DISS. ETH NO. 25277

Aerosol effects on climate, with an emphasis on the Arctic

A thesis submitted to attain the degree of

DOCTOR OF SCIENCES of ETH ZURICH
(Dr. sc. ETH Zurich)

presented by

WAN TING KATTY HUANG

MSc in Atmospheric and Oceanic Sciences, McGill University
born on 16.12.1990
citizen of Canada and Taiwan

accepted on the recommendation of

Prof., Dr. Ulrike Lohmann
Dr. Luisa Ickes
Assoc. Prof., Dr. Risto Makkonen

2018

Abstract

As the global climate warms, the Arctic environment is changing rapidly, with temperature increases up to two times higher than in lower latitudes. As a consequence, the aerosol population in the Arctic as well as the environment with which it interacts is expected to change in the future. In this thesis we examine two particular processes which have been newly implemented into the model as part of the thesis, involving aerosol-induced forcing in the Arctic region which may change in the future following changes in the natural and anthropogenic environment: the impact of heterogeneous ice nucleation, particularly by marine organic aerosol (MOA), and the darkening impact induced by deposited black carbon (BC) on snow. A general assessment of the relative importance of both processes is performed under present day conditions, followed by a look into how they may change in the future.

Firstly, as the sea ice retreats further during summer months, more of the ocean surface will be exposed in the future. This increases the potential for local marine aerosol emissions in the Arctic. Aside from the expected emission of sea salt particles, the ocean has also been found to be a source of organic material, which may be emitted in the gaseous or particulate phase. Recent re-emergence of interest in these marine organic emissions include their ability to act as ice nucleating particles (INPs) for the formation of ice crystals in supercooled clouds, which are prevalent in the Arctic. As this is still a relatively new subject of research, a sensitivity study is first performed to assess the importance of primary marine organic aerosol (MOA) as INPs on the global scale. MOA is contrasted to dust as immersion-mode INP, and found to contribute to more heterogeneous ice nucleation than dust during up to 50 % of the time in large parts of the mixed-phase temperature regions. This percentage, however, is highly dependent on the freezing onset temperature and parametrisation chosen for each INP species, as well as the choice of INP species considered. On the seasonal mean, an increase in both ice crystal number concentration and frequency of cloud ice occurrence in the high latitude near surface regions is found in the summer hemisphere. On the annual mean, a slight but statistically significant decrease in the ice crystal effective radii is observed in the high latitude low altitude regions, likely to have resulted from ice crystals nucleated in the warmer regions closer to the surface (which would be smaller in size than those which have grown during sedimentation from higher levels). Overall, however, MOA acting as INP is not found to have any significant influence on the global radiative balance nor other bulk cloud and precipitation properties.

Following the sensitivity study on MOA as INPs, changes in heterogeneous ice nucleation in the Arctic in the future are examined using a newly coupled aerosol-earth system model MPI-ESM1.2-HAM. A decrease in the number of immersed INPs available for freezing is found throughout the Arctic atmospheric column except near the surface below 2.5 km where an increase in the number of immersed MOA can be observed. The former can be associated with the decrease in dust and anthropogenic aerosol emissions in the lower latitudes as well as a possible increase in aerosol coagulation due to warming temperatures. The increase in immersed MOA, on the other hand, results from an increase in local emissions from the exposed Arctic Ocean surface. When changes in the environment (in particular shifting of the isotherms and specific humidity to higher altitudes) are also considered, a 50 to 200 % decrease in the overall heterogeneous freezing rate (relative to the mean over the present day and future periods) is observed in the future at all levels and seasons in the Arctic except near the surface in summer, where an increase in freezing rate is found. Aside from a decrease in INP activity with increasing temperature at each height level, this can be attributed to an overall lower freezing contribution because cold mixed-phase clouds become rarer due to both warmer temperatures and fewer INPs.

Lastly, the importance of snow surface darkening by deposited BC is examined. Under present day conditions, a localized instantaneous clear-sky shortwave forcing at the surface of up to 1.3 W m^{-2}, associated with an albedo decrease of up to 0.005,

can be found to result from BC deposited and mixed in the surface snow. This impact is most pronounced during the Arctic melt season of May and June. When feedbacks with the atmosphere are included, this leads to a clear-sky surface effective radiative forcings (ERF) of up to 9 W m^{-2}, associated with albedo decreases of up to 0.03. These changes are, however, not found to be statistically significant, and blend into the background variability when clouds are also considered (i.e. for the all-sky ERF). When comparing the present day impact to that in the future, a decrease in the instantaneous forcing can be found. This is associated with both decreases in the spatial extent of the snow coverage and a decrease in the BC concentration in the surface snow layer in the future.

Zusammenfassung

Mit der Erwärmung des globalen Klimas verändert sich die Arktis besonders stark mit einem Temperaturanstieg, welcher den in den niedrigeren Breiten um das bis zu zweifache übersteigt. Es ist daher anzunehmen, dass sich sowohl die Aerosolpopulation in der Arktis als auch die Umgebung, mit welcher diese interagiert, in der Zukunft verändern wird. In dieser Dissertation untersuchen wir zwei spezielle Prozesse, welche als Teil dieser Arbeit neu in das Modell implementiert wurden. Bei beiden Prozessen handelt es sich um aerosol-induzierte Strahlungsantriebe in der Arktis, welche sich in Zukunft aufgrund von Änderungen der natürlichen und anthropogenen Umgebung verändern könnten. Der erste Prozess beschreibt den Einfluss von heterogener Eisnukleation, insbesondere durch marine organische Aerosole (MOA), während der zweite den Verdunkelungseffekt von Ruß (BC, *engl. black carbon*) auf der Schneeoberfläche betrachtet. Eine allgemeine Bewertung der relativen Bedeutung beider Prozesse wird unter heutigen Bedingungen durchgeführt, gefolgt von Untersuchungen, wie diese sich in der Zukunft ändern könnten.

Wenn sich das Meereis während der Sommermonate weiter zurückzieht, wird in Zukunft mehr von der Meeresoberfläche freigelegt. Dies erhöht das Potenzial für lokale marine Aerosolemissionen in der Arktis. Abgesehen von der Emission von Meersalzpartikeln, ist der Ozean auch eine Quelle für organisches Material, welches in der gasförmigen oder teilchenförmigen Phase emittiert werden kann. Das kürzlich wiederkehrende Interesse an marinen organischen Emissionen ist auf deren Wirkung als Eiskeim (INP, *engl. ice nucleating particle*) in unterkühlten Wolken zurückzuführen, welche in der Arktis weit verbreitet sind. Da dies noch ein relativ neues Forschungsgebiet ist, wird in dieser Arbeit zunächst eine Sensitivitätsstudie durchgeführt, um die Bedeutung von primären MOA als INPs auf globaler Ebene zu untersuchen. MOA wird als immersiver INP im Vergleich zu Staub kontrastiert. Es zeigte sich, dass MOA in 50 % der Fälle in weiten Teilen des mischphasigen Temperaturbereichs mehr zur heterogenen Eisnukleation beiträgt als Staub. Dieser Prozentsatz ist jedoch stark abhängig von der für jede INP-Art gewählten Gefriertemperatur und Parametrisierung, sowie der Wahl der betrachteten INP-Arten. Im saisonalen Mittel ist auf der Sommerhalbkugel ein Anstieg sowohl der Eiskristallzahl als auch der Häufigkeit des Auftretens von Wolkeneis in den oberflächennahen Regionen der hohen Breitengrade festzustellen. Im Jahresmittel ist ein leichter, aber statistisch signifikanter Rückgang der effektiven Radien der Eiskristalle in den hohen Breiten in niedriger Höhe zu beobachten, der wahrscheinlich auf Eiskristalle zurückzuführen ist, die in den wärmeren Regionen näher an der Oberfläche entstanden sind (welche in ihrer Größe kleiner sind als diejenigen, die während Sedimentation aus höheren Lagen gewachsen sind). Insgesamt hat MOA als INP jedoch keinen signifikanten Einfluss auf die globale Strahlungsbilanz der Erde oder andere Wolken- und Niederschlagseigenschaften.

Im Anschluss an die Untersuchung der Sensitivität von MOA als INP werden zukünfitge Veränderungen der heterogenen Eisnukleation in der Arktis mit einem neu gekoppelten Aerosol-Erdsystem-Modell MPI-ESM1.2- HAM untersucht. Ein Rückgang in der Anzahl der zum Gefrieren verfügbaren immersiven INP ist in der gesamten arktischen Atmosphärensäule zu beobachten, außer in der Nähe der Oberfläche unter 2,5 km, wo ein Anstieg der Anzahl der immersiven MOA beobachtet werden kann. Ersteres kann mit dem Rückgang der Staub- und anthropogenen Aerosolemissionen in den niedrigen Breiten sowie einer möglichen Erhöhung der Aerosolkoagulation durch Erwärmung in Verbindung gebracht werden. Der Anstieg der immersiven MOA hingegen resultiert aus einem Anstieg der lokalen Emissionen aus dem exponierten Arktischen Ozeanoberfläche. Berücksichtigt man auch Umweltveränderungen (insbesondere die Verschiebung der Isothermen und der spezifischen Luftfeuchtigkeit), so ist in der Arktis in Zukunft ein Rückgang der gesamten heterogenen Gefrierrate (bezogen auf den Mittelwert der heutigen und zukünftigen Perioden) auf allen Ebenen und Jahreszeiten zu beobachten, außer in der Nähe der Oberfläche im Sommer, wo eine Zunahme der Gefrierrate festgestellt wird. Neben einer Abnahme der INP-Aktivität mit zunehmender Temperatur auf allen Höhen kann dies einem generell niedriegeren Gefrieren

zugeschrieben werden, weil kalte Mischphasenwolken seltener werden, zum einen wegen der wärmeren Temperaturen, zum anderen wegen der wenigeren INP.

Abschließend wird die Bedeutung der Verdunkelung der Schneeoberfläche durch die Ablagerung von BC untersucht. Unter den gegenwärtigen Bedingungen kann ein lokalisierter und instantaner kurzwelliger Strahlungsantrieb unter wolkenfreien Bedingungen (*engl. clear sky*) an der Oberfläche von bis zu 1.3 Wm^{-2}, verbunden mit einer Albedo-Abnahme von bis zu 0.005, gefunden werden, die aus dem im Oberflächenschnee abgelagerten und gemischten BC resultiert. Diese Auswirkungen sind während der arktischen Schmelzsaison im Mai und Juni am deutlichsten ausgeprägt. Werden Rückkopplungen mit der Atmosphäre einbezogen, führt dies unter *clear sky* Bedingungen zu einem effektiven Strahlungsantrieb (ERF, *engl. effective radiative forcing*) an der Oberfläche von bis zu 9 W m^{-2}, verbunden mit einer Albedo-Abnahme von bis zu 0.03. Diese Veränderungen sind jedoch statistisch nicht signifikant und fügen sich in die Hintergrundvariabilität ein, wenn auch Wolken berücksichtigt werden (z.B. für den *all-sky* ERF). Vergleicht man die Auswirkungen der Gegenwart mit denen der Zukunft, so lässt sich ein Rückgang des momentanen Strahlungsantriebs feststellen. Dies ist sowohl mit einer Abnahme der räumlichen Ausdehnung der Schneebedeckung als auch mit einer Abnahme der BC Konzentration in der Oberflächenschneeschicht in der Zukunft verbunden.

Contents

Chapter 1

Introduction: the Arctic environment

1.1 Warming in the Arctic

The Arctic is a region of particular interest for climate scientists mostly due to its faster rate of warming when compared to the global mean (e.g. Serreze and Francis, 2006; Bekryaev et al., 2010; Holland and Bitz, 2003). A widely cited mechanism for the amplified Arctic response to climate change is the ice-albedo feedback, where warming induces sea ice retreat, exposing the darker ocean underneath that reflects much less of the incoming shortwave radiation, and thus leading to a positive feedback of further warming (Manabe and Stouffer, 1980). The reduction in sea ice cover can also lead to increased heat flux into the ocean during the warm seasons, which would subsequently contribute to increased heat flux from the ocean, delayed re-freezing of the sea ice, thinner ice cover overall, and thus warming during autumn and winter (Manabe and Stouffer, 1980). Other pathways inducing stronger warming in the Arctic have also been proposed, such as the water vapour and cloud cover feedback where increased specific humidity in the Arctic leads to a greenhouse effect (Graversen and Wang, 2009). Changes in ocean circulation at high latitudes have also been suggested to extend a degree of control on the Arctic amplification (Holland and Bitz, 2003). Pithan and Mauritsen (2014), on the other hand, found the strongest driver behind Arctic amplification in the Coupled Model Intercomparison Project Phase 5 (CMIP5) models to be the temperature feedback, where warming induces a stronger increase in energy being radiated away from the surface in the lower latitudes compared to the higher latitudes (due to the weaker relative increase in blackbody radiation per degree of warming at colder temperatures and the difference in the vertical warming profiles). Looking more at the impact of changes in the atmospheric aerosol concentration, Acosta Navarro et al. (2016) found that the decrease in European aerosol burden in the past decades could have led to warming in the Arctic through an overall increase in oceanic heat transport into the Arctic and an increase in the atmospheric heat transport in summer (when the Arctic warms less as most of the energy goes into melting the ice while Europe warms more following the reduction of scattering aerosol), leading to more sea ice melt that extends to subsequent warming in autumn and winter.

1.2 Clouds in the Arctic

Clouds in the wintertime Arctic are characterized by two distinct and persistent states, where the atmosphere is either radiatively clear or opaquely cloudy (Morrison et al., 2012;

Stramler et al., 2011; Pithan et al., 2014; Graham et al., 2016). During the cloudy period, little net longwave radiative cooling occurs at the surface, the surface is warmer, and the temperature inversion is weaker and more elevated, while during the radiatively clear period, a strong surface radiative cooling leads to a strong surface temperature inversion (Stramler et al., 2011; Pithan et al., 2014; Graham et al., 2016). Studies by Pithan et al. (2014) have pointed to a tendency of the CMIP5 models to under-predict the cloudy phase, which they attributed to deficiencies in the models' mixed-phase cloud microphysics. The radiatively clear state, on the other hand, is likely to contain clear sky precipitating ice crystals, which is a prevalent phenomenon during the Arctic winter (Curry et al., 1996).

During summertime, Arctic clouds are either mixed-phase, with cloud-top radiative cooling driving the formation of ice crystals, or purely liquid, in which case the atmosphere tends to be stably stratified and the cloud too thin to drive mixing through radiative cooling (Sotiropoulou et al., 2014). Low level clouds are ubiquitous (found during 80 to 90 % of the time) in the Arctic summer, where clouds below 3 km are most commonly mixed-phase (Shupe, 2011). Despite the thermodynamically unstable state of mixed-phase clouds, they are found to persist for extended periods of time in the Arctic, with a supercooled layer above and frozen precipitation falling out of the cloud (e.g. Morrison et al., 2012; Pinto, 1998; de Boer et al., 2009). An example schematic of the complex processes maintaining such mixed-phase clouds is illustrated by Morrison et al. (2012) and shown in Fig. 1.1.

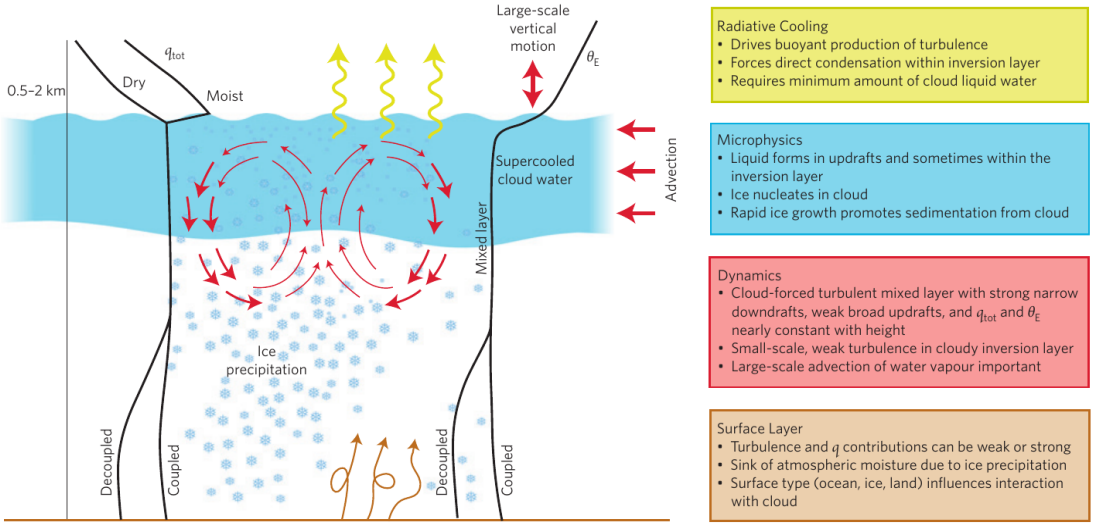

Figure 1.1: A schematic of the main processes involved in Arctic mixed-phase clouds, from Morrison et al. (2012). Features summarized in the text boxes are colour-coded according to the diagram.

Over the year, the Arctic is found to be persistently cloudy (58 to 83 % of the time, based on six observational sites; Shupe et al., 2011), with peak cloudiness during summer and the lowest percentage of cloud occurrence during winter (Intrieri et al., 2002b). Using measurements from aboard a ship drifting with the pack ice in the Arctic Ocean for a full year between 1997 and 1998, Intrieri et al. (2002b) found 73% of the lidar-observed clouds to be liquid-containing. When examined seasonally, mixed-phase and pure liquid clouds dominate during summer while ice cloud occurrence dominates during winter (Yin and Min, 2014). Supercooled droplets are found to persist to temperatures below -20 °C (Curry, 1995), with the lowest cloud base heights lower than 1 km (Intrieri et al., 2002b). When analysing data from three surface-based observational sites, however, Shupe (2011)

noted that ice clouds are the most prevalent cloud type in the Arctic, followed by mixed-phase clouds and lastly pure liquid clouds. This conclusion was derived in part by the lower occurrence of liquid-containing clouds at the Eureka site in northern Canada. Based on Cloud-Aerosol Lidar and Infrared Pathfinder Satellite Observation (CALIPSO) observations, on the other hand, Cesana et al. (2012) found substantial liquid-containing cloud fraction during all seasons (though significantly lower in winter; see Fig. 1.2).

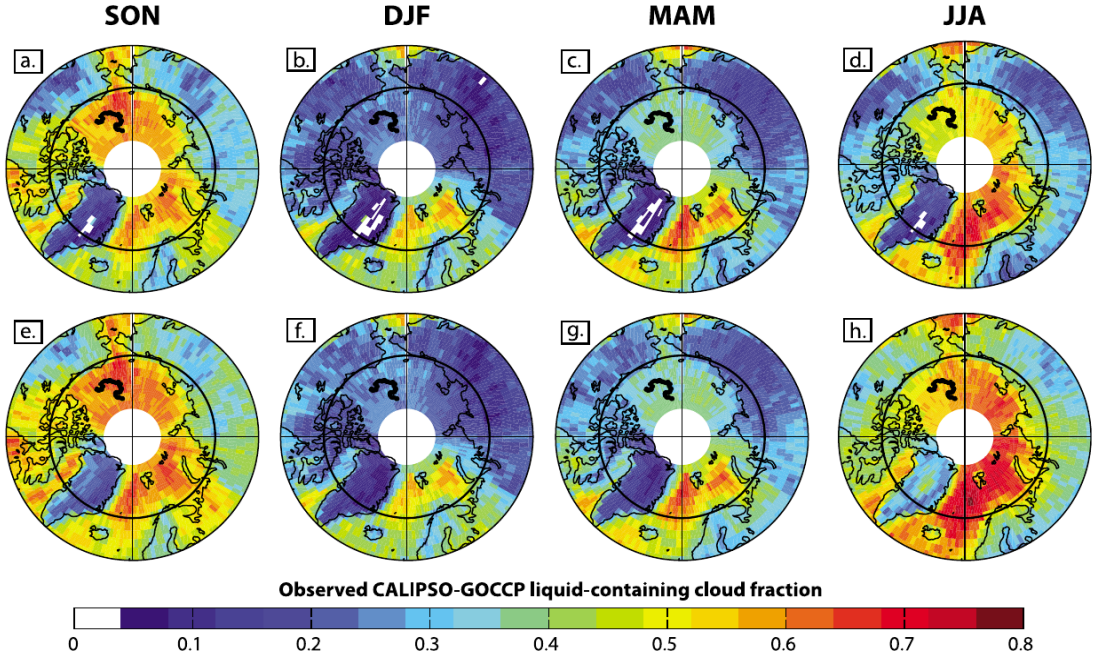

Figure 1.2: 2006 to 2011 seasonal mean (autumn to summer) liquid-containing cloud fractions from CALIPSO-GOCCP satellite observations, for low level clouds (up to 3.36 km above sea level; top row) and for clouds at all levels (bottom row). Figure from Cesana et al. (2012).

In terms of cloud radiative forcing, the longwave effect dominates during most of the year and induces a warming at the surface, while during midsummer, the shortwave effect becomes more important and clouds induce a cooling at the surface (Intrieri et al., 2002a; Shupe and Intrieri, 2004). Despite the more common occurrence of pure ice clouds, mixed-phase stratiform clouds are found to be the dominant driver in the Arctic cloud forcing at the surface (Shupe and Intrieri, 2004; Graham et al., 2016), where 80 % of the radiatively significant clouds had cloud bases below 1 km and temperatures warmer than -23 °C (Shupe and Intrieri, 2004). For summer, this value increases to cloud base temperatures warmer than -10 °C for 95 % of the radiatively significant clouds.

With sea ice retreat, the cloud response was examined using a set of observational data and found to be minimal in summer due to the near surface temperature inversion as well as low air-sea temperature gradient, while in early autumn, formation of low clouds was found over the newly opened ocean surface (Kay and Gettelman, 2009). By applying an assessment method including feedback processes, however, Liu et al. (2012) concluded that the Arctic can be expected to get cloudier with sea ice retreat. In particular, they noted that an increase in cloudiness by 0.3 to 0.5 % was found with each 1 % decrease in sea ice cover. In a modelling study, Holland and Bitz (2003) also found a significant correlation between the amplified Arctic warming and increases in the Arctic cloud cover.

1.3 Aerosols in the Arctic

Due to its remote location and cold climate, the Arctic is characterized by a low background concentration of aerosol particles. A seasonal cycle can be observed with the highest concentration near the surface occurring during late winter/spring, while the lowest concentrations are generally found during summer/early autumn (Freud et al., 2017). A stronger temporal variability can be observed during months with lower mean aerosol concentrations, when individual events may lead to more notable changes. Monthly averaged number concentrations of particles smaller than 500 nm in diameter vary between 50 to 100 cm^{-3} at ground-based measurement stations around the Arctic (Freud et al., 2017). During an April field campaign, however, Brock et al. (2011) found the aerosol concentration in the sea ice boundary layer north of Alaska to rather be in the range of 100 to 200 cm^{-3}, while the tropospheric background above the boundary layer showed a hazy concentration of between 200 to 680 cm^{-3}, which can reach up to 500 to 1700 cm^{-3} within atmospheric layers influenced by anthropogenic or biomass burning plumes. Aside from more long range transport, the higher aerosol concentrations in the free troposphere can result from the minimal precipitation scavenging in the upper levels in the Arctic (Brock et al., 2011). As transport through adiabatic processes would require the origin air mass to be of similar temperature as the Arctic (Iversen, 1984), transport into the Arctic is facilitated if the air mass originates from within the Arctic front. Thus as the Arctic front extends to lower latitudes over the Eurasian continent during winter, transport from these regions can lead to higher aerosol concentrations in the Arctic in winter (Law and Stohl, 2007). Additionally, the slow rate of aerosol removal during the dry and stable Arctic winter may also have contributed to the accumulation of aerosol particles during this season (Law and Stohl, 2007).

In terms of the aerosol composition, Chang et al. (2011) found a dominance of sulphate near the surface in the central Arctic Ocean during summer from both marine biogenic and continental sources, while around a third of the total aerosol is noted to be rich in organic material from either marine or continental sources. A similar proportion of organics is also found in the free tropospheric background haze population, during an April campaign north of Alaska (Brock et al., 2011). The authors of this latter study, however, attributed the organic material to be from past biomass or bio-fuel burning.

Aside from the shielding effect of the polar front, transport pathways into the Arctic have been identified to either occur at low altitudes, followed by possible ascent once in the Arctic region, or at higher altitudes after air mass ascent outside the Arctic which then descend in the Arctic following large-scale subsidence (Stohl, 2006). While transport from Europe can follow any of the proposed pathways, they found that those from North America and Asia are more likely to be transported following large-scale subsidence. Using the Goddard Earth Observing System Chemistry-Climate Model (GEOSCCM), Orbe et al. (2015), on the other hand, found that Arctic air masses below 700 hPa tend to originate (in terms of last contact with the planetary boundary layer) from regions north of 60° N, while those in higher levels are more likely to originate from mid-latitudes. On a seasonal scale, they found that these upper level air masses are more likely to originate from oceanic regions during winter and from continental regions (mostly Asia) during summer.

In terms of local sources, a series of papers from Leck and Bigg (e.g. 1999; 2010) have proposed a marine biogenic source of aerosols in the central Arctic Ocean, either from open leads in the sea ice or from the open ocean, and both nucleation-sized particles as well as larger primary aerosol emissions are discussed. Measurements by Held et al. (2011), however, found that open water leads constitute a weak aerosol source that only

explains 5 to 10 % of the variation in particle number concentration close to the surface in the central Arctic.

With future changes in the global environment, the amount of aerosol reaching the Arctic may also be expected to change. This may result from changes in the aerosol emissions, such as an increase in boreal forest fires, which may result in increased biomass burning aerosol being transported to the Arctic (Stocks et al., 1998). Changes in the atmospheric transport pattern may also occur due to climate change, and a possibility is the decreased meridional temperature gradient leading to a weakening of the Arctic front and thus more transport into the Arctic (Law and Stohl, 2007). Finally, studies have also pointed to the possibility of a positive trend in the North Atlantic Oscillation (NAO) index leading to more airmasses being transported into the Arctic region (Burkhart et al., 2006; Eckhardt et al., 2003).

1.4 Impacts of aerosols on the Arctic climate

The impacts of aerosols on the Arctic climate can be broadly divided into three types: direct radiative effects associated with reflectivity and absorptivity of the aerosol, indirect effects involving aerosol-cloud interactions, and finally impacts on radiation through darkening of the surface after deposition of absorbing aerosols.

While aerosol particles in the atmosphere are generally associated with a surface cooling due to reflectance of incoming shortwave radiation, this effect is diminished in the Arctic due to the lack of solar radiation for significant parts of the year, and due to the high surface albedo. During summer, however, this effect may still be relevant. Struthers et al. (2011), for instance, found that an increase in sea salt emission due to sea ice retreat leads to an approximately 23 % increase in the natural aerosol optical depth, which resulted in a radiative forcing of between -0.2 to -0.4 W m^{-2} at the surface north of 70° N during the summer months. MacCracken et al. (1986), however, noted that the shortwave effect of carbonaceous aerosols over bright surfaces is likely to be compensated by the longwave effect (increased emission from the atmosphere to the surface due to aerosol-induced warming of the atmosphere) and leading to a net warming at the surface. This longwave heating effect is found to be of importance in the Arctic for even slightly absorbing aerosols with single scattering albedos as high as 0.98 (Pueschel and Kinne, 1995). During polar nights, the direct thermal radiative forcing of aerosols has been measured at Svalbard to amount to 2.99 to 4.66 W m^{-2} in the downwelling, and -0.23 to 1.17 W m^{-2} in the outgoing longwave radiation (Ritter et al., 2005). Using a set of idealized simulations, Flanner (2013) also found an altitude dependence of the forcing induced by black carbon (BC) aerosol, with the most significant warming observed when the aerosol resides in the lowest atmospheric layer, as opposed to a cooling effect for high altitude (230 hPa) BC. The magnitude and sign of the forcings, however, was noted to be dominated by feedback processes in the climate system such as the ice-albedo feedback and changes in the meridional energy transport.

In terms of aerosol-cloud indirect effects, studies have particularly noted the influence of the first indirect effect in the Arctic, whereby increased aerosol concentrations lead to an increase in the cloud droplet number concentration and a decrease in the droplet radius, assuming constant liquid water content (Twomey, 1977). Due to the frequent occurrence of thin liquid clouds in the Arctic, whose longwave emissivity can vary due to changes in the droplet size (as opposed to thicker liquid clouds at lower latitudes where the emissivity is close to unity regardless of droplet size), the longwave component of the first indirect effect is also of relevance in the Arctic (Curry, 1995; Garrett et al., 2002). Measurements obtained from near Barrow, Alaska, for instance, have noted an increase

in the surface longwave radiative fluxes of 3.3 to 5.2 W m^{-2} when thin liquid clouds coincide with pollution plumes (Lubin and Vogelmann, 2006b; Garrett and Zhao, 2006). Lubin and Vogelmann (2006a), however, also noted that during March and April, the shortwave component of the first indirect effect induces a compensating cooling, while in May and June, the shortwave effect dominates. Model simulations by Alterskjær et al. (2010) comparing the indirect effects induced by present day and pre-industrial aerosol emissions, on the other hand, found an Arctic-wide (north of 71° N) annual average longwave forcing between 0.10 and 0.85 W m^{-2}, while the shortwave forcing lies in the range of -1.29 to -0.52 W m^{-2}. The annual mean net cloud forcing was found to be mostly negative, with a value of up to -0.98 W m^{-2}. By simulating a complete removal of sea ice in a model, Browse et al. (2014) found a negligible change in the cloud condensation nuclei despite increases in local emissions of aerosols and precursor gases. They attributed this to the efficient scavenging of the aerosols by drizzle from the stratocumulus decks.

Aside from impacts on the cloud liquid properties, aerosols also play a role in the formation of ice crystals. In particular, aerosols can act as ice nucleating particles (INPs), which aid in the formation of critical ice germs and thus lowers the temperature and supersaturation required for ice crystal formation. This process is termed heterogeneous ice nucleation, whereas in the absence of INPs, ice crystals are formed through homogeneous freezing of supercooled liquid droplets at colder temperatures (<-38 °C; Kanji et al., 2017). Thus the absence of INPs can lead to persistence of supercooled liquid droplets under sub-zero environmental conditions. The presence of INPs, on the other hand, has the potential to lead to glaciation of clouds through the Wegener-Bergeron-Findeisen process where ice crystals grow rapidly by depositional growth due to the lower saturation vapour pressure over ice than over liquid, causing cloud droplets to evaporate. The ability of specific aerosol species to nucleate ice crystals (ice activity) and their relevance in the atmosphere, however, is still a topic of active research (e.g. Kanji et al., 2017). One widely accepted INP species in the atmosphere is mineral dust particles (e.g. Atkinson et al., 2013), while bacteria and fungal spores (e.g. Huffman et al., 2013), marine organic aerosol (e.g. Wilson et al., 2015), and black carbon (e.g. Gorbunov et al., 2001) have also been suggested as potentially important INPs. In the Arctic where persistent mixed-phase clouds are prevalent, such mixed-phase microphysics is of particular importance. Indeed, modelling studies have pointed to a sensitivity of the simulated Arctic mixed-phase cloud properties to the INP concentration and ice activity, though the extent of the influence is still variable (e.g. Fu and Xue, 2017; Fan et al., 2009; Morrison et al., 2008).

Due to the high albedo of snow in the visible range, the presence of minimal amounts of absorbing impurities in snow can already have non-negligible impacts on the snow albedo (Warren and Wiscombe, 1980). A collection of papers by Flanner et al. (2007, 2009); Flanner (2013) have examined in particular the impact of BC, the most absorptive aerosol species in the atmosphere, deposited on and mixed in with snow on the ground and sea ice in various contexts. In a study of the present day global forcing of black carbon in snow (Flanner et al., 2007), they found a global annual mean forcing of 0.054 W m^{-2} for a year with strong boreal fires, of which 80 % is attributed to anthropogenic activities. A particularly strong response to the boreal fires was also noted in the Arctic, with a warming of 1.61 °C due to inclusion of BC in snow when climate feedbacks are considered. An idealized set of simulations performed by Flanner (2013) also indicated a warming effect of BC in surface snow that can counteract cooling effects induced by the same order of magnitude radiative forcing in the Arctic. When examining the effects of BC in snow outside of the polar regions, they found that due to strong feedback processes, BC deposition on snow contributed to nearly as much of the snow melt over Eurasia as anthropogenic carbon dioxide (Flanner et al., 2009). In an overview paper by Dou and

Xiao (2016), the strongest forcing induced by BC in snow is found to occur over the Arctic ice cap during summer (due to the compounding effect of increased snow grain size with age), but the radiative effect is secondary to that induced by widespread melt ponds during this season. A model study by Namazi et al. (2015), on the other hand, concluded that BC emission changes between the 1950's and the 2000's had negligible impacts on the snow albedo, and that the overall impact of BC in snow on the cryosphere is small. Lastly, a multi-model Aerosol Comparisons between Observations and Models (AeroCom) assessment quoted a global annual mean radiative forcing due to BC in snow of 0.17 W m^{-2} (Jiao et al., 2014).

1.5 Thesis outline

With global warming, decreases in summer sea ice cover in the Arctic have been observed in recent years, and the trend is expected to continue into the future, leading to increased exposure of the ocean surface. From the perspective of aerosols, this indicates a potential for increased local aerosol emissions from the ocean. On the other hand, anthropogenic aerosol emissions are also expected to change in the future, with decreases in mid-latitude industrial emissions due to economic and technological advancement, and possible increases in local emissions due to opening up of the Arctic shipping route. In this thesis, two aerosol processes which have the potential to impact the Arctic climate are implemented into a global aerosol-climate model, and assessments are made for their importance in the present day and in the future. More specifically, we address the following questions:

1. What is the global relevance of marine organic aerosol as ice nucleating particles under the present day climate?
2. How does heterogeneous ice nucleation change in the future Arctic?
3. How does black carbon deposited on snow impact the Arctic climate?

In the rest of this thesis, an overview of the model versions used for the investigations is first provided in chapter 2, followed by three chapters addressing the above posed research questions, in the listed order, and lastly closing with a summary and outlook chapter.

Chapter 2

Model description

All model simulations in the current thesis are performed using variations of the ECHAM6.3-HAM2.3 global aerosol-climate model (Tegen et al., 2018), which consists of the global atmospheric model ECHAM6 (Stevens et al., 2013) and the HAM2 aerosol module (the Hamburg aerosol model; Stier et al., 2005; Zhang et al., 2012) (hereafter referred to as ECHAM-HAM, ECHAM, and HAM, respectively). This can be additionally coupled to an ocean-sea ice model (the Max Planck Institute ocean model, MPIOM; Marsland et al., 2003; Jungclaus et al., 2013). When considering interactive carbon cycling between the various components (Giorgetta et al., 2013a), this forms the earth-system model (ESM) MPI-ESM-HAM. An overview of the key components of the model (Fig. 2.1) will be given in this chapter, with special notes on differences between the model versions used in the present thesis.

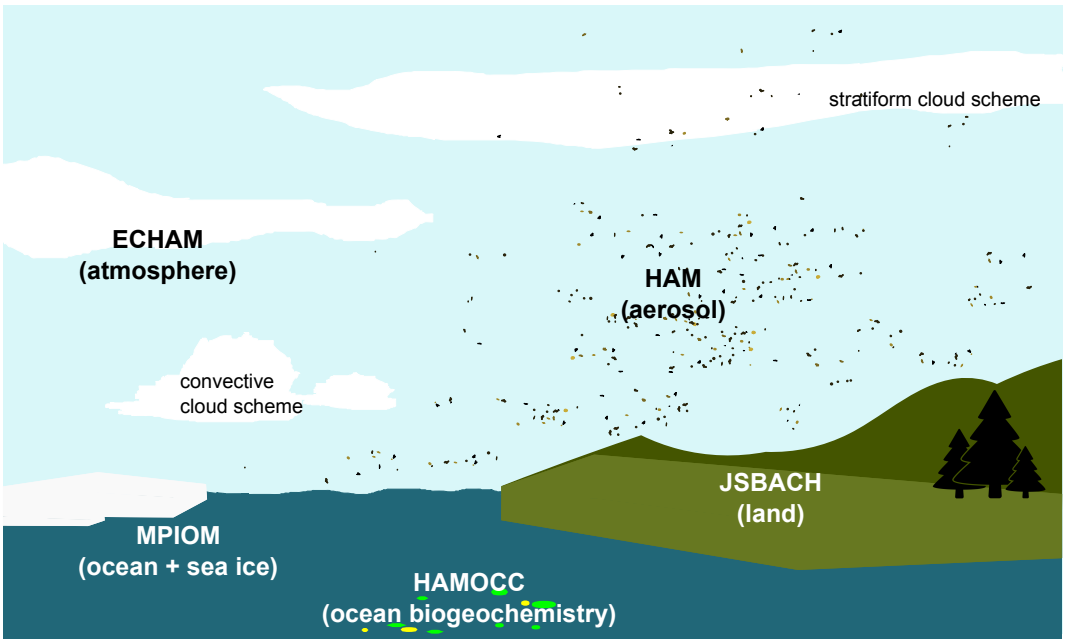

Figure 2.1: A schematic of the various model components discussed in this chapter.

2.1 ECHAM

The atmospheric part of MPI-ESM-HAM (ECHAM) includes parametrisations for the radiative transfer, turbulence, gravity waves, and clouds, as described in detail in Giorgetta et al. (2013b). As the land surface property plays an important role in both radiative and thermodynamic balances, a version of the JSBACH land surface model (Roeckner et al., 2003) is also included.

Clouds and precipitation are handled by two different cloud schemes in the model, one for cumulus convection and another for stratiform clouds. For convective systems, the lifetime of the main updraft (convective core) is assumed to be less than one model time step (12 minutes), such that no convective core would be visible to the radiation scheme. Rather, the parametrisation serves to transport moisture, heat, and momentum upward in the atmosphere, which can lead to either moistening of the upper levels or formation of detrained clouds, which are considered in the stratiform cloud scheme. As the convective parametrisation is a single-moment scheme (i.e. only one hydrometeor property is prognosed while the rest are either prescribed or diagnosed), it considers only the specific humidity being transported but neither the mass mixing rate nor the number concentration of hydrometeors. Should saturation be reached following detrainment from the convection, the mass flux is fed into the stratiform cloud scheme for the formation of detrained clouds which can persist over several time steps.

In the original ECHAM model (without HAM), the stratiform cloud scheme is also single-moment (source and sink processes are prognosed only for the hydrometeor mass concentration, while the number concentration is prescribed and the size is diagnosed). This is however changed to a two-moment scheme (such that the hydrometeor number concentration is also prognosed) when ECHAM is coupled to the aerosol module (Lohmann et al., 2007). The change is essential for the coupling between aerosol and clouds, as the main influence of aerosol particles on clouds is through changes in the number concentration of hydrometeors formed. Since it is not part of the standard ECHAM distribution, the two-moment stratiform cloud scheme is described separately in the subsequent section.

Radiative transfer in ECHAM is calculated based on considerations for the surface and cloud properties as well as transmisivity of the atmosphere. Sub-grid clouds in adjacent model layers are assumed to be maximally overlapping, while if the layers are not directly adjacent to each other, they are assumed to be randomly overlapped. The large-scale winds are calculated based on a set of governing equations in the dynamical core of the model, while turbulence, which is a sub-grid feature, is parametrised in terms of the turbulent kinetic energy (TKE; Brinkop and Roeckner, 1995) scheme.

In this thesis, JSBACH is run with 11 vegetation and one bare surface types, each of which is prescribed using different characteristics and is treated separately during process calculations in the model. Forcing from the atmosphere is uniform across the surface types, and the grid mean properties are calculated based on a combination from all surface types present. The initial ratio of the various surface types at each geographical location is then prescribed based on an input file. Changes in the ratio over time can be explicitly calculated in the model based on competition between the vegetation types, a set of rules for anthropogenic (e.g. agricultural, forestry activities) land transitions (Hurtt et al., 2006), and influences by the climate conditions (Reick et al., 2013). This feature, called dynamical vegetation, is by default turned off in ECHAM-HAM. It is thus only used in the ESM simulations in the subsequent chapters. For atmosphere-only simulations, the ratio of coverage by the various vegetation types at each grid box remains fixed. Properties of the land within each surface type, however, can change due to modelled forcings from the atmosphere.

A number of different model resolution are available for ECHAM, but for all results included in this thesis, the T63 horizontal grid (which has a resolution of $1.88° \times 1.88°$) is used. Two different vertical resolutions are applied, one with 31 hybrid levels, which is used for the atmosphere-only simulations and reaches up to 10 hPa, and another with 47 hybrid levels, which includes the stratosphere up to 0.01 hPa and is used in the ESM simulations. The model vertical resolution in the troposphere, from around 500 m in the lower troposphere to 1 km around the tropopause, however, is identical between the two set-ups (Roeckner et al., 2006).

When not coupled to an ocean model, the sea ice cover and sea surface temperature are prescribed based on input data representing either the conditions for individual years or a climatology. Aside from nudged simulations, where the model is set up to replicate the atmospheric condition for specific years, all atmosphere-only simulations in the current thesis use a mean climatology for the 1979 to 2008 sea ice and sea surface temperature conditions from the AMIP dataset (Taylor et al., 2000). In addition, present-day climatological greenhouse gas and ozone concentrations as well as the solar irradiance are prescribed and do not change in these simulations.

2.2 Stratiform clouds

Stratiform clouds are parametrised in ECHAM-HAM following the two-moment microphysics scheme described in Lohmann et al. (2007, 1999). Two prognostic hydrometeors are considered: cloud droplets and ice crystals. Each hydrometeor type is then characterized by its mass mixing ratio and number concentration, which are predicted separately following considerations of various microphysical processes. Precipitating hydrometeors, namely rain and snow, are diagnosed as sink terms for the cloud droplets/ice crystals once they grow to a sufficiently large size. The precipitation is then assumed to fall to the ground within one time step.

As the model horizontal resolution is coarser than the length scale of individual clouds, a cloud cover scheme is needed in order to consider sub-grid scale moisture inhomogeneity. This allows for cloud formation below grid-wide saturation of water vapour. Cloud cover is determined based on the Sundqvist et al. (1989) scheme, which represents cloud cover as a function of the relative humidity. Cloud microphysical processes are then computed for the cloudy part of the grid box.

2.3 HAM

Two different types of aerosol size distribution representations are available from the HAM model: the M7 modal bulk scheme where the distribution of aerosols in each size mode is represented by a lognormal size distribution function (Vignati et al., 2004), and the SALSA sectional bin scheme where the size distribution is divided into individual bins without assumptions of the shape of the overall distribution (Bergman et al., 2012). Due to advantages concerning computational costs and as a bulk representation of the aerosol size distribution is sufficient for the studies conducted, all simulations discussed in the current thesis utilize the M7 scheme.

The M7 scheme (Fig. 2.2) represents the entire aerosol population in seven different modes, each represented by a lognormal size distribution function constrained by a fixed shape parameter. The seven modes are comprised of four size modes (nucleation: $\bar{r} \leq 0.005$ µm, Aitken: 0.005 µm $< \bar{r} \leq 0.05$ µm, accumulation: 0.05 µm $< \bar{r} \leq 0.5$ µm, and coarse: 0.5 µm $< \bar{r}$, where $\bar{r}$ is the number median radius) and all but the smallest size

mode are further divided into two modes of different mixing states/solubility (internally mixed/soluble, and externally mixed/insoluble). The aerosol species considered in this thesis are sulphate, organic carbon (OC), black carbon (BC), dust (DU), sea salt (SS), and in addition to the standard HAM module, also marine organic aerosol (MOA). For internally mixed modes, the aerosol species are assumed to be equally distributed between all the particles such that only one number concentration is considered per mode. The proportion of the various species present in the aerosol mode is then represented by the mass concentration of each species. For the externally mixed modes, the number and mass concentrations are traced in the same way, but as only carbonaceous particles exist in the externally mixed Aitken mode and only dust resides in the externally mixed accumulation and coarse modes, each particle in these modes contains essentially one aerosol species. As neither sulphate nor SS is present in these particles, the externally mixed modes are also referred to as the insoluble modes. The nucleation mode, which also contains only one aerosol species (sulphuric acid), on the other hand, is a soluble mode.

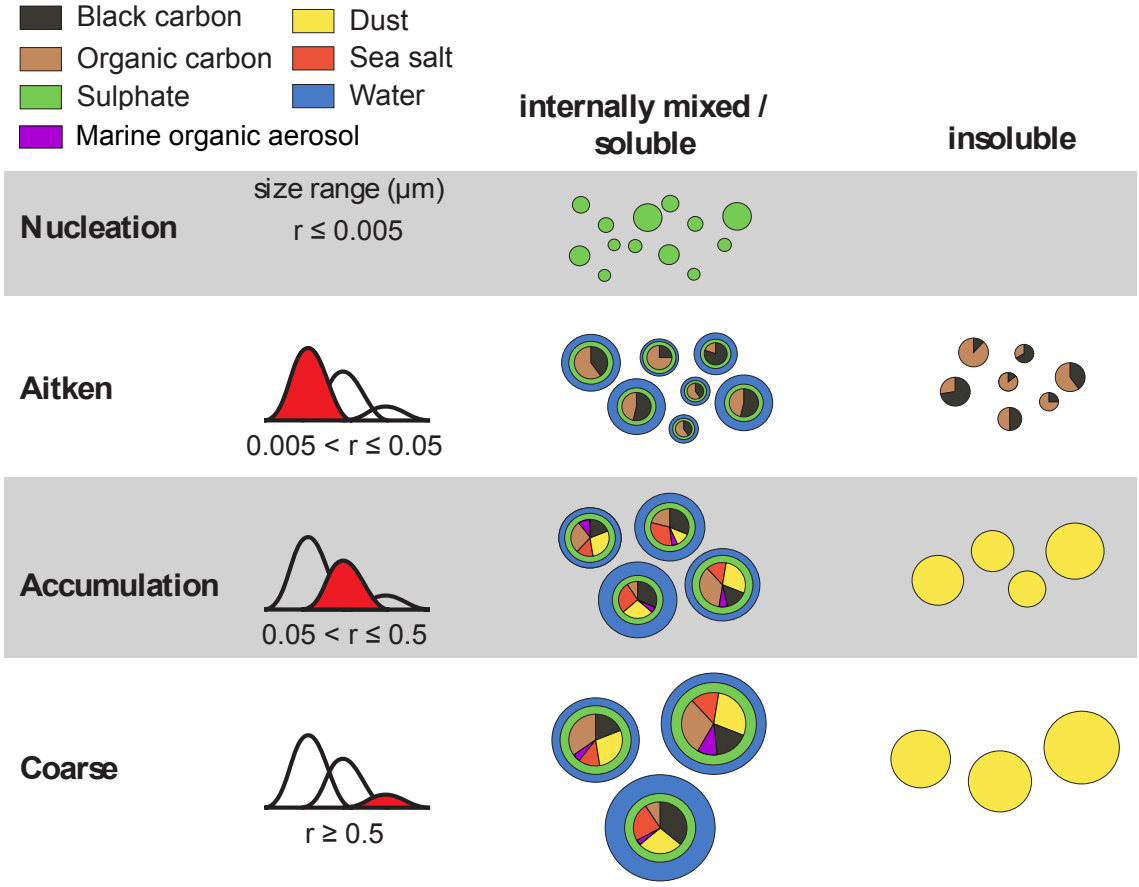

Figure 2.2: A schematic of the aerosol modes and species considered in the M7 scheme. Original figure courtesy of Elias Zubler, modified to include MOA.

Aerosol emissions are either prescribed as inputs to the model or calculated online based on the model environmental conditions. They are prescribed should the processes controlling the emissions not be explicitly represented in the model (e.g. anthropogenic and fire emissions), and calculated online otherwise (e.g. for dust and SS). Prescribed monthly mean emissions are separated by the source sector (e.g. ships, domestic, industry, grass fire, etc.), each of which can lead to emissions of several aerosol species. Online emissions, on the other hand, are parametrised and calculated at each model time step.

All atmosphere-only simulations in this thesis use the Long et al. (2011) sea salt emission parametrisation with an additional sea-surface temperature dependence following Sofiev et al. (2011), while for the ESM simulation, the previous model distribution default (Guelle et al., 2001) is used. Notably, the newer implementation based on Long et al. (2011) results in significantly less emissions of SS in the Southern Ocean. Dust emission follows that described in Tegen et al. (2002) for all cases, and MOA is emitted by scaling up the Rinaldi et al. (2013) parametrisation by two-fold in the default set-up.

2.4 Aerosol-cloud-climate coupling

Direct coupling between aerosols and clouds in ECHAM-HAM is through activation of cloud droplets and formation of ice crystals. The former is parametrised following Abdul-Razzak and Ghan (2000), which is based on Köhler theory and dependent on the aerosol species, size, and the environmental supersaturation. For the formation of ice crystals in the mixed-phase temperature regime (-35 to 0 °C, where liquid droplets can persist under supercooled conditions without freezing homogeneously), the default parametrisation following Lohmann and Diehl (2006) is not used in the current thesis. Instead, the default set-up is changed to consider immersion freezing of dust following the single-α classical nucleation theory parametrisation by Ickes et al. (2017) and that of MOA following Wilson et al. (2015). Immersion freezing requires that the relevant aerosol be immersed in a cloud droplet before it can nucleate ice. For temperatures colder than -35 °C, only homogeneous ice nucleation, which is independent of aerosols, is included.

Aside from acting as cloud condensation nuclei (CCN) and ice nucleating particles (INPs), aerosol can impact the model climate through the direct radiative effect (scattering of radiation) and warming due to absorptive aerosol species (BC) suspended in the atmosphere. Reduction of surface albedo and subsequent warming due to deposited BC on snow is additionally included (contrary to the default ECHAM-HAM distribution) in all simulations in this thesis except those in chapter 3.

2.5 MPIOM

When run as an ESM, ECHAM-HAM is coupled to the ocean-sea ice model MPIOM (Marsland et al., 2003; Jungclaus et al., 2013), which simulates the ocean dynamics and thermodynamics as well as those of sea ice. An ocean biogeochemistry sub-model HAMOCC (Ilyina et al., 2013) is also included, in which the photosynthesis and transformation of biogeochemical constituents in the ocean are simulated. The overall ocean model is run on a bipolar (over Greenland and Antarctica instead of north and south poles) GR15L40 grid with 40 vertical levels and an approximate horizontal resolution of 1.5°. Information is exchanged between the atmosphere and ocean components of the model once per simulated day.

Chapter 3

Global relevance of marine organic aerosol as ice nucleating particles

This chapter is published on Atmospheric Chemistry and Physics, with the citation: Huang, W. T. K., Ickes, L., Tegen, I., Rinaldi, M., Ceburnis, D., and Lohmann, U.: Global relevance of marine organic aerosol as ice nucleating particles, Atmospheric Chemistry and Physics, 18, 11423-11445, doi:10.5194/acp-18-11423-2018, 2018.

Abstract

Ice nucleating particles (INPs) increase the temperature at which supercooled droplets start to freeze. They are therefore of particular interest in mixed-phase cloud temperature regimes, where supercooled liquid droplets can persist for extended periods of time in the absence of INPs. When INPs are introduced to such an environment, the cloud can quickly glaciate following ice multiplication processes and the Wegener–Bergeron–Findeisen (WBF) process. The WBF process can also cause the ice to grow to precipitation size and precipitate out. All of these processes alter the radiative properties.

Despite their potential influence on climate, the ice nucleation ability and importance of different aerosol species is still not well understood and is a field of active research. In this study, we use the aerosol–climate model ECHAM6-HAM2 to examine the global relevance of marine organic aerosol (MOA), which has drawn much interest in recent years as a potentially important INPs in remote marine regions. We address the uncertainties in emissions and ice nucleation activity of MOA with a range of reasonable set-ups and find a wide range of resulting MOA burdens. The relative importance of MOA as an INP compared to dust is investigated and found to depend strongly on the type of ice nucleation parameterisation scheme chosen. On the zonal mean, freezing due to MOA leads to relative increases in the cloud ice occurrence and in-cloud number concentration close to the surface in the polar regions during summer. Slight but consistent decreases in the in-cloud ice crystal effective radius can also be observed over the same regions during all seasons. Regardless, MOA was not found to affect the radiative balance significantly on the global scale, due to its relatively weak ice activity and a low sensitivity of cloud ice properties to heterogeneous ice nucleation in our model.

3.1 Introduction

In regions with scarce ice nucleating particles (INPs), liquid cloud droplets can remain supercooled for extended periods of time before the drops freeze homogeneously (Rogers

and Yau, 1989). In the presence of INPs, phase change is facilitated, and supercooled cloud droplets can freeze at temperatures warmer than the homogeneous freezing temperature (Kanji et al., 2017). Together with the Wegener–Bergeron–Findeisen (WBF) process through which ice crystals grow at the expense of liquid droplets due to their difference in saturation vapour pressure, INPs can alter the radiative properties of clouds and thus climate through glaciation and possible precipitation (Korolev, 2007; Lohmann, 2002). Representation of INPs and their freezing ability is therefore of importance in climate modelling, especially for studies investigating aerosol–cloud effects.

Indeed, the subject of INPs is an area of active research in both modelling as well as laboratory and field work (e.g. Hoose and Möhler, 2012; Coluzza et al., 2017; Kanji et al., 2017). Suggested INP candidates, such as mineral dust, terrestrial biogenic material, and black carbon, are mostly of terrestrial origin. Recently, however, more interest has been drawn to oceans being possible sources of ice-active organic matter (Bigg, 1973; Knopf et al., 2011; Wang et al., 2015; Wilson et al., 2015; DeMott et al., 2016; McCluskey et al., 2017). While likely not as ice active as mineral dust especially in the colder mixed-phase temperatures, the difference in geographical locations of their emission sources may cause such marine organic aerosol (MOA) to become an important source of INPs in remote marine regions (Vergara-Temprado et al., 2017).

MOA can either be emitted directly as primary aerosol from the ocean surface by bubble bursting (e.g. Caroline and Keith, 2005) or formed through a secondary process involving the condensation of biogenic volatile organic compounds (BVOCs) emitted from the ocean (e.g. Bonsang et al., 1992), and the resulting aerosol can either be water insoluble (WIOM; water insoluble organic matter) or water soluble (WSOM). The type relevant for ice nucleation is the insoluble organic matter, which originates mainly from primary emissions (Ceburnis et al., 2008). In this study, therefore, we will only focus on the primary emitted WIOM and thus only refer to such WIOM when discussing MOA.

In investigating the global impact of MOA as INPs using general circulation models, an earlier study by Yun and Penner (2013) found MOA to be the dominant source of heterogeneously formed ice crystals in the Southern Hemisphere compared to contributions from dust and black carbon. They also noted a better comparison of modelled ice water path to satellite observations from the International Satellite Cloud Climatology Project (ISCCP) when MOA is added as an additional source of INPs. Due to the lack of more measurement data at the time of publication, however, the representation of MOA ice activity in their study is constrained by a fixed ratio of nucleation efficiency at $-15\,^{\circ}\mathrm{C}$ that is 3 times higher over the Antarctic Ocean at $40^{\circ}\,\mathrm{S}$ than over Australia, based on Schnell and Vali (1976)'s evaluation of the Bigg (1973) INP data. It assumes, therefore, implicitly that MOA alone accounts for any shortfall in the model in representing the difference in ice nucleation ability of aerosol over Australia and the Southern Ocean. This would render the calculated MOA ice activity dependent on aerosol transport and the ice nucleation ability of other species in the model, while at the same time discounting other sources of INPs not yet considered. Thus, while a better agreement with observational data could be obtained, MOA may not be the sole missing INP responsible for the model shortfall.

In terms of the relative contribution of MOA to the global INP population when compared to other sources, Burrows et al. (2013) found a greater contribution of MOA compared to terrestrial biogenic aerosol over nearly all regions except central continental areas, and a greater contribution compared to dust over the Southern Ocean. A recent paper by Vergara-Temprado et al. (2017) also found MOA to be the dominant source of INPs in remote locations, particularly in the southern high latitudes during austral autumn to spring. Notably, they also found MOA to be the more dominant source of INP compared to dust (K-feldspar) on 10–30 % of days in the Northern Hemisphere.

MOA can also have impacts on climate through cloud properties of warm liquid clouds. This was investigated by Meskhidze et al. (2011) and Gantt et al. (2012), who concluded a weak influence of MOA on the global CCN concentration but up to a 20 % localised increase in the annually averaged low-level cloud droplet number concentration (CDNC) over remote oceans, as well as up to a 7 % decrease in the anthropogenic aerosol indirect forcing (though their MOA emission rates remained fixed between present-day and pre-industrial periods). These potential effects, however, will not be the focus of the current study.

The goal of this study is to quantify possible contributions of MOA to heterogeneous ice nucleation and its subsequent influence on cloud properties on the global scale. We hypothesise a potential impact in remote marine regions and test our hypothesis while considering various uncertain aspects in the representation of MOA ice nucleation in a global climate model.

Table 3.1: List of aerosol species present in each of the seven modes. In bold are tracers added in the current study.

Size mode	Internally mixed/soluble	Externally mixed/insoluble
Nucleation	Sulphate	
Aitken	Sulphate, OC, BC	OC, BC
Accumulation	Sulphate, OC, BC, SS, dust, **MOA**	Dust
Coarse	Sulphate, OC, BC, SS, dust, **MOA**	Dust

3.2 Methodology

3.2.1 The aerosol–climate model

Simulations in this study are performed using the aerosol–climate model ECHAM6-HAM2. The main atmospheric component is ECHAM6 (Stevens et al., 2013), except for a two-moment cloud microphysics scheme that is coupled to the aerosol module HAM2 (Lohmann et al., 2007). Aerosols are represented as a superposition of seven lognormal size distributions, representing aerosol populations in four size modes and two different mixing states, except for the nucleation mode (number median radius $\overline{r} \leq 0.005\,\mu m$) which only contains sulphate aerosol in the internally mixed/soluble mode. All other size modes (Aitken: $0.005\,\mu m < \overline{r} \leq 0.05\,\mu m$, accumulation: $0.05\,\mu m < \overline{r} \leq 0.5\,\mu m$, coarse: $0.5\,\mu m < \overline{r}$) are divided into an internally mixed/soluble mode in which particles are assumed to contain a fraction of all species present, in particular the soluble sulphate aerosol, and an externally mixed/insoluble mode in which each particle is assumed to contain one species only. Only one size distribution (with one total number concentration, median radius, and standard deviation) is considered per mode, while the contribution of each species is represented by their individual masses, which are traced separately.

Various aerosol processes are explicitly represented as described in Zhang et al. (2012). Changes in recent model updates include the use of the Abdul-Razzak and Ghan (2000) scheme for aerosol activation to form cloud droplets, which is based on Köhler theory, and the use of the Long et al. (2011) sea salt (SS) emission parameterisation with a sea surface temperature dependence applied following Sofiev et al. (2011). Also, anthropogenic emissions are fixed at year 2000 levels in the following simulations and the minimum CDNC is $10\,cm^{-3}$. In the base version used in the current study, aerosol species considered include sulphate, dust, black carbon (BC), organic carbon (OC), and SS, among

which dust is allowed to nucleate ice through immersion freezing, following either Ickes et al. (2017) or Niemand et al. (2012) as opposed to Lohmann and Diehl (2006) in the default model set-up. No other type of heterogeneous ice nucleation is considered. Ice multiplication is also not represented in the current model version, as a previous study has found ECHAM6-HAM2 to be insensitive to inclusion of the Hallett–Mossop process following Levkov et al. (1992) (David Neubauer, personal communication, 2017). The relative importance of the various sources of cloud ice crystals in mixed-phase clouds, however, remains an unconstrained property and can thus vary between models.

In the current study, MOA is implemented as an additional species in the internally mixed accumulation and coarse modes, as shown in Table 3.1 which lists the species present in each of the seven aerosol modes. Aitken-mode MOA is not considered as our model does not consider sea spray production in that size mode. MOA is allowed to nucleate ice through immersion freezing, as described in the following section.

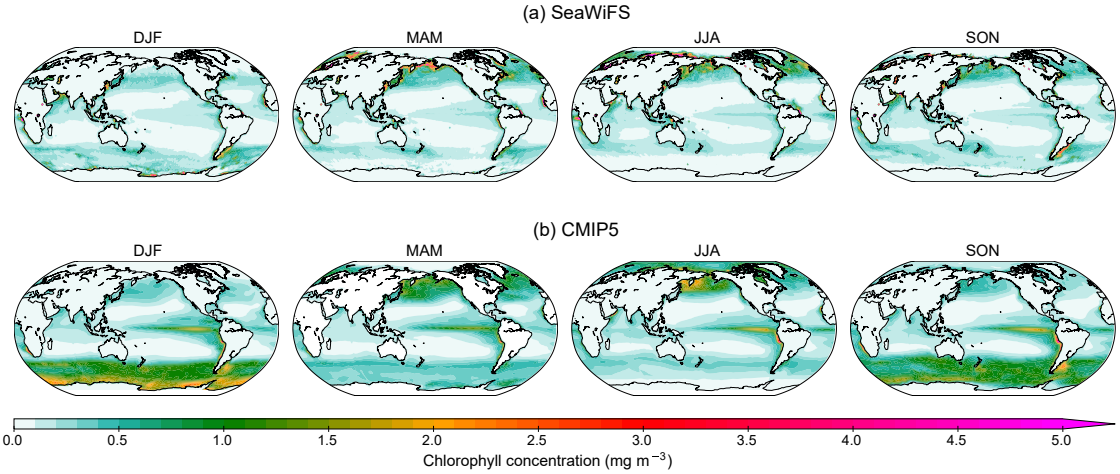

Figure 3.1: Maps of seasonal mean chlorophyll concentrations used as input files for the nudged simulations. The top row shows maps from the SeaWiFS satellite observational dataset from March 2003 to May 2009, and the bottom row shows the mean from CMIP5 historical simulations for the years 2000–2005.

3.2.2 MOA implementation

3.2.2.1 Emission of MOA

MOA emission is calculated online and depends on the SS emission, such that the total sea spray emitted is the sum of the two (i.e. sea spray is the combination of SS and MOA), with the organic mass fraction (OMF) defined as $\mathrm{OMF} = \frac{\mathrm{MOA}}{\text{total sea spray}} = \frac{\mathrm{MOA}}{\mathrm{MOA+SS}}$. SS is emitted following Long et al. (2011) and remains independent of the MOA emission for all cases except where specified. MOA is then emitted additionally as

$$\mathrm{MOA}_{\text{mass flux}} = \frac{\mathrm{SS}_{\text{mass flux}} \times \mathrm{OMF}}{1 - \mathrm{OMF}}. \tag{3.1}$$

The only exception is when MOA is emitted following Long et al. (2011), in which case the SS emission is reduced due to partitioning of some of the emitted mass into MOA. The density of MOA is set to be $1000\,\mathrm{kg\,m^{-3}}$ (Vignati et al., 2010), with radiative properties identical to those of organic carbon and a hygroscopicity parameter κ of zero. Due to

the lack of measurement data, the latter two properties are chosen for simplicity and, for the last case, consistency with other potential INP candidates such as dust particles. While sensitivity to the chosen radiative properties of MOA has yet to be investigated, a previous study by Gantt et al. (2012) has not shown a strong dependence of the results on the chosen hygroscopicity parameter.

No additional number flux due to MOA is considered, as we assume it to be always internally mixed with SS during emission. This is treated differently in different studies, with most emitting MOA as an internal mixture with SS (e.g. Long et al., 2011; Vergara-Temprado et al., 2017) while studies by Meskhidze et al. (2011) and Gantt et al. (2012) have noted a stronger impact of MOA on the modelled CDNC when they are assumed to be externally mixed during emission (that is, with an additional number flux but still emitted into internally mixed modes). Unfortunately, no measurement data are available to quantify such potential externally mixed number flux nor the division between internally and externally mixed emissions. Should some of the MOA be emitted separately from SS, they would be part of the externally mixed/insoluble mode in our model. However, as we are interested in the immersion freezing property of MOA, which requires immersion of the aerosol in a cloud droplet that can only occur for soluble/internally mixed particles, for simplicity, we emit all of the MOA into the internally mixed mode directly in order to give an upper estimate of the potential impact of MOA as INP.

Various OMF parameterisations are available in the literature (e.g. Vignati et al., 2010; Gantt et al., 2011; Rinaldi et al., 2013; Burrows et al., 2014; Vergara-Temprado et al., 2017), which produce a wide range of MOA fluxes when applied to the global scale, as was also shown in Meskhidze et al. (2011) and Lapina et al. (2011). A measure of marine biological activity is often used in these parameterisations, while some also consider a negative dependence on the near-surface wind speed based on the argument of oceanic mixing leading to a reduction in surface organic enrichment. The performance of each parameterisation is thus also highly dependent on the model wind speeds and choice of representation of the marine biological activity, in addition to the model's SS emission.

In this study, only ocean surface chlorophyll is used to represent the marine biological activity. Despite ongoing debate on the validity of chlorophyll as a proxy for the organic fraction in emitted sea spray, it has been shown that there is currently no better alternative for global coverage and available data (Rinaldi et al., 2013; O'Dowd et al., 2015). Instead, we address the dependence on ocean biological activity data by using two different sources of chlorophyll datasets. In most simulations, multi-year monthly mean level 3 observational data from the Sea-viewing Wide Field-of-view Sensor (SeaWiFS; Hu et al., 2012) were fed into the model. Free simulations, as will be described later in Sect. 3.2.3, use the full 12 years of available observational data from 1998 to 2010, while for the nudged simulations, a subset corresponding to the nudged period from March 2003 to May 2009 is used. The two choices of averaging time periods result in only very slight, localised differences in the chlorophyll concentrations (not shown). Such satellite-based observations, however, have a limited coverage in the polar regions in the winter hemisphere that can create a data void as far equatorward as 50° (though in the less biologically active winter hemisphere). Also, in light of the possibility to accommodate pre-industrial and future simulations, a sensitivity study is performed using chlorophyll concentration data from the CMIP5 multi-model ensemble outputs (Taylor et al., 2012). Monthly mean chlorophyll maps were created using results from the last 6 years (2000–2005) of the Earth system model (ESM) historical simulations, from which only eight models contain chlorophyll data, as listed in Table 3.5 in the Appendix. A comparison of the two sets of maps is shown in Fig. 3.1. Notable deviations of the modelled data from observational means include the lack of peak values near coastlines, which could be due to unresolved coastal processes, coarse model

resolution, and averaging across models and/or errors in observations near coastlines; a more widespread coverage of medium concentrations in the high-latitude regions of the spring–summer hemisphere, especially over the Southern Ocean; and persistent local peak concentration in the equatorial upwelling region off the west coast of South America. The impact of such differences is discussed in the results.

Offline calculations were performed to compare the various OMF parameterisations when applied to our model to long-term observations at Amsterdam Island in the southern Indian Ocean (Sciare et al., 2009) and Mace Head in Ireland (Rinaldi et al., 2013), as described in Appendix 3.A. The Rinaldi et al. (2013) parameterisation, which has a maximum OMF set to 78 %, was found to outperform others at both stations when applied to our model. Thus, despite the circular logic of the parameterisation having been derived by using the exact same Mace Head data which we used for validation, the Rinaldi et al. (2013) parameterisation is chosen for our control set-up. This does not, however, guarantee the most realistic emission rate when applied at the global scale. More long-term measurements from different parts of the globe would be required for a better validation of the model simulations.

MOA is emitted into the internally mixed accumulation mode and allowed to grow through coagulation and condensation of sulphate into the coarse mode. This is consistent with the Rinaldi et al. (2013) OMF parameterisation, which is based on observations of submicron emissions. Previous studies have noted a difference in the organic fraction of accumulation- and coarse-mode sea spray, with a higher fraction in the smaller size mode (Facchini et al., 2008). Thus, it would not be appropriate to extrapolate the emission parameterisation to coarse-mode particles, and emission of MOA in the coarse mode is not considered in our simulations.

3.2.2.2 Heterogeneous ice nucleation of MOA

Quantification of the ice nucleation ability of MOA is still a topic of active research. Currently, only one published parameterisation is available in the literature, namely that of MOA immersion freezing from Wilson et al. (2015). This is an empirical fit to droplet freezing measurements performed using samples collected from the marine microlayer, which gives a purely temperature-dependent parameterisation for the number of INPs per mass of total organic carbon. It should be noted, however, that this parameterisation is developed based on sea surface microlayer samples, which does not necessary reflect the concentration of INPs in the MOA that actually gets aerosolised and emitted into the atmosphere (McCluskey et al., 2017). To convert from the number of INPs per mass of total organic carbon to that per mass of total organic matter, division by a conversion factor of 1.9 is applied. This value lies at the lower end of the range of factors recommended by Turpin and Lim (2001) for non-urban cites, and is chosen since we are only considering water insoluble organics, which are associated with lower carbon-to-molecule conversion in their study. Subsequent publications which investigated airborne sea spray aerosol in the field and produced in laboratory settings (DeMott et al., 2016; McCluskey et al., 2017) have, however, indicated lower ice nucleation efficiencies than that described by Wilson et al. (2015). Therefore, a sensitivity study is also performed by producing a fit to data published in DeMott et al. (2016). Both parameterisations are extrapolated to cover the entire temperature range relevant for mixed-phase clouds (-35 to $0\,^{\circ}\mathrm{C}$ in ECHAM6-HAM2). The former is applied to accumulation- and coarse-mode MOA, while the latter, which is a fit representing the ice activity of the total sea spray, is applied to the sum of MOA and SS in the two size modes. For comparison, the parameterisations are plotted together with the n_{s}-based parameterisation of Niemand et al. (2012) for dust aerosol in

Fig. 3.2. Weaker ice activity of MOA compared to dust aerosol can be noted, but MOA could still be important in more remote regions where dust concentrations are low.

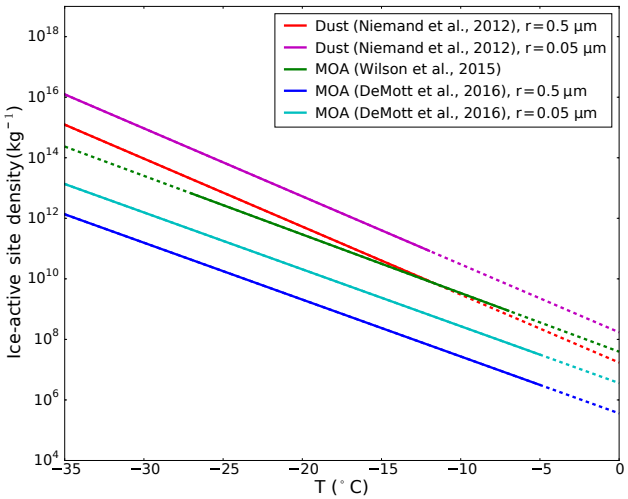

Figure 3.2: Ice-active site density per unit mass (n_{m}) of the Wilson et al. (2015) parameterisation and of the fit to the DeMott et al. (2016) data, for marine aerosol, as well as the Niemand et al. (2012) parameterisation for dust aerosol. The Wilson et al. (2015) parameterisation is converted from INP number per total organic carbon mass to INP number per MOA mass by dividing by the conversion factor of 1.9. The DeMott et al. (2016) fit and Niemand et al. (2012) parameterisation are converted from the original representation of ice-active site density per unit surface area (n_{s}) by division by their respective density and multiplication by the spherical surface-to-volume ratio using the two extremes in accumulation-mode median radius in our model. The inverse dependence of the ratio on the radius induces higher ice activity of the smaller particle when converting from n_{s} to n_{m}. Solid lines represent the range in which the parameterisations are valid, and dotted lines represent temperature ranges where the parameterisations are linearly extrapolated.

The surface active site density (n_{s}) approach described in Connolly et al. (2009) is extended to consider active site density per mass (n_{m}) and applied to calculate a frozen fraction (FF) given the mean particle mass (m_{MOA}) and temperature. This is then multiplied by the number concentration of MOA immersed in cloud droplets ($N_{\mathrm{MOA,imm}}$), such that the number of drops frozen per time step (N_{frozen}) is

$$\begin{aligned} N_{\mathrm{frozen}} &= N_{\mathrm{MOA,imm}} \times \mathrm{FF} \\ &= N_{\mathrm{MOA,imm}} \times \left[1 - \exp\left(-m_{\mathrm{MOA}} \times n_{\mathrm{m,MOA}}\right)\right]. \end{aligned} \tag{3.2}$$

$N_{\mathrm{MOA,imm}}$ is defined as

$$N_{\mathrm{MOA,imm}} = N_{\mathrm{TOT,act}} \times \left(\frac{V_{\mathrm{MOA}}}{V_{\mathrm{TOT}}}\right)^{2/3}, \tag{3.3}$$

following Hoose et al. (2008), where V_{MOA} is the total volume of MOA in the mode calculated by dividing the mass by the density, and V_{TOT} is the summed volume of all species in the internally mixed mode. $\left(\frac{V_{\mathrm{MOA}}}{V_{\mathrm{TOT}}}\right)^{2/3}$ is therefore a surface area fraction which considers that although the species are internally mixed in the mode, not every particle will contain MOA. A surface area fraction is used as this is the relevant property for

ice nucleation. $N_{\mathrm{TOT,act}}$ is the number of aerosol particles in the internally mixed mode that can be activated to cloud droplets under current conditions, as calculated following Abdul-Razzak and Ghan (2000). This is equal to the actual CDNC only if the cloud cover or liquid water content in the grid box increased from the last time step, and only if the newly activated number is greater than the previous CDNC (Lohmann et al., 2007).

Table 3.2: List of nudged simulations. In bold are fields which are changed from the control (ctl) set-up. Fields marked with dashes (–) are not relevant for the set-up. "CMIP5chl" uses the chlorophyll concentration from CMIP5 models; "GuelleSS" replaces the SS emission parameterisation by Guelle et al. (2001); "LongMOA" replaces the Rinaldi et al. (2013) MOA emission by Long et al. (2011); for "2xctlMOA", the control MOA emission is scaled up by two times; and lastly, MOA is not emitted in the "noMOAndg" simulation.

Name	MOA emission	Chlorophyll	SS emission
ctl	Rinaldi et al. (2013)	SeaWiFS	Long et al. (2011); Sofiev et al. (2011)
CMIP5chl	Rinaldi et al. (2013)	**CMIP5 mean**	Long et al. (2011); Sofiev et al. (2011)
GuelleSS	Rinaldi et al. (2013)	SeaWiFS	**Guelle et al. (2001)**
LongMOA	**Long et al. (2011)**	SeaWiFS	Long et al. (2011); Sofiev et al. (2011)
2xctlMOA	**Rinaldi et al. (2013) × 2**	SeaWiFS	Long et al. (2011); Sofiev et al. (2011)
noMOAndg	–	–	Long et al. (2011); Sofiev et al. (2011)

Further pertaining to Eq. (3.2), the mean mass of MOA in the size mode (m_{MOA}) is obtained by dividing the total mass of MOA in the mode by the total number scaled by the surface area fraction as defined above, and $n_{\mathrm{m,MOA}}$ is the temperature-dependent number of active sites per mass, calculated using the Wilson et al. (2015) parameterisation. A slight modification is required for the fit to data from DeMott et al. (2016), which expresses the number of active sites per surface area of total sea spray instead of per mass of MOA. The surface area fraction therefore becomes $\left(\frac{V_{\mathrm{MOA}}+V_{\mathrm{SS}}}{V_{\mathrm{TOT}}}\right)^{2/3}$, and the mean surface area of sea spray per particle is defined as

$$s_{\mathrm{mean}} = 4\pi\overline{r}^2 \exp\left(2\ln^2\sigma\right)\left(\frac{V_{\mathrm{MOA}}+V_{\mathrm{SS}}}{V_{\mathrm{TOT}}}\right)^{2/3}, \tag{3.4}$$

where $\overline{r}$ is the median radius of all particles in the mode and σ is the standard deviation of the lognormal distribution, which is a size-mode-dependent constant. The s_{mean} is then multiplied by n_{s} in the calculation for FF.

One problem with the above method of determining heterogeneous ice nucleation is that, in ECHAM6-HAM2, aerosol particles are not removed due to activation. Rather, in-cloud wet removal only occurs due to precipitation in the form of rain or snow. This leads to possible repeat freezing of the same aerosol across time steps. Indeed, the active site density approach of Connolly et al. (2009) represents the integrated number of ice crystals that can be frozen when the temperature drops from 0 °C to the current temperature, which would overestimate freezing if the full range of the temperature drop from 0 °C is assumed at each time step. One method to address this is to subtract the ice crystal number concentration (ICNC) from the previous time step from the newly nucleated number, such that only when the latter is greater than the former, does ICNC change due to heterogeneous freezing. This method has the drawback that it assumes that all ice crystals

in the mixed-phase temperature range are produced through heterogeneous nucleation. In fact, the largest contributor to mixed-phase ICNC in our model has been found to be sedimentation from cirrus clouds, which can lead to suppression of contributions from heterogenous freezing (Ickes et al., 2018). Thus, in the case that the above method does not lead to an increase in ICNC, a second method is applied where n_{frozen} calculated using the previous time step's temperature is subtracted from that calculated using the current temperature, such that new ice crystals are produced if the temperature decreased since the last time step. This second method, in turn, does not consider transport of aerosol or changes in moisture between time steps and does not have a memory beyond the previous time step. A combination of both methods is therefore applied to achieve a best estimate of the immersion freezing rate.

Table 3.3: List of 10-year free-running simulations. Fields marked with dashes (–) are not relevant for the set-up. "MOA" refers to the control free-running simulation where the Rinaldi et al. (2013) MOA emission is scaled up by two times; "MOADeMott" refers to a simulation where immersion freezing by MOA is replaced by the fit to the DeMott et al. (2016) data for total sea spray; "noMOAfrz" refers to a simulation where MOA is emitted but not acting as INP; "MOADUns" is the same as "MOA" but with the dust freezing parameterisation replaced by the n_{s} scheme following Niemand et al. (2012); "noMOAfrzDUns" is the same as "noMOAfrz" except with a different dust freezing parameterisation; and lastly, "noMOA" is a free-running simulation where MOA is not emitted. CNT indicates classical nucleation theory.

Name	MOA emission	MOA ice nucleation	Dust ice nucleation
MOA	Rinaldi et al. (2013) $\times 2$	Wilson et al. (2015)	CNT (Ickes et al., 2017)
MOADeMott	Rinaldi et al. (2013) $\times 2$	Based on DeMott et al. (2016)	CNT (Ickes et al., 2017)
noMOAfrz	Rinaldi et al. (2013) $\times 2$	–	CNT (Ickes et al., 2017)
MOADUns	Rinaldi et al. (2013) $\times 2$	Wilson et al. (2015)	n_{s} (Niemand et al., 2012)
noMOAfrzDUns	Rinaldi et al. (2013) $\times 2$	–	n_{s} (Niemand et al., 2012)
noMOA	–	–	CNT (Ickes et al., 2017)

3.2.3 Simulations

Summarised in Table 3.2 is a range of sensitivity runs nudged to the same meteorology from March 2002 to May 2009 in order to investigate the impact of different set-ups on the MOA distribution while minimising influences from internal variability. The nudging period is chosen to correspond to the maximum period covered by the MOA concentration measurements performed at the two observational sites, described in Sect. 3.2.4. As mentioned previously, sensitivity to the chlorophyll concentration is investigated by replacing the SeaWiFS observations with the CMIP5 model mean outputs, while sensitivity to the SS emission is studied by using two different parameterisation schemes. Aside from the default set-up, the Guelle et al. (2001) parameterisation, which was the default SS emission set-up in a previous version of ECHAM6-HAM2 and has a much higher emission rate, is also tested.

In most simulations, the Rinaldi et al. (2013) parameterisation for OMF is used, for it was found to fit best to observations when calculated offline using ECHAM6-HAM2

outputs as mentioned in Sect. 3.2.2.1 and shown in the Appendix. This type of offline calculations, however, does not allow for proper consideration of particle size dependence, which is included in various size-resolved parameterisation schemes (e.g. Gantt et al., 2011; Long et al., 2011). Thus, an additional sensitivity study is performed by using the size-resolved MOA emission parameterisation from Long et al. (2011), which also provides a consistent emission scheme for both SS particles and MOA. In the control set-up and the simulations with the same SS emission scheme, the total sea spray according to the Long et al. (2011) parameterisation, which includes both SS and organic matter, is emitted as SS. MOA mass is then emitted additionally and separately while the SS emission is kept untouched. To be consistent with the original intention of the parameterisation, when both MOA and SS are emitted following Long et al. (2011), the total sea spray is divided between SS and MOA components. This therefore leads to decreases in the SS emission rates when compared to the control simulation.

Lastly, an additional simulation is performed where the MOA emission following Rinaldi et al. (2013) is doubled, and another one where MOA is not emitted at all. The rationale behind these simulations will be shown and discussed in Sect. 3.3.2 and 3.3.4.3.

Following the nudged runs, six free-running sensitivity simulations are performed as listed in Table 3.3. The MOA emission set-up follows the "2xctlMOA" simulation, and is chosen based on the nudged run which best compares to observations, as discussed in Sect. 3.3.2. Each set-up is run for 10 years (plus 3 months of spin up) with fixed year-to-year external forcing, and a 10-year mean is used during analysis to account for internal variability. As the goal of these free simulations is to investigate the impact of ice nucleation by MOA and its climate feedback, focus is placed on the ice nucleation parameterisations.

MOA ice nucleation rates are studied by using the Wilson et al. (2015) parameterisation and a fit to data from DeMott et al. (2016), which has an ice-active surface site density that is around 2 orders of magnitude lower when converted to the same units. Two different immersion freezing parameterisations for dust, which is the only other heterogeneous freezing candidate in this study, are also tested. Control simulations are performed using a physically based classical nucleation theory (CNT) single-α parameterisation described in Ickes et al. (2017). Properties of montmorillonite as the ice nucleating dust type and an ice nucleation time integration of the first 10 s of each time step are chosen. Another set of simulations is done with the Niemand et al. (2012) ice-active surface site density (n_s)-based freezing parameterisation for Saharan dust, which provides a more straightforward comparison to the ice-active site density parameterisation of MOA. The n_s parameterisation is extrapolated over the whole mixed-phase temperature regime as is consistent with that of MOA.

Two simulations are done where MOA is emitted but not allowed to nucleate ice, each with a different dust freezing parameterisation (CNT vs. n_s), and finally one simulation is set up where MOA is not emitted in the model at all. Analyses of results from all of the above-mentioned simulations are discussed in Sect. 3.3.

3.2.4 Comparison to observations

Very limited long-term observations of MOA are available for validation of the model results. The two main sites with available data are Mace Head in Ireland and Amsterdam Island in the southern Indian Ocean. Measured water insoluble organic carbon (WIOC) concentrations from Mace Head spans the time period of 2002–2009 (Rinaldi et al., 2013), while that from Amsterdam Island covers the years 2003–2007 (Sciare et al., 2009). For comparison with observations, model simulations nudged towards the meteorology of the

Table 3.4: Annual global mean MOA and SS emissions and burdens from nudged simulations. The ratio of MOA to SS emission rates (MOA / SS emission) is a global area-weighted average of the ratio calculated at individual grid boxes. Note that MOA is only emitted in the accumulation mode, while SS is emitted in both accumulation and coarse modes. In the "2xctlMOA" and "CMIP5chl" simulations, slightly different MOA emission properties are considered as explained in Table 3.2; for "GuelleSS", a different SS emission is used; and lastly for "LongMOA", changes are present in both the MOA and SS emissions when compared to the "ctl" run.

Name	MOA emission ($Tg\ y^{-1}$)	MOA burden (Mg)	SS emission ($Tg\ y^{-1}$)	SS burden (Mg)	MOA/SS emission (%)
ctl	9	67	1005	4135	1.6
2xctlMOA	16	132	956	4142	3.2
CMIP5chl	19	119	1004	4136	3.2
GuelleSS	11	63	5741	10 556	0.3
LongMOA	11	62	1114	4189	1.0

respective measurement periods are used. The measured WIOC concentration is converted to WIOM (i.e. MOA) by multiplying by 1.9 as discussed in Sect. 3.2.2.2. Due to the limited spatial coverage of satellite-observed chlorophyll concentrations over single months, multi-year monthly mean chlorophyll measurements from SeaWiFS over the time period from March 2002 to May 2009 are used repeatedly for all simulation years. Should the dependence of MOA emissions on chlorophyll concentrations be strong in reality and the chlorophyll concentrations be highly variable from year to year, this will cause biases and inconsistencies in the modelled concentrations when compared to observations. Results from the comparisons are shown in Sect. 3.3.2.

3.3 Results

3.3.1 Distribution of MOA concentrations

A summary of MOA and SS annual emissions and global burdens from the various simulations is shown in Table 3.4. A dependence on both the choice of chlorophyll concentration data and the SS emission scheme can be observed, as expected. Notably, a rough doubling of the MOA burden resulted from the doubling of the Rinaldi et al. (2013) MOA flux, indicating a linear dependence of MOA burden on the emission rate. The same cannot be said, however, when the emission parameterisations are changed (for instance, when comparing the "ctl" simulation with "GuelleSS"), which resulted in changes in the spatial distribution of emitted MOA and thus diverging changes in emission and burden.

All emission rates are roughly in line with other quotes in the literature, which consider varying degrees of size resolution (e.g. Langmann et al., 2008; Spracklen et al., 2008; Long et al., 2011) and span a wide range of around 5 to $55\,Tg\,y^{-1}$ of organic matter. While studies that emit MOA in all size modes and consider both primary and secondary sources can obtain MOA fluxes of over $140\,Tg\,y^{-1}$ (Roelofs, 2008), most studies quote emission rates of less than $20\,Tg\,y^{-1}$, especially in the submicron size mode (e.g. Vignati et al., 2010; Lapina et al., 2011; Gantt et al., 2011). On the global annual average, the mass emission of submicron primary MOA is less than 3.2 % of the SS mass emission in all our simulation set-ups.

Annual mean global emission distributions and zonal mean cross sections of the mass concentration are shown in Fig. 3.3. Using the Rinaldi et al. (2013) parameterisation

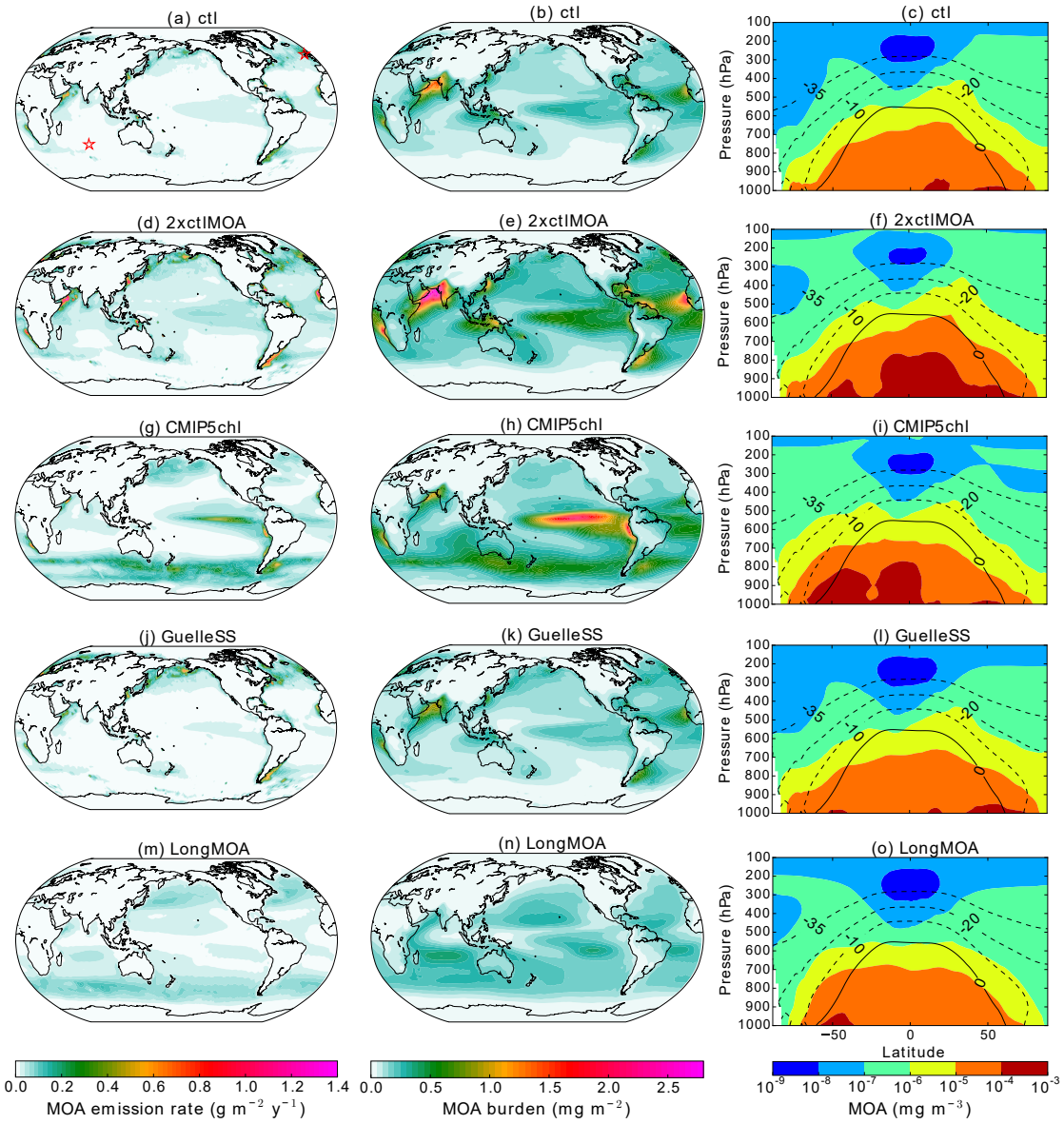

Figure 3.3: Multi-annual mean emissions **(a, d, g, j, m)**, burdens **(b, e, h, k, n)**, and zonal mean cross sections **(c, f, i, l, o)** of MOA from the various nudged simulations described in Table 3.2 for the period from March 2002 to May 2009. Contour lines in the zonal mean plots are zonal mean isotherms in °C in the mixed-phase temperature range. Red stars in panel **(a)** indicate locations of Mace Head in the Northern Hemisphere and Amsterdam Island in the Southern Hemisphere, where long-term observations of MOA are available.

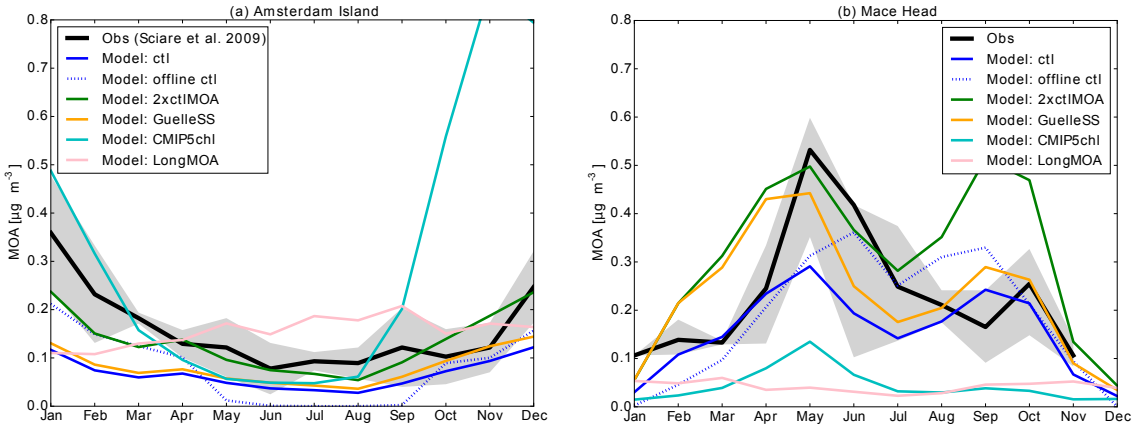

Figure 3.4: Monthly mean observed MOA concentrations at Amsterdam Island **(a)** and Mace Head **(b)** compared to model simulated outputs as described in Table 3.2. The dotted blue curve ("offline ctl") corresponds to an offline calculation of MOA concentration based on the same parameterisation as the control case. The shaded area corresponds to ±1 standard deviation of the observed mean for the Amsterdam Island case, while for Mace Head, it corresponds to the 25th to 75th percentiles. In both cases, the bold black line is the observational monthly mean. Note that no measurements are available for Mace Head in December. Model outputs are averaged over the entire nudging period (March 2002 to May 2009) for comparisons to observations at Mace Head, and averaged over the period of May 2003 to November 2007 for Amsterdam Island, corresponding to the measurement periods.

(all but "LongMOA"), the spatial pattern of MOA emission largely follows that of the chlorophyll concentration. For the simulations using SeaWiFS chlorophyll maps (all but "CMIP5chl"), MOA emissions peak in coastal and equatorial upwelling regions. Due to higher surface wind speeds, a lower emission rate is found in mid-to-high-latitude open ocean regions despite having chlorophyll concentrations comparable to the tropics. Notably, and contrary to expectations based on previous literature (e.g. Burrows et al., 2013; Yun and Penner, 2013; Vergara-Temprado et al., 2017), we do not obtain a high concentration of MOA in the Southern Ocean with the Rinaldi et al. (2013) emission, likely also due to the higher wind speeds and moderate chlorophyll concentrations (when using SeaWiFS maps) in these regions. When using CMIP5 mean chlorophyll concentrations, emissions from coastal upwelling regions are reduced, while those from the equatorial upwelling become more pronounced. Much higher MOA emission rates can also be found in mid-to-high-latitude open waters and the Southern Ocean (mainly occurring during the respective hemispheric summer months), as was observed in the chlorophyll concentrations (Fig. 3.1). An anomalously high emission rate of MOA off the coast of the Arabian Peninsula in boreal summer, observable even in the annual mean in all simulations, is mostly due to the southwest monsoon-associated ocean upwelling and particularly strong SS fluxes. The annual mean signal is weaker in the "LongMOA" simulation, which exhibits a weaker dependence on the wind speed and chlorophyll concentration. This leads to peak MOA emissions off the coast of the Arabian Peninsula only during boreal summer, while relatively high emission rates are also present during boreal autumn and winter in the other simulations, corresponding to the chlorophyll map. The secondary peak in ocean productivity during winter months is associated with deep water mixing caused by colder air blowing over the water surface during the northeast monsoon season (Mann and Lazier, 2005; Wiggert et al., 2000).

The annual mean MOA burden mostly mirrors the emission pattern, with notable accumulations over source regions that are subject to limited precipitation washout. The peak burden in the equatorial South Pacific found in all simulations, for instance, can be associated with the dry zone related to the South Pacific convergence zone that is largely caused by orographically induced subsidence (Takahashi and Battisti, 2007), as well as contributions from subsiding branches of the Hadley and Walker circulations. On the other hand, high emission rates in the northern North Pacific and North Atlantic oceans as well as along the Southern Ocean in the "LongMOA" simulation are not reflected in the annual mean burden, due to washout along the storm tracks.

In the zonal mean cross section, MOA mass is mainly concentrated in the lower altitudes below 700 hPa, and is in general not transported very high up into the atmosphere, as can be expected since MOA is mainly emitted from relatively calm waters. Despite this, non-negligible amounts of MOA still reach mixed-phase temperatures, especially in subpolar regions. All simulations produced similar patterns, with some having a more poleward extent of higher MOA concentrations than others, depending on the emission rates.

3.3.2 Comparison of MOA concentrations to the observed annual cycle

A comparison of the monthly mean MOA concentrations simulated using the various nudged set-ups listed in Table 3.2 to the observations at Amsterdam Island and Mace Head is shown in Fig. 3.4. Notably, the offline-calculated MOA concentration using the same set-up as the control simulation, which was used for choosing the OMF parameterisation as described in Sect. 3.2.2.1, is also plotted. It can be observed that even with the same parameterisation set-up, offline calculations yielded a stronger seasonal cycle than online calculations. Possible reasons for this deviation include errors in estimating the source regions (since the back trajectories are not explicitly computed using our model), seasonal variations in the aerosol source regions that are not considered in the offline calculations, and a lack of consideration for depletion and sedimentation during transport of MOA to the measurement site. As most MOA emission parameterisations are developed using similar offline methods, it may be worthwhile to note the possible deviation for future parameterisations. Due to the rather low bias of the control simulation, an additional simulation is set up where the control MOA emission using the Rinaldi et al. (2013) OMF parameterisation is increased by a factor of 2 (green curve in Fig. 3.4), and a better agreement to observations is obtained, despite a rather high bias at Mace Head in March and a low bias in January at Amsterdam Island. This increased emission is thus used as the standard set-up for all subsequent free-running simulations.

In examining other simulations with various SS or MOA emission set-ups, we found a general and consistent underestimation of MOA concentrations at both stations. One exception is the simulation using the Guelle et al. (2001) SS parameterisation, which produced reasonable MOA concentrations at Mace Head and hit the lower range of observations at Amsterdam Island except in the first 4 months of the year. The control simulation underestimated MOA concentrations at both stations. Simulation with MOA emitted following the size-resolved Long et al. (2011) parameterisation, on the other hand, was not able to reproduce the annual cycle of MOA concentrations well, despite yielding higher concentrations at Amsterdam Island. By replacing the SeaWiFS chlorophyll observations with CMIP5 mean modelled outputs, a significant underestimation of MOA concentrations resulted at Mace Head, while for Amsterdam Island, a relatively good fit to the observed annual cycle of MOA concentration is produced except for the months of October to December, where the CMIP5 models produced a widespread peak in chlorophyll concentrations in the Southern Ocean not observed by the satellite. This led to the

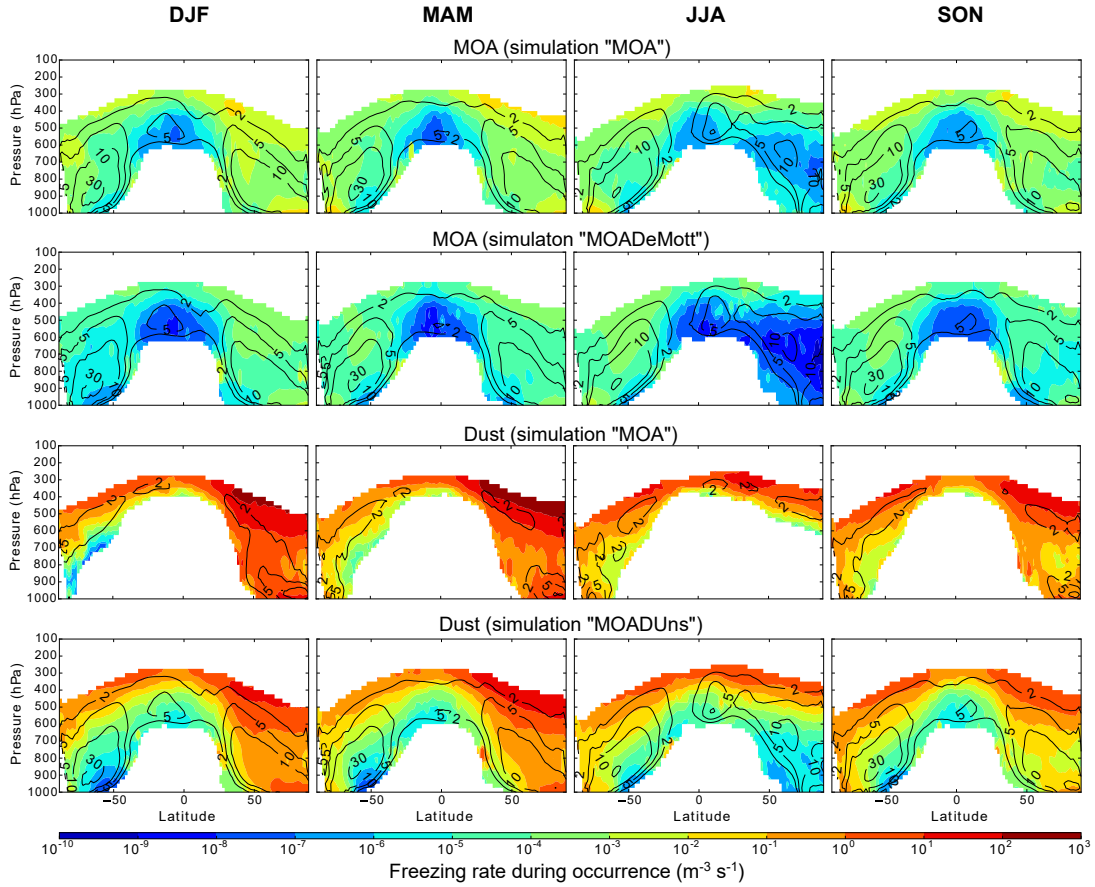

Figure 3.5: Seasonal and zonal mean freezing rates due to MOA and dust aerosol during freezing occurrence. Contour lines denote the frequency with which freezing occurs in %. All plots are averages from the 10-year free-running simulations. Only rates where the freezing occurs more often than 0.1 % of the time are plotted.

decision to not use the CMIP5 mean chlorophyll map for the longer-term simulations, and points to the need for more MOA measurement sites and improvements in the simulation of chlorophyll concentrations in ocean models, as well as a need for caution in future MOA-related model studies where modelled chlorophyll concentrations need to be used. Notably, however, the "CMIP5chl" simulation is the only simulation which is able to reproduce the strong peak in MOA concentrations during the austral summer months (DJF) at Amsterdam Island, which may point to an underestimation of the multi-year mean SeaWiFS chlorophyll concentrations in these months or to other missing marine organic sources not directly associated with chlorophyll.

3.3.3 Heterogeneous ice nucleation

Ice nucleation rates due to immersion freezing of MOA and dust aerosol and their respective frequencies of occurrence when applying the various parameterisations are shown in Fig. 3.5. One clear observation is the at least 3 order of magnitude difference between the peak freezing rates of dust aerosol and MOA. Aside from this, freezing occurs with the same frequency for all active site density schemes (contour lines in Fig. 3.5). Freezing calculated using this parameterisation approach occurs whenever the environmental condition is conductive for freezing at an ambient temperature between 0 and $-35\,^{\circ}\mathrm{C}$, the

relevant ice-active aerosol species is present in sufficient amounts (relative to the respective ice activity), and the considerations for refreezing as described in Sect. 3.2.2.2 are fulfilled. This indicates that, in most cases, MOA and dust aerosol are both present in sufficient amounts, and thus freezing occurs for both species if the environmental factors allow.

Such direct conclusions cannot be drawn from comparison with the CNT results, however. While the CNT-based dust freezing scheme produces a lower freezing occurrence frequency overall and especially in the warmer temperatures compared to MOA (Fig. 3.5), a similar difference in freezing occurrence frequency can also be noted between the results from the two dust freezing schemes, which points to the parameterisation as the main reason behind the difference. The sharp decrease in freezing occurrence at warmer temperatures following Ickes et al. (2017) when compared to the results using the Niemand et al. (2012) dust parameterisation indicates a faster decrease of the dust ice activity with increasing temperature for the former set-up, which is shown in Fig. 3.6. Indeed, the FF of 0.5 µm radius particles following Ickes et al. (2017) quickly drops below that following Niemand et al. (2012) at around −31 °C, and below that of MOA following Wilson et al. (2015) at around −29 °C. At −20 °C, even with the maximum monthly mean immersed dust concentration on the order of 100 cm^{-3}, only around 10 droplets per cubic kilometre of air will freeze. Without sufficiently large dust particles and/or sufficiently high number concentrations, the Ickes et al. (2017) CNT parameterisation will thus not lead to much ice nucleation occurrence in the warmer mixed-phase temperatures. Interestingly, a surface active site density approach for montmorillonite (consistent in dust type with the CNT parameterisation), which is also compared in Fig. 3.6, can be noted to have a less steep slope than the CNT approach, though still a faster decrease in FF than that from Niemand et al. (2012). As the Niemand et al. (2012) parameterisation considers a mixture of dust mineral types, this indicates that the difference in freezing rates between the Ickes et al. (2017) CNT parameterisation and the Niemand et al. (2012) parameterisation may be a consequence of both a difference in parameterisation method (CNT vs. n_s) and the considered dust type (montmorillonite vs. Saharan dust). A CNT-based parameterisation for MOA cannot be formulated, however, due to the lack of measurement data. It is therefore impossible to conclude how much of the difference in the frequency and regions of occurrence between freezing by MOA and CNT-parameterised dust is related to the different INP species and how much is simply due to differences in the parameterisation approach.

3.3.3.1 Immersion freezing by dust

Dust freezing rates following CNT (Ickes et al., 2017) and the surface active site density approach using the Niemand et al. (2012) parameterisation show consistent results in the spatial distribution and magnitude of peak values mainly in the colder mixed-phase temperature range. The Niemand et al. (2012) parameterisation, which is extrapolated for temperatures warmer than −12 °C, leads to more frequent freezing occurrence, especially notable at warmer temperatures, albeit with significantly lower freezing rates when compared to that in colder regions. This is associated with the differing slopes of the two parameterisations, as discussed in the previous section and shown in Fig. 3.6. When expressed as the onset freezing temperature, defined as the temperature at which a FF of 0.001 is reached, this translates to −21 °C for Niemand et al. (2012) and −28 °C for Ickes et al. (2017), assuming spherical aerosol of radius 0.5 µm.

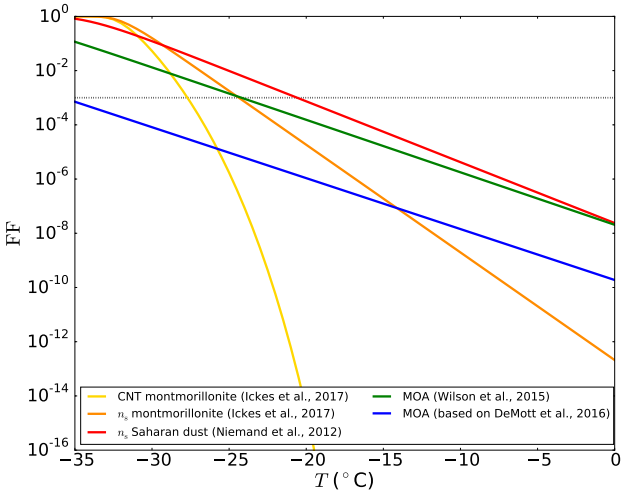

Figure 3.6: Frozen fraction (FF) vs. temperature (T) of the various parameterisations used for dust aerosol (montmorillonite and Saharan dust) and MOA in this study. Spherical aerosol of radius 0.5 µm and an ice nucleation time of 10 s for the CNT method are assumed. In addition to the parameterisations previously discussed in the text, an additional n_s-based parameterisation for montmorillonite is also plotted following Ickes et al. (2017). The dotted black line indicates the freezing onset (0.001 FF).

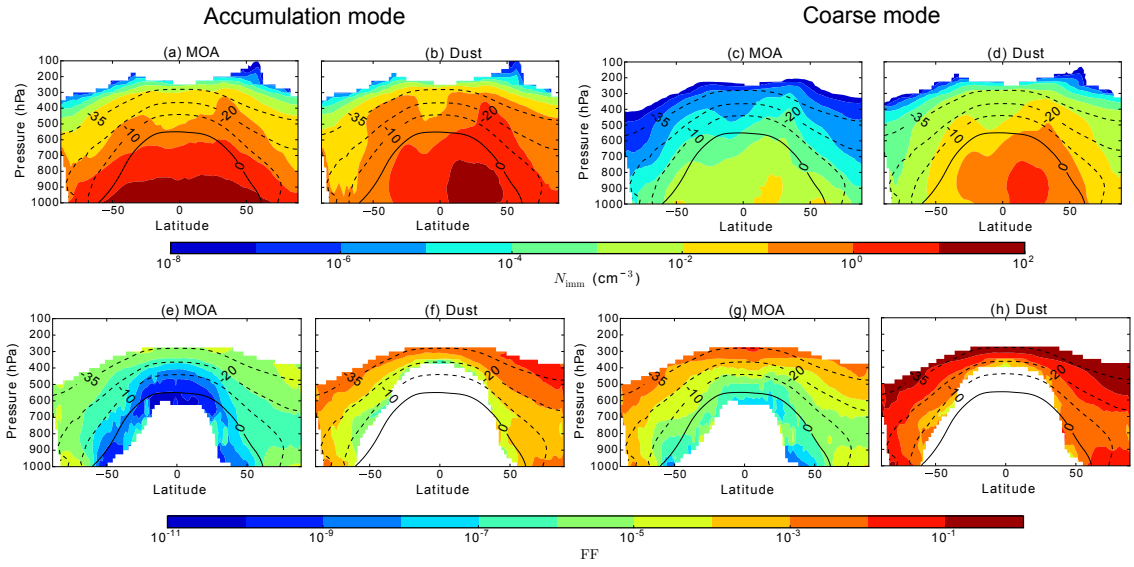

Figure 3.7: Multi-annual, zonal mean number of accumulation-mode **(a, b, e, f)** and coarse-mode **(c, d, g, h)** particles immersed in droplets (N_{imm}; **a**–**d**) and the frozen fraction (FF; **e**–**h**) for MOA (**a**, **e** and **c**, **g**) and dust aerosol (**b**, **f** and **d**, **h**), from the free "MOA" simulation with the Wilson et al. (2015) freezing parameterisation for MOA and CNT for dust. Contour lines denote isotherms in the mixed-phase temperature range. FF is only plotted where the freezing occurs more frequently than 0.1 % of the time.

3.3.3.2 Immersion freezing by MOA

The MOA freezing rate scales proportionally with the ice-active site density, with freezing rates increasing by around 2 orders of magnitude (depending on the aerosol size) when using the Wilson et al. (2015) parameterisation compared to the DeMott et al. (2016) parameterisation. The freezing onset temperatures of MOA for the same conditions as described above for dust are -36 and $-24\,^{\circ}\mathrm{C}$, respectively, for the parameterisation in the "MOADeMott" and "MOA" set-ups.

3.3.3.3 MOA vs. dust as INP

The immersion freezing rate, as described by Eq. (3.2), is calculated by multiplication of the number of aerosol particles available for freezing, which depends on the abundance and distribution of the aerosol as defined in Eq. (3.3), and the FF, which depends on the property of the aerosol (size- and temperature-dependent ice activity). A decomposition of these two components for MOA and dust is shown in Fig. 3.7. Here, it can be noted that the number concentrations of immersed MOA and dust aerosol span similar orders of magnitude in the accumulation mode, while in the coarse mode the abundance of dust aerosol can be up to 2 orders of magnitude larger. The FF, on the other hand, shows a more uniform 2–3 order of magnitude difference between dust aerosol and MOA regardless of the size mode. Thus, the temperature-dependent aerosol ice activity can be attributed as the main controlling factor behind the number concentration of nucleated ice crystals as compared to the availability of the particles. This can also be concluded by noting the small change in MOA freezing rates when different SS emission parameterisations or chlorophyll maps are used (not shown). Nonetheless, the larger amount of MOA near the surface can contribute to higher ice nucleation rates in polar near-surface regions despite the warmer temperature.

So far, only seasonal or annual mean freezing rates have been shown. However, monthly mean dust concentrations in the air could be dominated by episodic dust events which would mask potential contributions from MOA during periods of low dust concentrations. Thus, online diagnostics of the time frequency when the freezing rate of MOA is greater than that of the dust aerosol is performed for cloudy mixed-phase grids containing supercooled droplets and shown in Fig. 3.8. Different combinations of MOA and dust freezing parameterisations are investigated.

When comparing the diagnostic results with varying set-ups of freezing by MOA, no systematic differences are present. In particular, no noticeable change in the frequency of occurrence resulted from a 2 order of magnitude decrease in the MOA ice activity, as can be noted from comparison between the "MOA" and the "MOADeMott" simulations. This can be attributed to the similarities between the frequency of MOA freezing occurrence of the two simulations as shown in Fig. 3.5 (contours).

While the choice of MOA freezing parameterisation does not have a significant qualitative influence on the result of such diagnostics, that of the dust ice nucleation parameterisation plays a significant role. This is due to the much lower freezing frequency from the CNT-based approach, especially in warmer temperature regimes. When the Wilson et al. (2015) parameterisation for MOA is combined with the Ickes et al. (2017) CNT parameterisation for dust (simulation "MOA"), the contribution from MOA frequently dominates over that from dust aerosol over much of the warmer mixed-phase regions. When the Niemand et al. (2012) n_{s} parameterisation is applied for dust, however, MOA only becomes more important than dust in the warmest mixed-phase regions near the surface in polar regions and in the Southern Hemisphere low altitudes. This difference

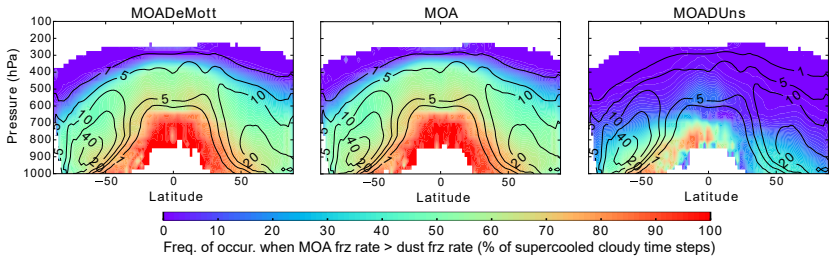

Figure 3.8: The annually and zonally averaged frequency of occurrence when the freezing contribution from MOA is greater than that from dust aerosol, diagnosed only for cloudy grid boxes containing supercooled droplets. Contour lines denote the frequency of occurrence (in %) of the above-mentioned favourable cloudy condition containing liquid droplets in the mixed-phase temperature range. All plots are from the respectively titled 10-year free-running simulations.

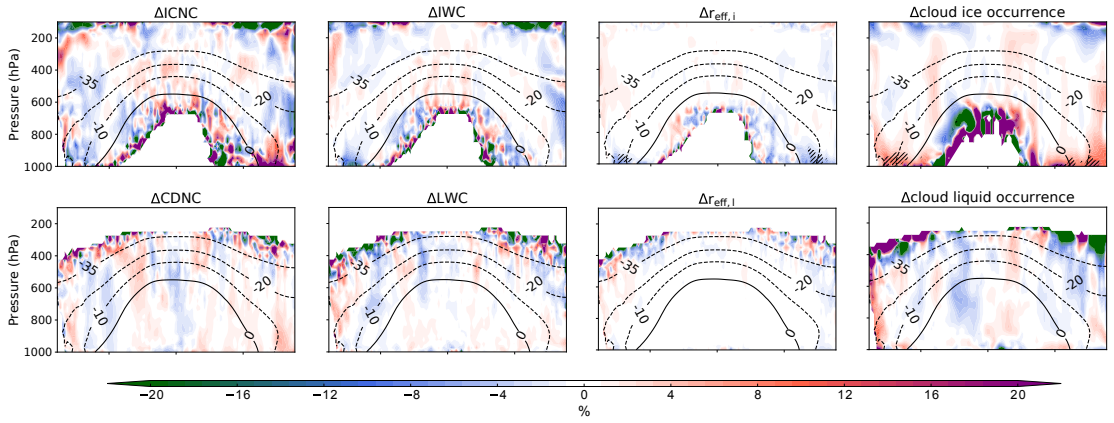

Figure 3.9: Annual and zonal mean relative change ("MOA" minus "noMOAfrz" divided by the mean of the two) in ice crystal number concentration (ICNC), ice water content (IWC), ice crystal effective radius ($r_{\mathrm{eff,i}}$), ice cloud occurrence frequency, cloud droplet number concentration (CDNC), liquid water content (LWC), cloud droplet effective radius ($r_{\mathrm{eff,l}}$), and liquid cloud occurrence frequency. All values are in-cloud changes (i.e. during liquid/ice cloud occurrence, respectively). Contour lines are zonal mean temperatures in the mixed-phase range in °C. Hatched areas indicate statistical significance at the 95 % level following the Wilks (2016) method for controlling the false discovery rate for data with moderate to strong spatial correlations.

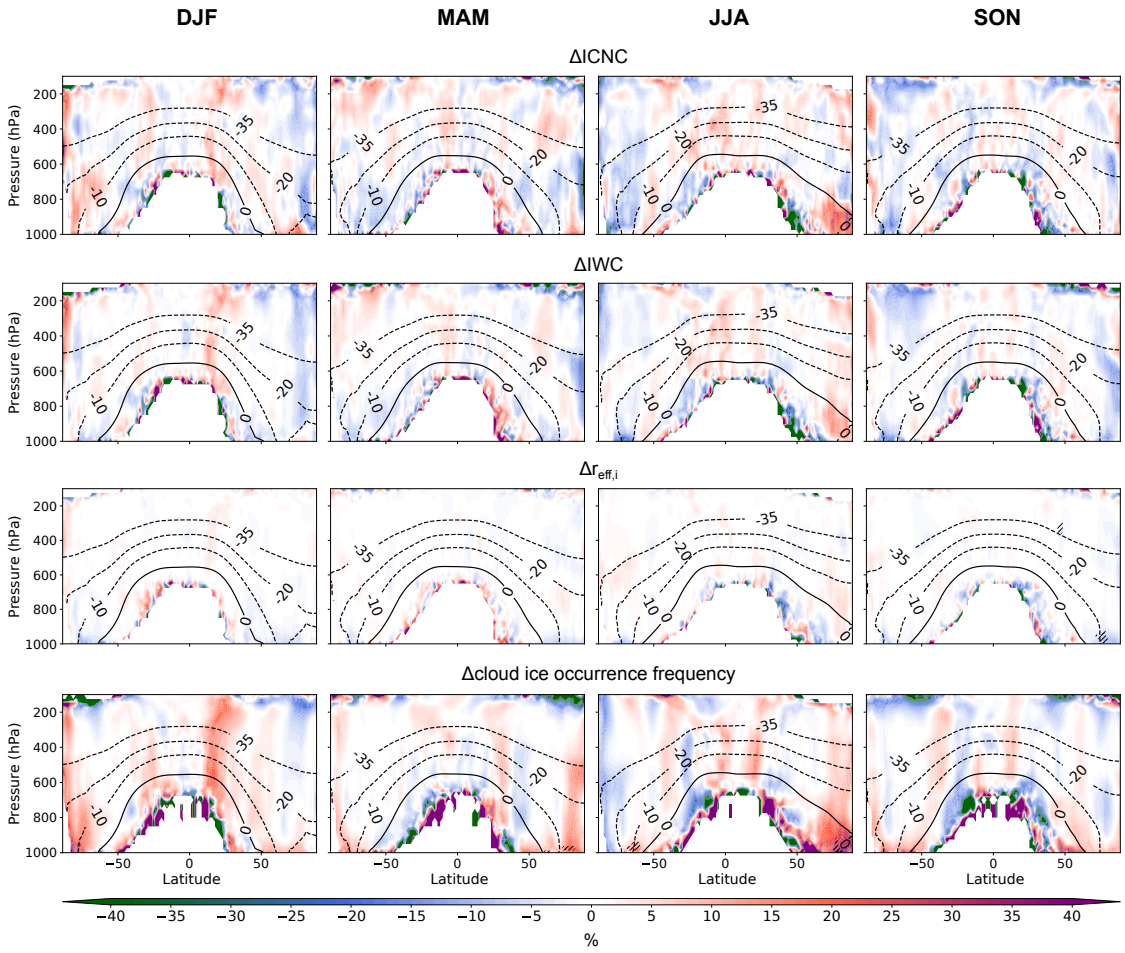

Figure 3.10: Same as in Fig. 3.9 but for seasonal mean changes in the cloud ice properties only.

can be attributed to the different slopes and dust freezing onset between the CNT and n_s parameterisations, as noted previously in Sect. 3.3.3.

Regardless of differences between different freezing parameterisation set-ups, MOA has been found to contribute to more freezing than dust during up to 20 to 70 % of the time in much of the mixed-phase cloud regions when using the Ickes et al. (2017) CNT dust scheme, and up to 60 % near the surface in the Southern Hemisphere when using the Niemand et al. (2012) dust scheme. This is largely comparable to the values found by Vergara-Temprado et al. (2017), who examined the percentage of days when the INP concentration at ambient temperatures from MOA is greater than that from K-feldspar. As their study also uses a n_s-based freezing parameterisation for dust, the most straightforward comparison would be with our "MOADUns" simulation, in which case slightly lower freezing contributions from MOA are found in our results. This is especially notable in the Northern Hemisphere and in higher altitudes in the Southern Hemisphere. Possible reasons for this include their choice of only considering freezing by a fraction of the dust (K-feldspar) instead of all dust aerosol in our case, which decreases the availability of dust particles in their study and leads to a more ready scavenging of the dust INP from the atmosphere due to the larger size of feldspar, as noted also by Vergara-Temprado et al. (2017). Additionally, the freezing parameterisations are not extrapolated to all mixed-phase temperatures in their study, and lastly, differences in emission, partitioning, removal, and transport of the

aerosol exist between models. It should be noted, however, that both the current work and the study by Vergara-Temprado et al. (2017) only consider MOA in combination with dust aerosol as the sole INP species. Should other INPs active at relatively warm temperatures be included (e.g. Vali et al., 1976), the relative importance of MOA may be dampened.

3.3.4 Impact on clouds and climate

3.3.4.1 Impact on clouds

INPs can impact clouds through freezing of supercooled liquid droplets and subsequent ice crystal growth at the expense of the remaining liquid drops, leading to glaciation of the cloud. The most direct impact of MOA as an INP would thus be expected in the cloud ice and liquid properties. This is shown in Fig. 3.9 as the annual mean in-cloud relative difference between one simulation where the expected impact of MOA acting as INP is greatest ("MOA") and the corresponding simulation where it is not allowed to initiate freezing ("noMOAfrz"). The most statistically significant changes in cloud properties are found near the surface in polar regions, with a decrease in the in-cloud zonal and annual mean ice crystal radius ($r_{\mathrm{eff,i}}$) by up to 3 to 9 % and an increase in the cloud ice occurrence frequency by 5 to 28 %.

To investigate the cause for the changes in $r_{\mathrm{eff,i}}$ and cloud ice occurrence frequency, seasonal mean changes in the cloud ice properties are shown in Fig. 3.10. Though mostly statistically insignificant following the strict Wilks (2016) criterion, strong relative increases in the cloud ice occurrence frequency, in-cloud ICNC, and to a lesser extent the in-cloud IWC can be observed in the polar regions especially during their respective summer months. A stronger signal can be noted in the Arctic during boreal summer, likely due to the higher temperatures in these regions leading to rare ice occurrences in general and thus stronger relative sensitivity to contributions by MOA.

The observed decrease in $r_{\mathrm{eff,i}}$, on the other hand, does not exhibit statistical significance on a seasonal scale (except in the Arctic during boreal autumn). Rather, a consistent but weak decrease in the ice crystal size can be observed near the surface over both polar regions for all seasons. A possible explanation is that since MOA initiates ice crystal formation at relatively warm mixed-phase temperatures closer to the surface, the newly formed ice crystals do not have enough time to grow further. This is particularly notable when compared to ice falling from higher levels, which is also more likely to reach lower levels if the crystal sizes are larger. The newly nucleated ice crystals therefore lead to a lower in-cloud ice crystal radius near the surface.

3.3.4.2 Impact on the TOA radiative balance

The change in the zonal mean top-of-atmosphere (TOA) radiative balance due to the emission and/or ice activity of MOA in the various free-running set-ups is shown in Fig. 3.11. When comparing our strongest MOA potential set-up ("MOA") to one where MOA is not emitted at all ("noMOA"), the TOA net solar radiation decreases by $0.16\,\mathrm{W\,m^{-2}}$ on the global mean with the added MOA, while the net outgoing terrestrial radiation decreases by $0.03\,\mathrm{W\,m^{-2}}$, leading to a decrease of $0.13\,\mathrm{W\,m^{-2}}$ in the net TOA radiation. When decomposing the contribution into that from the emission of MOA ("noMOAfrz"–"noMOA") and that from MOA acting as INP ("MOA"–"noMOAfrz"), neither process can be ruled out as a contributor to the change. This can include cooling at the surface due to the direct scattering effect of the emitted MOA and that due to the increased aerosol indirect effect on cloud radiative properties induced by MOA acting as INP, as well as further feedbacks triggered by the two processes.

In the shortwave (SW), a statistically significant decrease in the net TOA incoming radiation of around 0.3 W m^{-2} over Antarctica can be observed in association with the added MOA. Up to a 1.3 W m^{-2} decrease can also be noted in the Arctic region associated with the freezing of MOA. However, the pattern of change is mostly not consistent across the different set-ups. No consistent pattern north of 50° S can be observed in the changes due to MOA acting as INP when the dust ice nucleation parameterisation is changed from Ickes et al. (2017) to Niemand et al. (2012) (i.e. dark blue vs. light blue curves in Fig. 3.11). Similarly, differences in the MOA ice nucleation parameterisation (i.e. black vs. gray curves in Fig. 3.11) cause some non-statistically significant changes, especially in the Northern Hemisphere. This is indicative of internal variability of the system and feedback processes which are further examined in the next section.

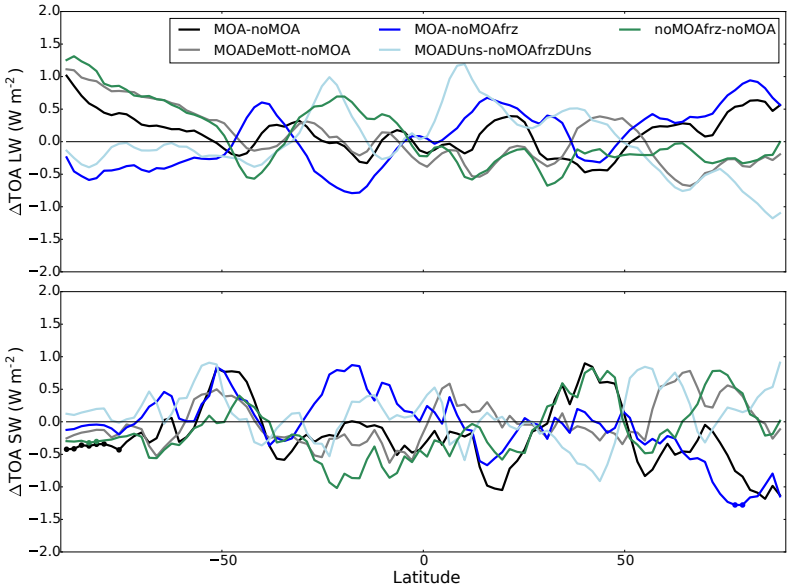

Figure 3.11: Zonal and multi-annual mean change in the top-of-atmosphere (TOA) solar (SW) and terrestrial (LW) radiative balance for the various free-running 10-year simulations. The black and gray curves indicate changes due to both the emission and ice nucleation of MOA, the blue-coloured curves correspond to changes stemming from MOA ice nucleation, and the green curve indicates changes due to the emission of MOA. It should be noted that the outgoing terrestrial radiation is defined to be negative, so a positive change is indicative of less outgoing radiation. Statistically significant changes at the 99 % level are marked with dots on the respective curves.

3.3.4.3 Impact on dynamics

The changes in the zonal mean aerosol and cloud properties together with the changes in TOA radiative balance due to the emission and ice activity of MOA in the "MOA" set-up are shown in Fig. 3.12a, d. In particular, the SW aerosol forcing mirrors rather well the increase in aerosol optical depth (AOD, global mean increase of 0.006) at the various latitudes, indicating an expected increase in scattering effect due to the added MOA. On the global mean, the TOA all-sky instantaneous aerosol forcing decreases by 0.069 and 0.008 W m^{-2} in the SW and LW, respectively, yielding a net decrease of 0.061 W m^{-2}. This does not, however, translate to changes in the TOA radiative balance, which is only significant in the shortwave radiation over the Southern Hemisphere high latitudes, as

discussed in Sect. 3.3.4.2. Rather, the latter signal may be due to internal variability and feedback processes.

To further investigate possible causes for the signal in radiative balance changes over Antarctica, the relevant simulations ("MOA" and "noMOA") are extended for an additional 10 years and the resulting changes shown in Fig. 3.12b, e. Notably, while the general pattern of the changes is preserved, the magnitude of the signal is largely diminished in nearly all properties, and no statistical significance remains in the changes in the TOA radiative balance. An exception is the increase in AOD over the Northern Hemisphere tropical latitudes and midlatitudes and the change in SW aerosol forcing, both of which show a stronger signal averaged over the 20-year simulation. Virtually no significance can be found, however, in any of the zonal mean cloud or environmental variables investigated. Therefore, we conclude that MOA emission and MOA acting as INPs do not have significant impacts on the global radiative balance and climate variables.

Lastly, to suppress feedback processes through dynamics, analyses of nudged simulations with otherwise the same set-ups ("2xctlMOA" and "noMOAndg") are performed where the vorticity and divergence of the flow fields are nudged toward the same meteorology for the two simulations. The changes in the climate and cloud properties are shown in Fig. 3.12c, f, where it can be noted that any changes in the examined properties are diminished and no significant impact of MOA on the modelled climate can be observed. The pattern of mirrored changes in the AOD and aerosol forcing is, however, consistent with other simulations.

3.4 Conclusions

In this study, a range of simulations is set up to investigate the emission and distribution of MOA on the global scale. Three different aspects that control the emission rate are tested, namely the SS emission parameterisation, the MOA emission parameterisation, and the chlorophyll map. A weaker dependence on the SS emission parameterisation is found compared to the choice of chlorophyll data and MOA emission parameterisation. In particular, the use of the CMIP5 mean modelled chlorophyll data to replace SeaWiFS observations leads to significant changes in the MOA spatial distributions. A cause for this is the systematic overestimation of total chlorophyll concentrations in the Southern Ocean that is common among global ocean models (Le Quéré et al., 2016). This should be taken into account for future simulations using modelled chlorophyll concentrations. The vertical distribution of MOA, however, is relatively similar between simulations, with the mass mostly concentrated in the lower levels.

Following previous studies proposing MOA as a potentially important INP (e.g. Burrows et al., 2013; Yun and Penner, 2013; Wilson et al., 2015; Vergara-Temprado et al., 2017), contributions of MOA to heterogeneous ice nucleation are investigated. When compared to dust aerosol, MOA is found to nucleate 3–4 orders of magnitude fewer ice crystals during freezing occurrence, depending on the choice of parameterisation, due to its weaker ice activity. When compared to the CNT-based dust parameterisation for montmorillonite (Ickes et al., 2017), however, MOA commonly contributes to more freezing of liquid droplets in 50 % of the cases in the mixed-phase temperature range. On the other hand, when applied together with the Niemand et al. (2012) parameterisation for dust aerosol, MOA only contributes to more heterogeneous ice nucleation than dust in the low-altitude regions. This occurs more often in the Southern Hemisphere, where the mass concentration of MOA is higher and where the dust concentration is lower due to the hemispheric dependence of dust emissions that favours the Northern Hemisphere. The difference between the comparisons to the two different dust parameterisations mainly stems

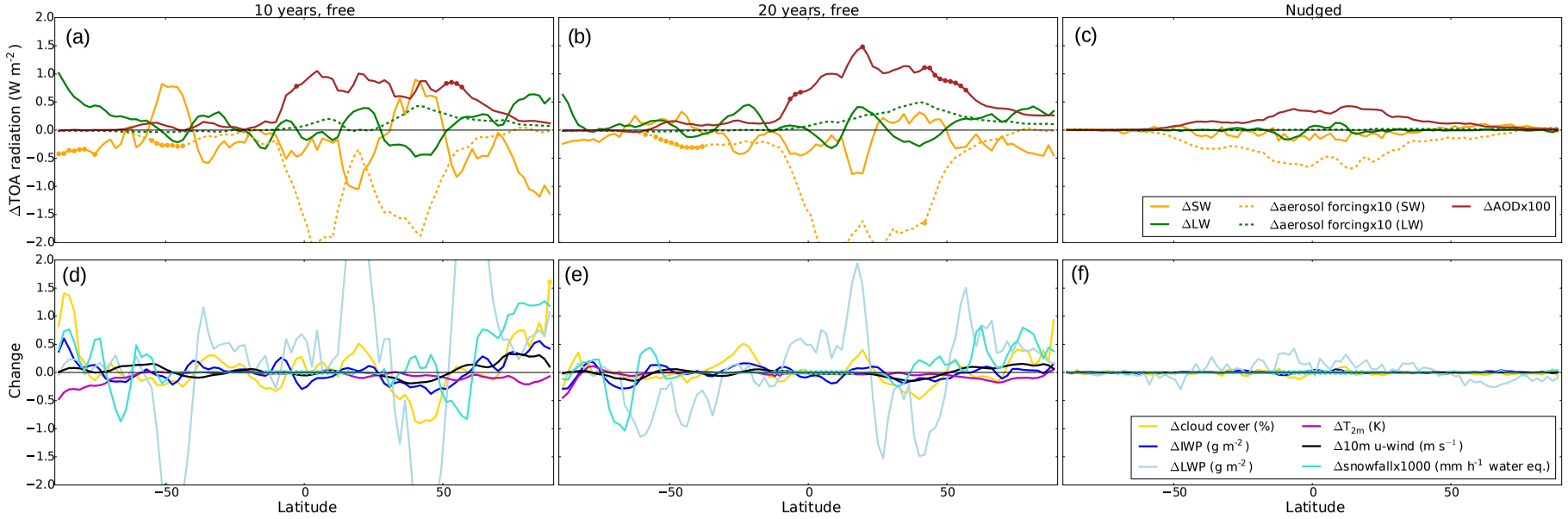

Figure 3.12: **(a–c)** Zonal, multi-year mean changes ("MOA"–"noMOA") in the top-of-atmosphere (TOA) solar (SW) and terrestrial (LW) radiation in all-sky conditions, the corresponding changes in aerosol forcing at the TOA scaled up by an order of magnitude, and the change in aerosol optical depth (AOD) at the 550 nm wavelength scaled up by 2 orders of magnitude to fit the same scale on the y axis. **(d–f)** Zonal, multi-year mean changes in cloud cover, ice water path (IWP), liquid water path (LWP), 2 m temperature ($T_{2\,m}$), 10 m zonal wind (10 m u wind), and water equivalent snowfall rate. Panels **(a)** and **(d)** are changes from the 10-year free-running simulations, **(b)** and **(e)** are changes from simulations identical to those on the left except they are extended for another 10 years, and **(c)** and **(f)** are from the nudged simulations. Small circles on the curves indicate statistical significance at the 99 % level.

from their differing rates of FF decrease with increasing temperature. When expressed in onset freezing temperature, this is 7 °C lower for the Ickes et al. (2017) CNT parameterisation compared to −21 °C for Niemand et al. (2012), assuming a spherical aerosol radius of 0.5 µm. The onset temperatures then further diverge with lower threshold FFs. The overall importance of MOA as an INP when compared to mineral dust is thus highly dependent on the choice of freezing parameterisations, for both MOA and dust. This points to the need for more measurement data to better constrain the parameterisations, especially at warmer temperatures. Additionally, as the current study disregards potential heterogeneous ice nucleation by other aerosol species aside from MOA and dust aerosol, the relative importance of MOA may be overestimated when compared to the case where other INPs are considered. This would be particularly relevant for INP species that have a high ice activity at warmer temperatures, where MOA is more ice active than dust aerosol in the current study, such as pollen and fungal spore (e.g. Dreischmeier et al., 2017; Fröhlich-Nowoisky et al., 2015). The global atmospheric relevance of the various species, however, can also depend on their abundance and various other factors (e.g. Hoose et al., 2010), and therefore their impact on the relative importance of MOA as an INP cannot be directly inferred.

Extending the analysis one step further, impacts of MOA on clouds and climate are also investigated in this study. In general, weak to no statistically significant changes in cloud and climate variables are found due to the addition of MOA and due to MOA acting as an INP. More specifically, a decrease in in-cloud $r_{\mathrm{eff,i}}$ by up to 3 to 9 % and an increase in cloud ice occurrence frequency by 5 to 28 % near the surface over both polar regions can be identified due to MOA initiating ice formation in the presence of supercooled droplets. In the climate variables, any statistically significant change is largely diminished when the simulations are extended to 20 years. This points to the possibility that a 10-year mean is not sufficient to rule out internal variability in high latitudes as the reason behind the observed signals, and has implications for future studies focusing on high-latitude regions where longer simulations may be advised. When dynamical feedbacks are suppressed through nudged simulations, the changes are further diminished. We therefore conclude that any potential impact of the emitted MOA or MOA acting as an INP on the model climate is masked by the internal variability of the model. This can be partly attributed to the weak sensitivity of our model to heterogeneous ice nucleation (due to the dominating contribution of cloud ice from sedimentation of ice crystals originating from cirrus levels; Ickes et al., 2018), as well as to the weak ice activity of MOA when compared to dust.

Appendix

3.A Offline comparison of OMF parameterisations

Offline calculated monthly mean MOA concentrations at the two observational sites are shown in Fig. 3.13 using various OMF parameterisations. Monthly mean modelled 10 m wind speeds and SS concentrations from a nudged simulation without MOA, averaged over the relevant period for each observational site (March 2002 to May 2009 for Mace Head and May 2003 to November 2007 for Amsterdam Island) are used in combination with the mean SeaWiFS observed chlorophyll concentrations from the longer period. Two emission source regions for the aerosol reaching the measurement site are considered for each observational site: one following the region noted in the cited literature with the observational data and the other approximated from Vergara-Temprado et al. (2017). The two differ slightly due to consideration of atmospheric-transport-based different observational and modelled

data, but both only serve as an approximation as the transport pattern in ECHAM6-HAM2 would again be different. OMFs are calculated offline for each source region using each OMF parameterisation and the chlorophyll concentrations and wind speeds from the corresponding region, as needed. Observed WIOC is converted to WIOM with a conversion factor of 1.9 as discussed in Sect. 3.2.2.2. As the OMF parameterisations are valid for the organic fraction during emission, the MOA concentration shortly after emission is approximated by taking the SS concentration in the lowest model level with the derived OMF, following Eq. (3.1). The MOA concentration for the measurement site is then taken as the average of the concentrations over the entire source region. A schematic of the source regions is shown in Fig. 3.14.

Notably, the calculated MOA concentration can vary by more than 0.1 µg m^{-3} with slight shifts in the chosen source region, as can be observed by comparing solid and dotted curves in Fig. 3.13. When both source regions are considered, the Rinaldi et al. (2013) parameterisation is chosen as the best fit to observations, though with a general slight underestimation. It should be noted, however, that the assessment for the wellness of fit to observations is highly model-dependent. Thus, while suitable for choosing an appropriate OMF parameterisation for this particular model, no generalisations should be drawn with regards to the individual parameterisations when applied to other models. Indeed, each of the OMF parameterisations has been separately validated in their respective studies and found to fit well to observations in its respective set-ups.

3.B CMIP5 models with chlorophyll concentration output

Monthly mean of near-present-day values from 2000 to 2005 of the historical ESM simulations are used for the "CMIP5chl" sensitivity study. The eight models for which such outputs can be obtained through the CMIP5 data portal, and thus used herein, are listed in Table 3.5.

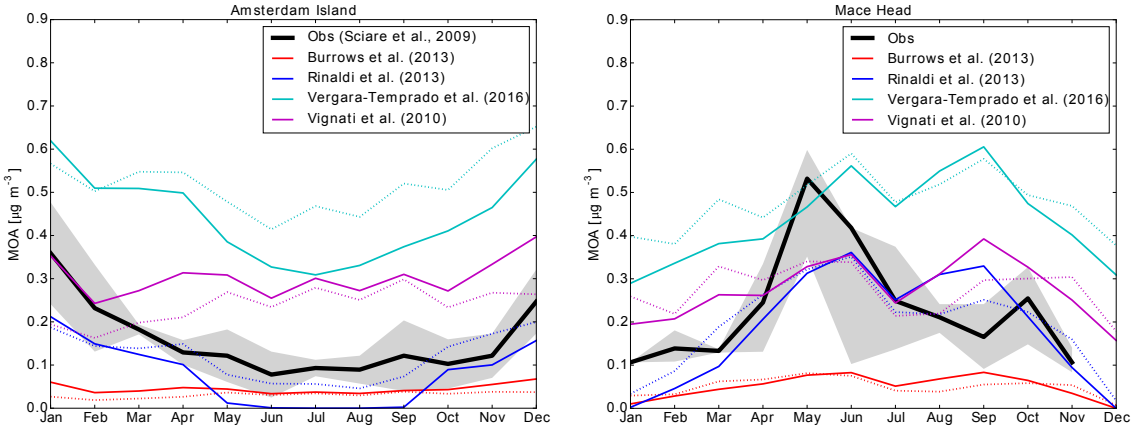

Figure 3.13: Comparison of MOA concentrations calculated offline using various OMF parameterisations. Coloured lines indicate offline calculated concentrations assuming the same source regions as the observational datasets; dotted lines of the same colours correspond to the same parameterisations except for the use of source regions from Vergara-Temprado et al. (2017). The black lines and shaded areas are the observational mean and the corresponding variances as described in Fig. 3.4.

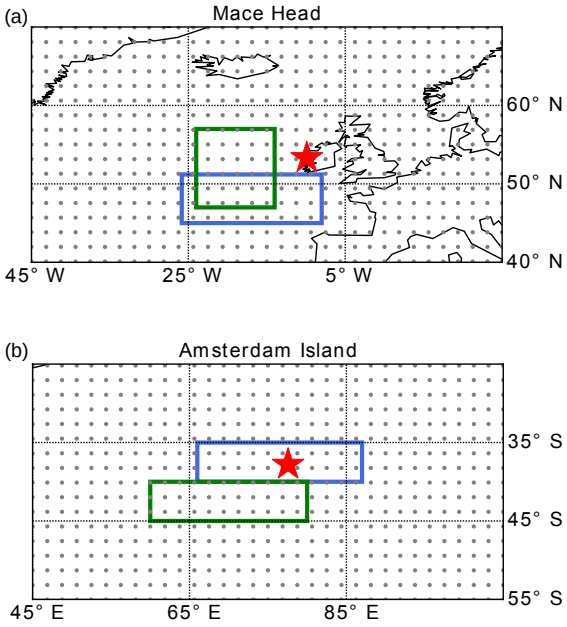

Figure 3.14: Source regions considered in offline calculations of MOA concentrations at Mace Head **(a)** and Amsterdam Island **(b)** according to various OMF parameterisations. The area boxed in green is the source region from the relevant publication related to each observational dataset, while that in blue is approximated from Vergara-Temprado et al. (2017). The red star indicates the location of the measurement station. The gray dots that fill the space are model grid points.

Table 3.5: List of CMIP5 models containing sea surface chlorophyll concentration data used for the "CMIP5chl" simulation.

Model name	Modelling centre or group	Mean of model versions, if multiple
CanESM2	Canadian Centre for Climate Modelling and Analysis	
CMCC-CESM	Centro Euro-Mediterraneo per I Cambiamenti Climatici	
CNRM-CM5	Centre National de Recherches Météorologiques/ Centre Européen de Recherche et Formation Avancée en Calcul Scientifique	
GISS-E2	NASA Goddard Institute for Space Studies	GISS-E2-H-CC, GISS-E2-R-CC
HadGEM2	Met Office Hadley Centre	HadGEM2-CC, HadGEM2-ES
IPSL-CM5	Institut Pierre-Simon Laplace	IPSL-CM5A-LR, IPSL-CM5A-MR, IPSL-CM5B-LR
MPI-ESM	Max-Planck-Institut für Meteorologie	MPI-ESM-MR, MPI-ESM-LR
MRI-ESM1	Meteorological Research Institute	

Chapter 4

Future changes in heterogeneous ice nucleation in the Arctic

4.1 Introduction

Due to its complexity and wide-ranging scales of relevance, there is still a large uncertainty associated with our understanding and quantification of aerosol-cloud interactions in the atmosphere (Seinfeld et al., 2016; Fan et al., 2016). With climate change and societal developments, however, the emissions of aerosols and the environment under which these particles interact with clouds is expected to change in the future. Questions then arise with regards to possible changes in the relevance of the various aerosol-cloud processes. In particular, a number of factors that may directly impact aerosol-cloud interactions are considered in the current study.

Firstly, given that the aerosol emissions from current industrial hubs are expected to decrease in the future (e.g. Riahi et al., 2007), an increase in sensitivity to local aerosol sources may result. This may be particularly relevant for regions downstream of major aerosol sources as well as more remote regions which depend on long-range transport as the main source of aerosol particles. Secondly, with increases in temperature, there is an upward shift of the isotherms in height, which may lead to changes in the cloud phase relative to the vertical gradient of aerosol concentrations.

A process that has the potential to be particularly affected by the above mentioned future changes is heterogeneous ice nucleation in mixed-phase clouds. This is because the concentration of ice nucleating particles (INPs) is relatively scarce in the atmosphere (Pruppacher and Klett, 1997). This may result in a strong sensitivity to any changes, and because it occurs in a narrow temperature range (limited to between -35 to 0 °C in the current study), it is subject to an upward shifting of the isotherms leading to mixed-phase clouds forming at altitudes with lower available INPs. In this study, focus is therefore placed on the future changes in heterogeneous ice nucleation.

The Arctic is chosen as an ideal testing ground for the analysis as: (a) it is expected to warm more strongly than the rest of the globe in the coming decades due to Arctic amplification (Serreze and Francis, 2006), (b) the environment is favourable for persistent mixed-phase clouds (Shupe, 2011; Morrison et al., 2012), and (c) long-range transport currently dominates as the source of aerosol particles in the region (Barrie, 1995; Garrett et al., 2004) but future local emission are expected to increase from the exposed ocean surface following sea ice retreat.

In the following sections, an overview of the model used for the analysis and the simulation set-up is provided first, followed by an evaluation of the present day (PD) aerosol

properties and their future changes on a global scale, and lastly a more detailed investigation into heterogeneous ice nucleation changes in the Arctic in the future is presented before the concluding summary.

4.2 Methodology

4.2.1 The coupled aerosol-earth system model

For this study, the newly available earth system model MPI-ESM1.2-HAM is used. This is based on the ECHAM6.3-HAM2.3 aerosol-climate model, which contains a more updated version of the global atmospheric climate model ECHAM6 (Stevens et al., 2013), including the land component handled by JSBACH (Roeckner et al., 2003; Reick et al., 2013), and a complex aerosol module HAM2.3 (Stier et al., 2005; Zhang et al., 2012; Tegen et al., 2018). In the earth system version used in this study, ECHAM6.3-HAM2.3 is additionally coupled with the ocean and sea ice model MPIOM (Marsland et al., 2003; Jungclaus et al., 2013), with an ocean biogeochemistry represented by the sub-model HAMOCC (Ilyina et al., 2013), and carbon cycling is considered between the various components (Giorgetta et al., 2013a).

Aerosols are represented following the M7 scheme as described in chapter 2. Anthropogenic emissions are defined based on the chosen Representative Concentration Pathways (RCP) scenario for the future, while the emission of SS (Guelle et al., 2001), MOA (Huang et al., 2018), and dust (Tegen et al., 2002) are computed at each time step based on the model conditions. In particular, MOA emissions are also coupled to the chlorophyll-a concentrations from the ocean model (more specifically HAMOCC), which serves as a proxy for the biological activity of the ocean. As chlorophyll-a is not prognosed in the model, the modelled phytoplankton concentration in the topmost ocean layer is converted to chlorophyll-a concentration by applying a Redfield phosphorus-to-carbon atomic ratio of 122 in phytoplankton and carbon-to-chlorophyll-a ratio of 0.2, consistent with the rest of HAMOCC. As the transfer of information between the atmosphere and ocean models only takes place once per simulation day, the computed chlorophyll-a concentration is updated daily in the MOA emission calculations.

A previous study has shown that the mean chlorophyll concentration from CMIP5 models tends to be overestimated in the open oceans when compared to SeaWiFS (Hu et al., 2012) satellite observations (Le Quéré et al., 2016; Huang et al., 2018). Concentrations diagnosed from MPIOM, in the context of MPI-ESM for the CMIP5 simulation, in particular, has been found to be especially high, though the fundamental cause for the bias is still a subject of investigation. Therefore contrary to the implementation in Huang et al. (2018), the emissions of MOA following the Rinaldi et al. (2013) parametrisation are not further increased in the current set-up. Regardless, the concentration of MOA simulated in the current study may be expected to be biased high, especially in the Southern Oceans. The relative change in MOA concentrations between the present day and the future, however, should still provide an insight into the impact of future changes in the climate.

4.2.2 Representation of heterogeneous ice nucleation in the model

Heterogeneous ice nucleation refers to the ice formation process involving an ice nucleating particle (INP) which decreases the energy barrier needed for the formation of an ice embryo (Kanji et al., 2017). In the current study, such processes are only considered in the mixed-phase temperature range (-35 to 0 °C), as at colder temperatures, ice is assumed to

form homogeneously (without the help of INPs). While there is still much research being conducted on identifying and describing INPs (e.g. Hoose and Möhler, 2012; Kanji et al., 2017), we consider two species in our model which can nucleate ice: dust and MOA. Both are assumed to only act in the immersion freezing mode, where the INP needs to be immersed in a droplet before initiating ice formation. The number of immersed particles (N_{imm}) is dependent on the number of particles activated into cloud droplets following Köhler theory and the relative mass/surface area fraction of the INP species compared to the total mass of the activated aerosol, following Hoose et al. (2008). For MOA, this is expressed as

$$N_{\text{MOA,imm}} = N_{\text{TOT,act}} \times \left(\frac{V_{\text{MOA}}}{V_{\text{TOT}}}\right)^{\frac{2}{3}}, \tag{4.1}$$

where V_{MOA} is the total volume of MOA in the size mode calculated by division of the mass by the density, and V_{TOT} is the total volume of all species in the respective size mode. The number of drops frozen per time step (N_{frozen}) due to MOA is therefore

$$N_{\text{frozen}} = N_{\text{MOA,imm}} \times FF \tag{4.2}$$

where FF is the frozen fraction, which is dependent on the properties of the INP species, its mean size in the respective grid box and size mode, and the temperature, as described in more detail in Ickes et al. (2017) and Huang et al. (2018).

4.2.3 Simulation set-up

For the current study, analyses are performed on a 55-year simulation starting from year 2000 following a historical run. The atmospheric component of the model uses a T63 horizontal grid (resolution of 1.88° by 1.88°), with 47 vertical levels, while a bipolar ocean grid is used for MPIOM, with horizontal resolution of approximately 1.5° and 40 levels in the vertical. The business-as-usual RCP8.5 scenario (based on the A2r development scenario described in Riahi et al., 2007) is used for prescribing future anthropogenic emissions. Dynamical vegetation is turned on, which allows for changes in the vegetation type in response to changing climate (Brovkin et al., 2013).

To investigate changes, the future (defined as the 10-year average centred around 2050) is contrasted against the PD (defined as the 10-year average centred around 2010) period, while relative changes are computed relative to the mean over the two time periods. For regional analysis, the Arctic region is defined as north of 75° N.

4.3 Global results

4.3.1 Comparison to observations

To assess the performance of the model in simulating global aerosol properties, comparison of the PD mean modelled aerosol optical depth (AOD, at 550 nm) are made against various satellite observational datasets. No temporal and spatial co-location and no satellite simulator was applied to the modelled data. The comparison therefore only serves as a first-order look into the performance of the model. Regardless, it is useful in providing insight into potential model biases in the aerosol distribution.

Due to observational uncertainties, data sparsity, and variations in processing techniques, four different observational AOD datasets are used for comparison. The first one is available from the Copernicus Atmosphere Monitoring Service (CAMS) reanalysis product, a successor of the Monitoring Atmospheric Composition and Climate (MACC) project

(Inness et al., 2013). It assimilates the satellite observations from Moderate Resolution Imaging Spectroradiometer (MODIS) into a global chemistry transport model and spans the years 2003 to 2007. A second dataset is available from the European Space Agency's Advanced Along-Track Scanning Radiometer (AATSR), available for the ten-year period from 2002 to 2012 (Popp et al., 2016). Version 2 of the Max-Planck-Institute Aerosol Climatology (MACv2), based on merger of observations from ground-based sun-photometer networks and an ensemble of complex aerosol models, covering the years 2000 to 2015, is also used (Kinne et al., 2013; Stevens et al., 2017). Lastly, a compilation of eight satellite observations spanning various time periods in the recent past is available and described in Kinne (2009).

The 550 nm AOD averaged over the entire available time period for the four observation-based datasets are shown with the modelled AOD for the PD period (2005 to 2014) in Fig. 4.1. Most notably, an overestimation of the AOD over China is found in our model, while an underestimation can be found over Africa, parts of central-south Asia, the Amazon regions, and North America. Slight differences exist in the AOD over oceans across the various observational dataset, where the modelled magnitude falls in the upper range of the spread. On the other hand, limited observational data is available over remote polar regions, but a first approximation indicates that our model may underestimate aerosol concentrations in these areas. Overall, the model performs relatively well in simulating the aerosol distribution across the globe, with a possible low-bias over polar regions.

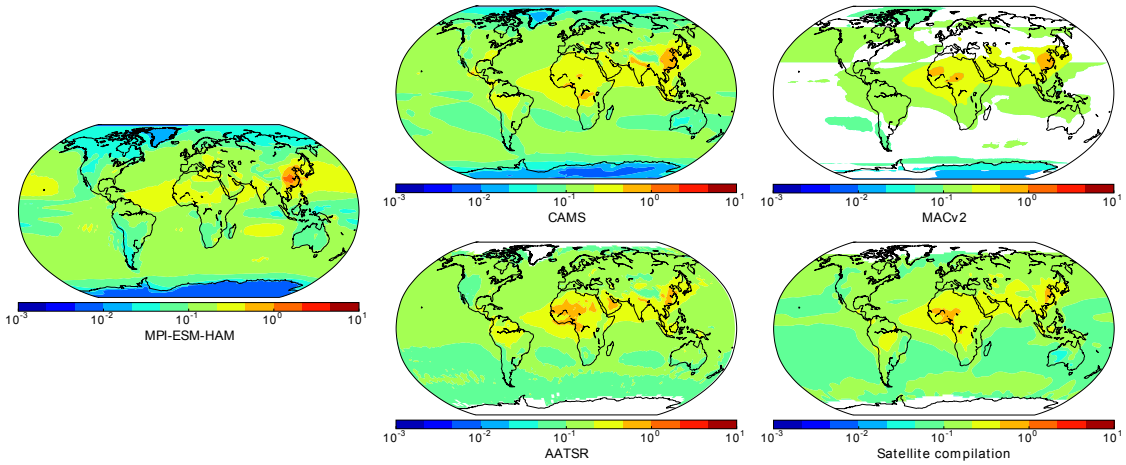

Figure 4.1: Present day multi-year annual average aerosol optical depth (at 550 nm) from the model (left) and four observation-based datasets (middle and right), as described in the text in Sect. 4.3.1.

4.3.2 Global aerosol changes

Following the RCP8.5 scenario, global aerosol emissions from anthropogenic sources are expected to decrease in the next decades due to air quality legislations (and later also economic and technological developments) that lead to decreases in emissions from industrial and residential sources (Riahi et al., 2011), as well as decreases in emissions from forest fires and deforestation. This trend is reflected in the global burden of OC, BC, and SO_4, where on the 5-year running mean, the global average burden of the three aerosol species combined decreases by around 1 mg m^{-2} from 2002 to 2052 (Fig. 4.2). It can also be noted, however, that the global mean trend of aerosol burden is largely dominated

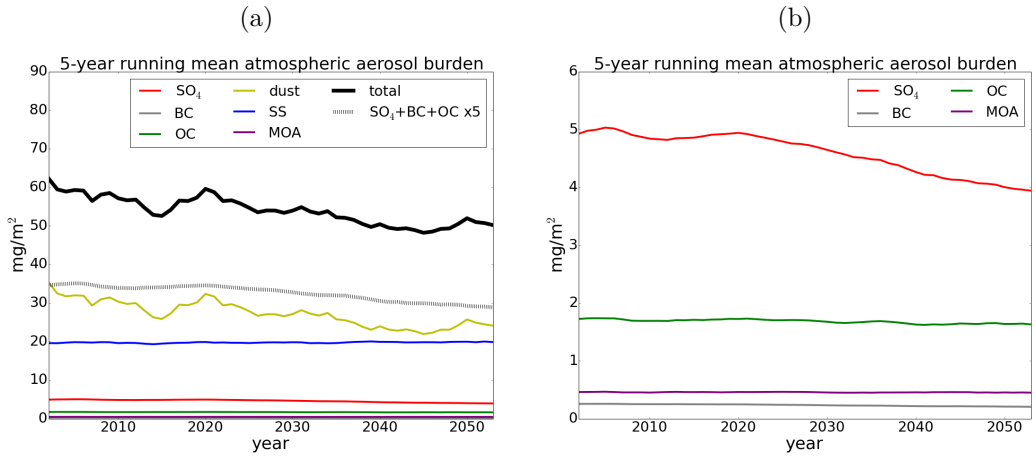

Figure 4.2: 5-year running mean time series of the global mean mass burdens shown for (a) all aerosol species, and (b) only those with mean burdens less than 10 mg m^2.

by changes in the dust burden, which has large inter-annual variability but also shows a decreasing trend in the next 50 years.

To investigate the reasons for these decreases in aerosol burden, global maps of changes in the online-emitted natural aerosol species (dust, SS, and MOA) as well as that of the rest of the aerosols with prescribed primary emissions (including growth and nucleation through the gas phase for sulphate aerosol) are shown in Fig. 4.3 together with the changes in the total aerosol burden. Here it can be clearly noted that the global pattern of aerosol burden changes between PD and the future is indeed dominated by decreases in the dust burden in the Northern Hemisphere mid-latitudes. Due to the high temporal variability of dust emissions, however, statistical significance in the change in total aerosol burden are mostly found in regions where there are significant changes of the same sign also in the other aerosol species.

For the BC, OC, and SO_4 burdens, for instance, significant decreases can be found nearly globally. The highest reductions are expected over industrialized regions such as China, Eastern Europe, and eastern North America. In the Southern Hemisphere, changes in aerosol burden are mostly dominated by marine aerosols (except over Australia where contributions from dust and BC+OC+SO_4 dominate and lead to a negative trend in aerosol burden), though still resulting in lower magnitude signals than that of dust. Over Antarctica, a notable decrease in aerosol burden can also be identified. This can be attributed to a general (though mostly not statistically significant) increase in zonal winds over the Southern Ocean which can hamper the transport of aerosols from lower latitudes to Antarctica.

In order to discern whether the reason behind the changes in aerosol burden in the atmosphere is driven by increased precipitation scavenging or decreased emission rates, global spatial distributions of the relative changes in source and sink terms for the total aerosol burden are plotted in Figure 4.4. The largest changes are simulated in the Arctic region, where an up to 200 % relative increase in aerosol emissions and sinks can be observed. This can be explained by the retreat of Arctic sea ice which allows for increased sea spray emissions from the ocean surface that in turn leads to increased scavenging at the surface (due to increased surface roughness), increased sedimentation (due to the larger size of locally emitted sea spray particles), and increased wet deposition (associated with increased precipitation). Interestingly, the relative increases in emission and sink terms roughly cancel out to yield minimal changes in the aerosol burden in the Arctic.

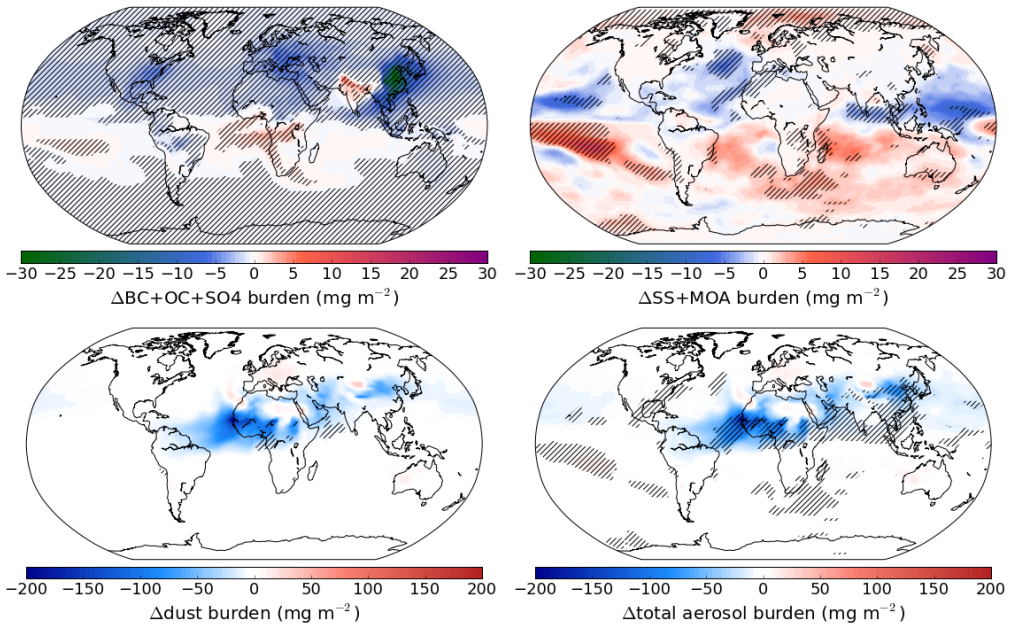

Figure 4.3: Global maps of changes in aerosol burden between PD and the future. Hatched areas indicate statistical significance of the yearly mean values at the 95 % level, but further restricted following the Wilks (2016) method for controlling the false discovery rate for data with moderate to strong spatial correlations. Note the nearly one order of magnitude difference in the colour scales between the upper and lower panels.

Secondly, it may be noted that outside of the Arctic, there is a general decrease in aerosol sinks over most of the globe, which is consistent with the decreased aerosol burden in the atmosphere. As the relative percentage of decreases in aerosol sink terms is of similar magnitude to the relative decrease in aerosol burden in the atmosphere, decreases in the sink terms seem to follow the decrease in the equilibrium aerosol concentration in the atmosphere rather than being their cause. The main driver, therefore, can only be in the emission rate, and this is reflected in particular by a strong and statistically significant decrease in aerosol emission over the Sahel region, which is dominated by changes in dust emissions.

4.3.2.1 What happens to the dust?

Dust is the greatest contributor to aerosol mass on the global scale in our model (as shown in Fig. 4.2). Any significant changes in its emission can therefore have a strong impact on the global aerosol burden and merit further investigation. In this case, the decrease in dust emissions from northern Africa is found to be attributable to the greening (increase in vegetated ratio) of the Sahel region (Fig. 4.5). While the coverage of potential dust source regions is prescribed and remains fixed in our model, the greening leads to increases in the surface roughness and therefore decreases in 10-metre wind speeds, which the dust emission parametrisation strongly depend on. In particular, following Tegen et al. (2002), dust emissions in our model are only active when a particle size-dependent threshold for wind speed is reached, and with the lower wind speeds (overall decrease in the mean by up to 0.7 m s^{-1} in the Sahel), the frequency of time when this threshold is surpassed decreases by up to 7.5 % on the annual mean.

A similar greening was also observed by Bathiany et al. (2014) in three CMIP5 models, and the reasoning is attributed to fertilization of vegetation by the increased CO_2 levels.

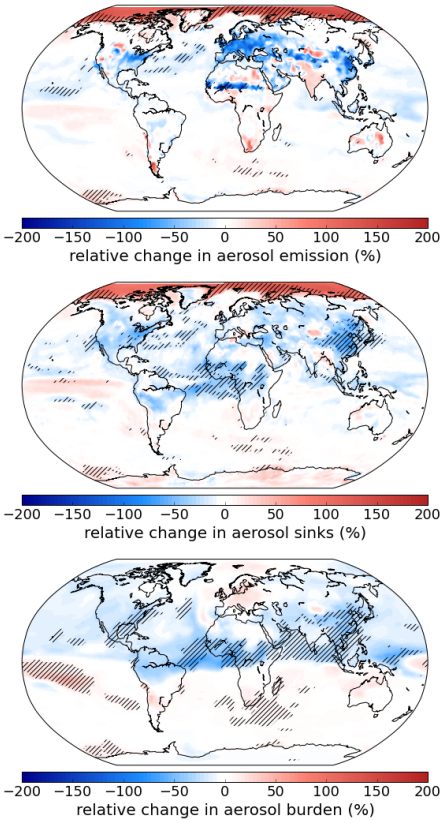

Figure 4.4: Global maps of the relative changes in the total aerosol sinks and emission between PD and 2050. Hatched areas indicate statistical significance of the yearly mean values at the 95 % level and further restricted following the Wilks (2016) method for suppressing the false discovery rate.

They noted, however, that mainly due to differing balancing response of precipitation and CO_2 fertilization, the greening effect does not persist after the first half of the 21st century across models, and the robustness of future greening or browning trends in the Sahel is still uncertain.

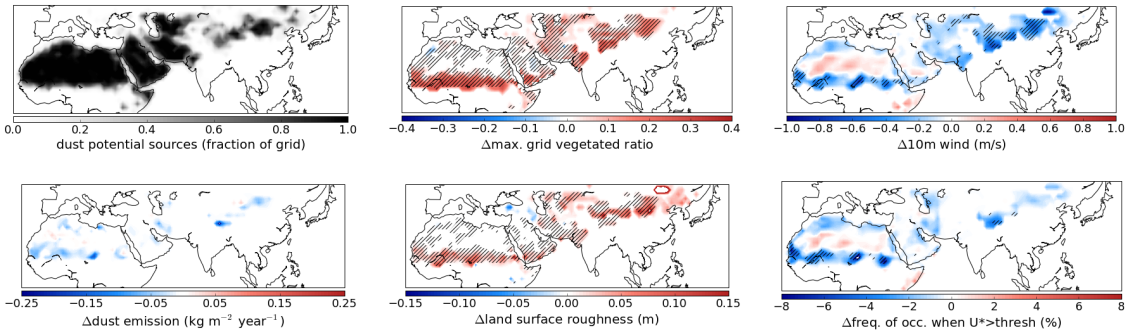

Figure 4.5: Factors contributing to the decrease in dust emissions. Plots are masked to the potential dust source regions (shown in the upper left figure). Hatches indicate statistical significance following the Wilks (2016) method applied at the 95 % significance level.

4.3.3 Changes in aerosol forcing

To quantify the effect of such changes in aerosol burdens in the atmosphere between the present day and the future, the all-sky and clear-sky top of atmosphere (TOA) net radiative forcing of aerosols is diagnosed by subtracting the respective TOA radiation balance calculated with and without aerosols in the radiation scheme of the model (Fig. 4.6). As expected, aerosols generally have a negative radiative forcing at the TOA. Exceptions are found in the polar regions where aerosols rather impede the reflectivity of the snow-covered surface, and in some regions under all sky conditions where the same effect can occur for aerosols above optically thick clouds.

In the simpler case of clear-sky diagnostics (i.e. clouds are ignored in the radiation calculations), the decrease in aerosol burden in the Northern Hemisphere mid-latitudes results in a decrease in the negative radiative forcing by up to 12 W m^{-2} over China and around 3 W m^{-2} over other regions with more significant aerosol changes (eastern North America, off the coast of West Africa, and Eastern Europe). In the Arctic, the positive radiative forcing decreases by 0.2 to 1 W m^{-2}, but this can mainly be explained by the decrease in surface albedo due to increased sea ice melt rather than aerosol burden changes (Gilgen et al., 2018). In the Southern Hemisphere, there is a general increase in the negative aerosol forcing consistent with increases in the burden of marine aerosols.

The negative radiative forcing associated with aerosols is generally reduced when clouds are also considered (all-sky conditions). In particular, the general latitude where the forcing becomes positive shifts more equatorward in the Arctic regions, and the magnitude of the positive forcing increases. When comparing 2050 to PD forcing, the magnitude decreases in the Northern Hemisphere regardless of the sign of the forcing, while in the Southern Hemisphere the forcing generally increases in magnitude. Signals over industrial hubs present in the clear-sky analysis, however, are largely absent due to masking by clouds. That is, while decreased aerosol concentration can lead to decreased reflection of incoming solar radiation under clear-sky conditions, this aerosol direct effect is largely irrelevant under cloudy conditions as clouds are already highly reflective.

In order to interpret the changes in aerosol radiative forcing when diagnosed under clear-sky and all-sky conditions, changes in cloud cover are also examined and shown in Fig. 4.6. Notable regions with significant decreases in cloud cover include eastern North America, Europe, the Norwegian Sea, Japan, central parts of South America, and southern parts of Central Africa. Under all-sky conditions, a decrease in cloud cover would lead to stronger instantaneous aerosol forcings as less of the potential impact of aerosols is masked by the clouds. However, as the clear-sky aerosol forcing is decreasing in magnitude in the Northern Hemisphere, this leads to a cancellation of the two aspects and thus a weaker signal in the all-sky net forcing.

4.4 Focusing on the Arctic

4.4.1 Changes in aerosol concentrations in the Arctic

To investigate how global aerosol changes translate to changes in the Arctic, 5-year running mean time series of the Arctic mean aerosol burden as well as the Arctic to Northern Hemisphere ratio of mean aerosol burdens, emissions, and depletions are shown in Fig. 4.7. From the first plot, it can be noted that similarly to the global trend, the aerosol mass burden in the Arctic is dominated by contributions from dust particles. The dust burden also shows a decreasing trend in the Arctic in the next half a decade, associated with greening of source regions, though also with a strong inter-annual variability. The sea salt

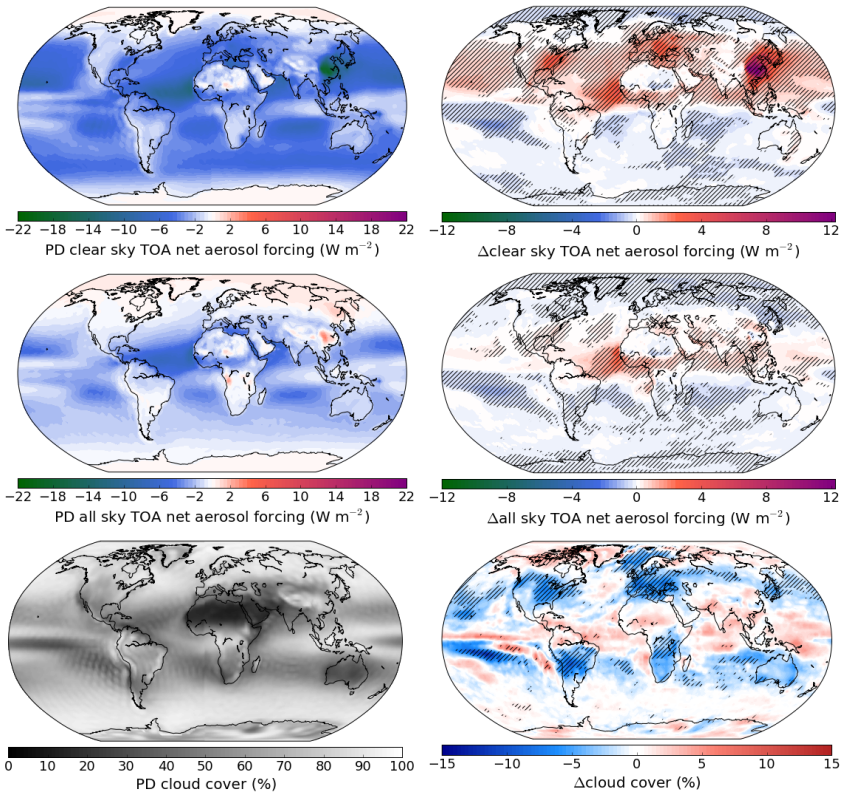

Figure 4.6: Left column: present day (PD) shortwave clear-sky and all-sky aerosol forcing at the top of atmosphere and total cloud cover; right column: changes in 2050 when compared to PD. Hatchings in the right column indicate statistically significant changes following the Wilks (2016) method applied at the 95 % significance level.

burden, on the other hand, shows a clear increasing trend (though overall a relatively low burden) due to increased local emissions from the exposed Arctic Ocean.

When comparing the mean burden in the Arctic region to that of the entire Northern Hemisphere (NH), most aerosol species show a lower mass burden in the Arctic than in the hemispheric mean. This is especially true of marine aerosols (sea salt and MOA), in which case the Arctic mean burden is consistently less than 10 % of the hemispheric mean. While this percentage does show an increase over time due to increased local emissions (40 % increase in the mean emission ratio in 50 years, as shown in Fig. 4.7c), the Arctic-to-NH mean ratio of aerosol sinks also show a similar increase. Thus less changes are found in the ratios of the burdens. On the other hand, all other aerosol species aside from sulphate have Arctic mean burdens that are between 20 to 60 % of the hemispheric mean. For sulphate, the mean burden in the Arctic is comparable to that in the NH. As local emissions of both sulphate aerosol and its gaseous precursor sulphur dioxide are minimal compared to the hemispheric mean, this indicates that sulphate is much more efficiently transported from the lower latitudes than the other species. A possible reason behind this is the smaller size of sulphate particles, which can be transported for longer distances before being removed from the atmosphere.

In terms of the temporal trend of the relative aerosol burdens in the Arctic compared to the NH mean, aside from marine aerosols, as discussed previously, all aerosol species show either no change (for dust), slight (for OC and BC), or greater (for sulphate) decreases over time. Possible causes that can contribute to these decreases include changes in the transport, emission, and/or depletion rates, as well as aerosol burden changes in

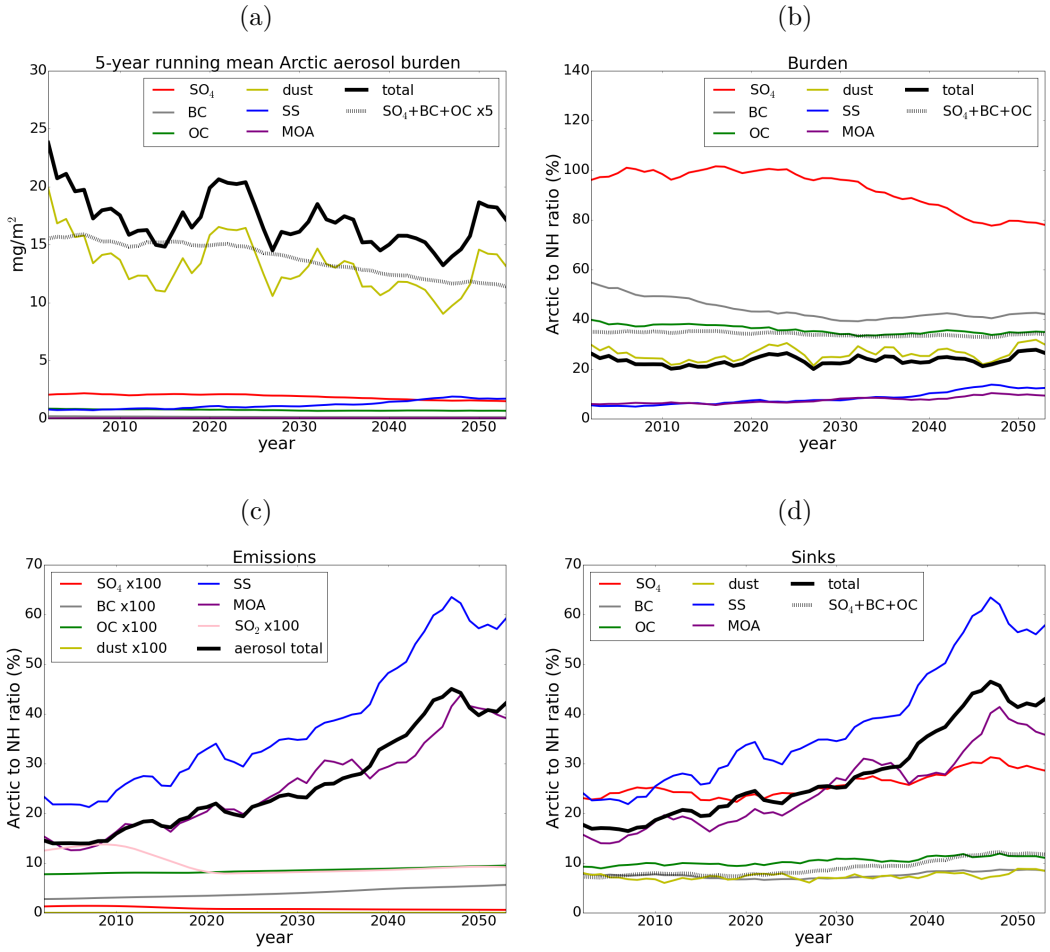

Figure 4.7: 5-year running mean time series of (a) mean aerosol burdens in the Arctic region (north of 75° N), and the ratio of the Arctic-mean to Northern Hemisphere-mean (b) burdens, (c) emissions, and (d) sinks.

the source regions where the transported airmass originate (e.g. if the airmass mostly originates from regions where there is a stronger decrease in the aerosol burden than the NH mean). Considering that there are minimal changes in the Arctic mean emissions relative to the NH mean (a slight increase for OC and BC, likely due to stronger decreases in anthropogenic emissions in the mid-latitudes), the changes in the relative burden over time are likely caused by the other factors. While the slight increase in the Arctic relative depletion rate of OC and sulphate may have contributed to their decreasing burdens, the changes in relative burden are likely also driven by a stronger anthropogenic burden decrease in the airmass source regions (when compared to the NH mean). This is supported by the similar time evolution (e.g. stronger sulphate burden decrease after 2025) of the Arctic-to-NH burden ratio and the global mean burden (which would also be dominated by regional changes). As dust emissions mostly originate in regions further south, airmasses that arrive in the Arctic are unlikely to be affected by local emission changes in the source regions. Thus the relatively constant (over time) Arctic to NH ratios of dust burden and dust sinks indicate that there are likely no significant systematic changes in the dusty airmasses that are transported into the Arctic.

The overall aerosol size, which can influence the number of aerosol particles activated into cloud droplets and therefore the number of immersed INPs, on the other hand, is

found to increase more strongly near the surface and less so (or even to decrease) aloft (Fig. 4.8c,d). The overall number concentration of accumulation and coarse mode aerosol particles decreases (except right at the surface in summer and autumn; Fig. 4.8b), partly due to a lower emission rate in the lower latitudes. Closer to the surface where aerosol mass increases due to local emissions, the number concentration still decreases in the future due to a higher rate of aerosol coagulation, which increases in efficiency with warmer temperature. In particular, a stronger decrease in the aerosol number concentration near the surface can be observed in winter, when the strongest temperature increase occurs, as opposed to summer, when the temperature warming is less significant. On the other hand, the slight increase in wind speeds (Fig. 4.9) over the Arctic Ocean cannot explain the change. Although larger sea spray particles can be lofted with higher wind speeds, this would lead to increases in both aerosol mass and number concentrations. Overall, this therefore results in a general decrease in the number of immersed aerosols available for ice nucleation (Fig. 4.10), despite an increase in the fraction of particles activated into cloud droplets.

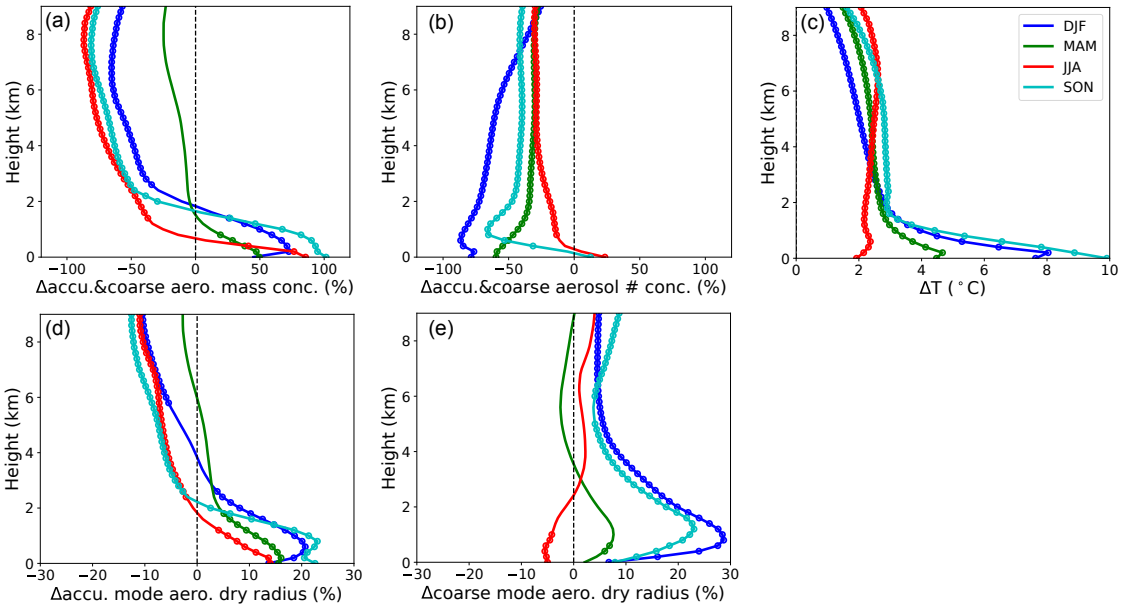

Figure 4.8: Shown on the left two columns are the Arctic seasonal mean relative changes in (a) the mass concentration of accumulation and coarse mode aerosols, (b) the number concentration of accumulation and coarse mode particles, (d) the mean dry radius of accumulation mode aerosols, and (e) that of coarse mode aerosols. Additionally shown on the right in (c) is the absolute changes in temperature. Circles indicate statistical significance at the 95 % level.

4.4.2 Changes in the Arctic environment

Climate change leads to an amplified temperature increase in the Arctic that is at least twice as large as in the global mean (Serreze and Francis, 2006). In our model, this translates to seasonal mean warming of 2 to 10 °C at the surface and 2 to 3 °C above 1.5 km height in the Arctic region (Fig. 4.11a). Specific humidity increases with a similar but slightly different trend at different altitudes. This leads to a general increase in seasonal mean relative humidity (RH; Fig. 4.11b) of less than 4 % below 2 km height (except autumn when there is a 5 % decrease in RH at the surface and up to 6 % increase

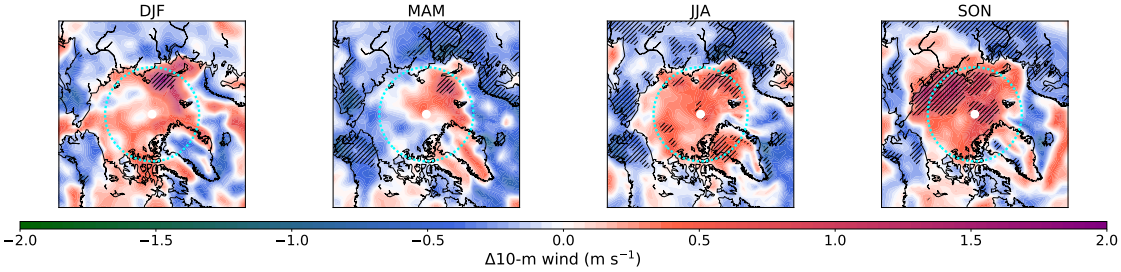

Figure 4.9: Changes in 10-metre wind speeds in the Arctic. Hatched areas are statistically significant following the Wilks (2016) method applied at the 95 % significance level. The dashed cyan circle indicates the 75° N latitude.

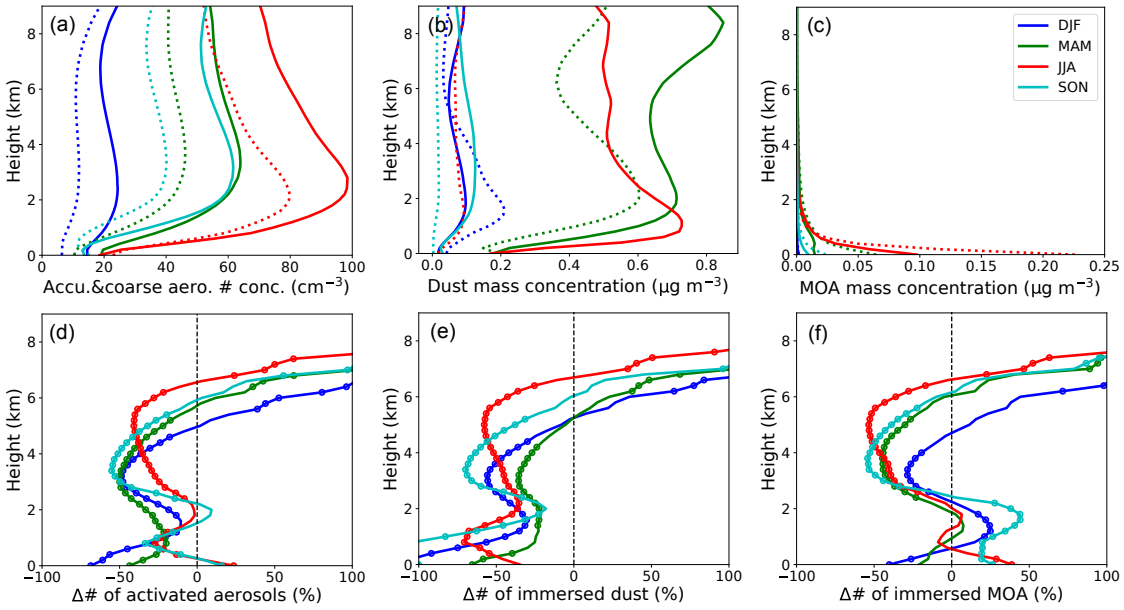

Figure 4.10: Arctic seasonal mean vertical profiles of PD (solid lines) and future (dashed lines) (a) number concentration of soluble aerosols in the accumulation and coarse modes, (b) mass concentration of dust aerosols and (c) of MOA. Also shown are the relative changes in (d) the number concentration of aerosol particles activated into cloud droplets and (e) the number concentration of dust aerosols and (f) MOA immersed in droplets. Circles indicate statistical significance at the 95 % level.

peaking at around 1 km height). In the higher altitudes, however, there is a general decrease in RH of up to 3 %. For the decrease in Arctic sea ice cover, a strong regional depletion is observed over the Barents Sea throughout the year, while on the seasonal mean, overall higher decreases across the entire Arctic region can be found in summer and autumn (Fig. 4.12).

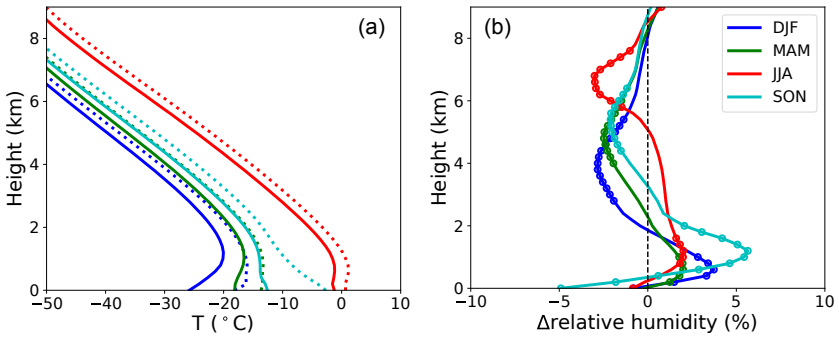

Figure 4.11: Arctic seasonal mean vertical profiles of (a) temperature in the PD (solid lines) and in the future (dashed lines), and (b) the absolute change (future-PD) in relative humidity. Circles indicate statistical significance at the 95 % level.

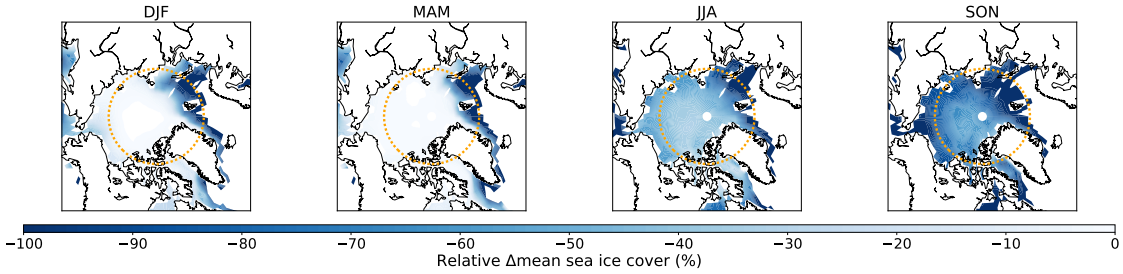

Figure 4.12: Relative (defined as (future-PD)/PD) seasonal mean changes in the Arctic sea ice cover. The orange dashed circle indicates the 75° N latitude, north of which is defined as the Arctic region in subsequent analyses. The extent of the shaded regions indicate where the sea ice cover is non-zero in the PD.

4.4.3 Changes in heterogeneous ice nucleation in the future

4.4.3.1 Freezing rate during occurrence

Heterogeneous ice nucleation in the Arctic can change in the future due to changes in both INP concentrations and the environmental condition that these aerosols are exposed to. As discussed previously, the concentration of dust aerosols decreases strongly in the Northern Hemisphere in the future in our model while MOA concentrations show a non-statistically significant increase near the surface and decrease aloft. The changes in aerosol concentrations, therefore, are likely to induce a decrease in heterogeneous ice nucleation rate in the Arctic except near the surface where contributions from MOA may lead to an increase in freezing rate.

Changes in the environment, on the other hand, are dominated by increases in temperature. Since the ice activity of both MOA and dust decreases sharply with increasing temperature, the upward shifting of isotherms is expected to contribute to a decrease in heterogeneous ice nucleation rate at each altitude in the future.

When considered together, the significant decrease in dust concentration and increase in temperature is expected to dominate, and this is indeed the case as shown in Fig. 4.13a,b, where the freezing rate of MOA and dust during occurrence are both shown to decrease by around 50 to 200 % in the future (except at the surface in summer for MOA).

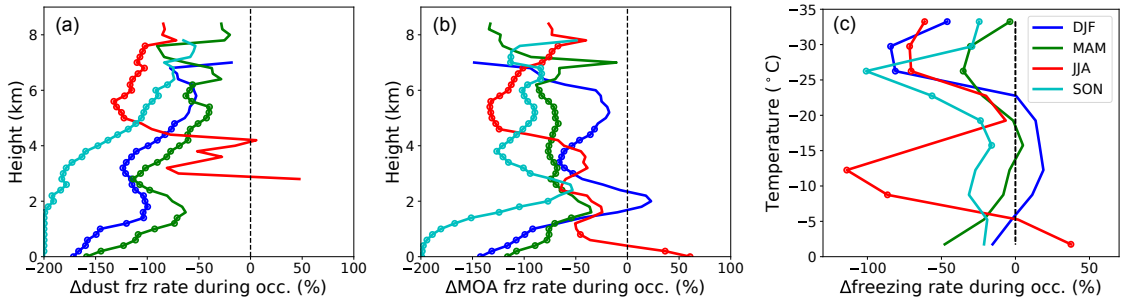

Figure 4.13: Arctic seasonal mean vertical profiles of relative changes in droplet freezing rate during occurrence due to (a) dust aerosols and (b) MOA, plotted against height and (c) of both species combined plotted against temperature bins. Circles indicate statistical significance at the 95 % level.

To rule out influences due to shifting of the isotherms, the freezing rate is binned by temperature in each time step and averaged over the respective periods. The relative difference between the future and PD is then taken for each temperature bin (Fig. 4.13c). Here a decrease in freezing rate during occurrence of around 20 to 100 % can still be noted, especially at temperatures colder than -20 °C which mostly occur at altitudes above 2 km where INP concentrations decrease considerably. The decreasing trend is extended to warmer temperatures in summer when the isotherm at 2 km is closer to -5 °C on average. An exception is during summer for the warmest temperature bin, where statistically significant increase in the freezing rate during occurrence can also be observed, resulting from the significant increase in MOA concentration near the surface.

All other seasons do not exhibit a significant change in freezing rate at the warmer temperatures. This is because MOA dominates over dust as the more ice-active INP at temperatures warmer than around -20 °C, and the change in the number concentration of immersed MOA available for ice nucleation is more variable and less statistically significant at levels below 2 km (Fig. 4.10f) where these temperatures tend to occur. In particular, during winter, the average temperature is generally below -15 °C at all levels and higher temperatures are rare.

Notably, significant increases in the number of immersed MOA can be observed during autumn at all levels below 2.5 km (Fig. 4.10f) but no notable increases in the freezing rate during occurrence can be seen in any of the temperature bins (Fig. 4.13c). Closer examination of the temperature changes reveals that during this season, temperatures warm on average by 3 to 10 °C in the Arctic, which would result in shifts across temperature bins (each with width of 3.5 °C). As the MOA concentration is highest close to the surface and sharply decreases aloft (Fig. 4.10c), shifts in isotherms can offset the increase in MOA concentration at all levels and result in statistically insignificant changes in the freezing rate during occurrence at each temperature.

4.4.3.2 Frequency of freezing occurrence

In terms of the frequency at which heterogeneous ice nucleation occurs in the Arctic, PD conditions lead to the most frequent occurrence near the surface below 1 km altitude in

our model. MOA causes nucleation of ice crystals during up to 17 % of the time steps in winter and 45 % in summer (Fig. 4.14b). Dust, on the other hand, nucleates ice only during up to 13 % of the time in all seasons except summer, when the peak freezing occurrence takes place at around 5 km altitude but occurs only around 5 % of the time (Fig. 4.14a), due to the limited temperature range at which nucleation of ice crystals on dust INP is relevant.

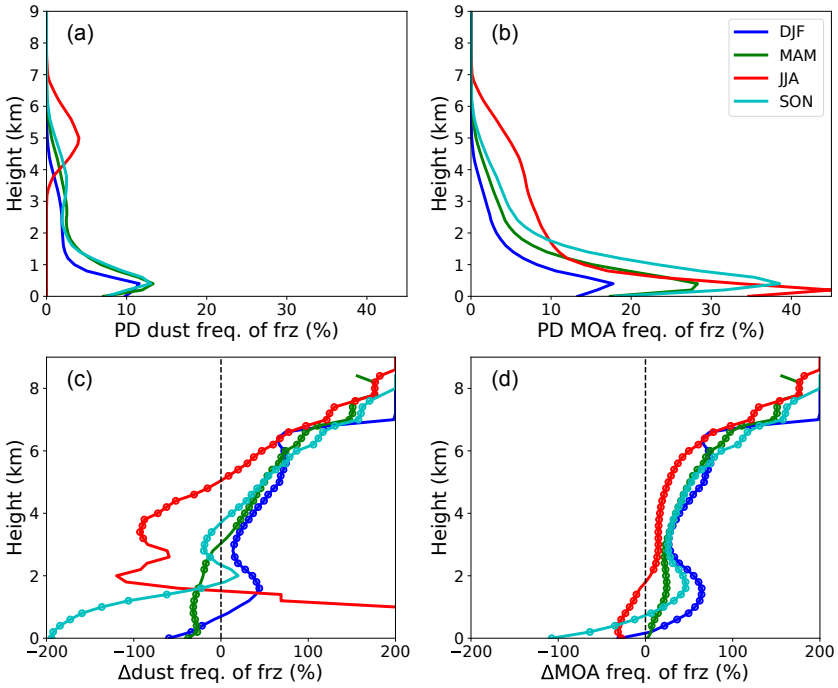

Figure 4.14: Arctic seasonal mean vertical profiles of PD freezing occurrence frequency due to (a) dust aerosols and (b) MOA. Relative changes of the respective properties are shown in (c) and (d). Circles indicate statistical significance at the 95 % level.

In the future, a general increase in ice nucleation occurrence is found at higher levels compared to the PD due to upward shifting of the isotherms, while closer to the surface the frequency decreases during warmer seasons as the temperature more frequently becomes too warm for the relevant nucleation process (Fig. 4.14c,d). Again, examining the changes for a given temperature bin (Fig. 4.15a,b,c) reveals more frequent freezing occurrence by up to 100 % of the time at warmer temperatures (>-15 °C in spring and autumn and >-23 °C in winter; Fig. 4.15a) and less frequent occurrence at colder temperatures. In summer, the decrease in freezing occurrence takes place mainly at the warmer temperatures (-13 °C to -5 °C) and only a slight increase can be noted for the warmest temperature bin. These trends mostly reflect the seasonal changes in the frequency of occurrence of the respective temperatures in each bin (Fig. 4.15b).

Ruling out the changes due to the increasing temperature, the frequency of freezing during temperature occurrence is shown in Fig. 4.15c. Here it can be observed that the strong increase in occurrence frequency at warmer temperatures is largely diminished. Instead, there is a notable decrease in nucleation frequency at the colder temperatures in autumn, increase in the medium temperature range in winter, and decrease at the warmer temperatures in summer. As immersion freezing requires that the INP particles be immersed in cloud droplets for freezing to occur, the frequency of occurrence can also be controlled by the availability of such liquid droplets. Indeed, a similar trend in the

change in the supercooled liquid fraction (which indicates changes in the mass of liquid droplets available for freezing) can be observed (Fig. 4.15d) as described above for the change in freezing frequency during each temperature occurrence (Fig. 4.15c).

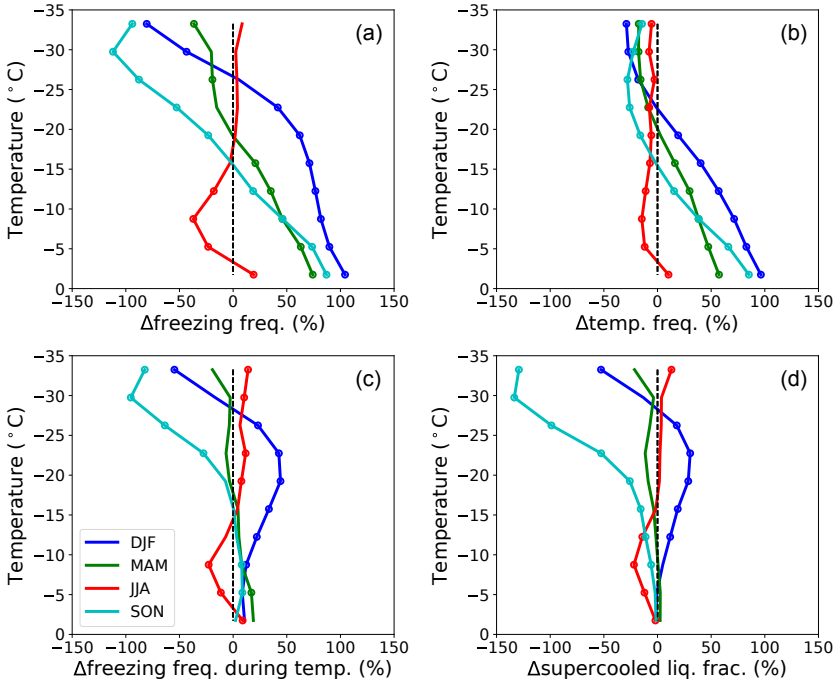

Figure 4.15: Arctic seasonal mean vertical profiles of relative changes in (a) freezing occurrence frequency (due to dust and/or MOA) plotted against temperature bins, (b) frequency of occurrence of each temperature bin, and (c) freezing frequency during temperature occurrence. Additionally, the relative change in the supercooled liquid fraction is shown in (d). Circles indicate statistical significance at the 95 % level.

4.4.3.3 Overall freezing rate

Combining the changes in both the freezing rate during occurrence and frequency of occurrence, future changes in the overall contribution of heterogeneous ice nucleation in the Arctic are shown in Fig. 4.16. Contributions by MOA and dust particles as INPs decrease by 50 to 200 % throughout all levels (except in summer near the surface, with an increase by nearly 50 %). Binned by temperature, the overall freezing rate decreases by 20 to 150 %, with the exception of winter when the increased occurrence of the warmer temperatures and increased presence of supercooled liquid droplets at the medium mixed-phase temperature range results in more ice nucleation at these temperatures. Additionally, freezing contributions from the warmest temperature bins also increase in summer and autumn, attributable to increases in the freezing rate during occurrence (summer) and frequency of occurrence (autumn).

By comparing Fig. 4.16b to Fig. 4.13c, the contribution of changes in freezing occurrence frequency (mostly due to increasing temperatures and changes in the available liquid droplets) to changes in freezing rate can be approximated. The most notable differences are in winter for temperatures above -20 °C and in autumn for the highest temperature bins, where increases in occurrence frequency contribute to an increase in seasonal freezing rate of around 70 %. For the coldest mixed-phase temperature bins, less frequent freezing occurrence contributes to a 20 to 120 % decrease in heterogeneous ice nucleation for all

seasons except summer (when the temperature change is minimum between PD and the future, as shown in Fig.4.11a).

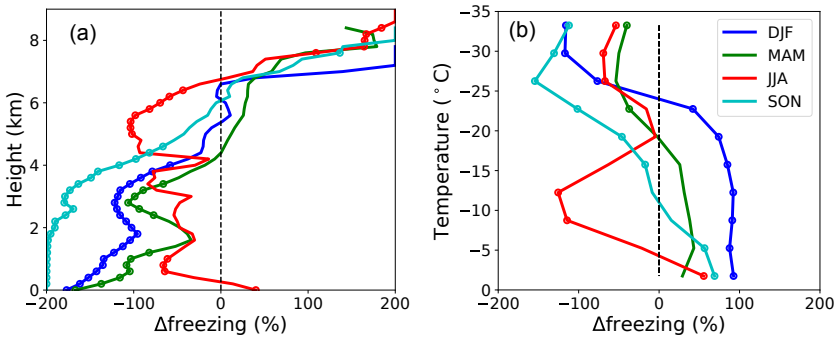

Figure 4.16: Arctic seasonal mean vertical profiles of relative changes in overall droplet freezing rate plotted against (a) height and (b) temperature bins. Circles indicate statistical significance at the 95 % level.

4.5 Conclusions

In this study, a first analysis using the newly available aerosol-earth system model MPI-ESM1.2-HAM is performed using a 55-year future simulation starting from year 2000 following the RCP8.5 scenario. The modelled PD AOD is found to compare well with observations, with a possible low bias in the polar regions. A general decrease in the global aerosol burden is found in the future, with contributions from decreases in anthropogenic emissions as prescribed by the RCP8.5 scenario. The dominating factor leading to the decrease in global aerosol burden, however, is the decrease in dust emissions, especially from the Sahel region, due to greening in the future leading to lower 10-metre wind speeds. While the change in dust emission is largely not found to be statistically significant due to high variability in its emission rate, it contributes to around 90 % of the global aerosol burden decrease from 2002 to 2052 (on a 5-year mean), while contributions from the mainly anthropogenic aerosols (SO_4, BC, and OC) are only around 1 mg m^{-2}. Thus changes in dust aerosols play an important role in subsequent analyses of the impact of aerosol changes on ice nucleation. Though also found in other CMIP models (Bathiany et al., 2014), the robustness of these dust trends in the future is unclear, thus pointing to a need for further research on the topic.

When focusing on the Arctic region and examining changes relevant for heterogeneous ice nucleation, we find a general decrease in the aerosol mass concentration above 1 to 2 km altitude and an increase below, due to a decrease in globally transported aerosols aloft and an increase in local sea spray emissions, respectively. For the two INP species considered, dust aerosol dominates the change in transported aerosols while for MOA, an increase in locally-emitted concentrations close to the surface can be found. The number concentration, however, decreases throughout all levels and seasons except during summer and autumn at the surface. This leads to an overall decrease in the number of immersed aerosol particles available for freezing, though the number of immersed MOA still shows increasing trends at varying levels below 2.5 km height in the various seasons except spring.

Considered together with other environmental factors such as upward shifting of the isotherms and changes in available supercooled liquid droplets, this leads to a 50 to 200 %

decrease in mean freezing rate at all levels and seasons in the Arctic, except near the surface in summer where an average increase of nearly 50 % can be noted. When inspected by temperature bins, this can be attributed to a decrease in freezing contribution from colder mixed-phase temperatures due to both warming in the Arctic and decreases in INP concentrations. An increase in freezing contribution from warmer mixed-phase temperatures, on the other hand, can be mainly traced back to increasing temperatures in winter and autumn and to aerosol changes in summer. Lastly, shifting of the isotherms in an environment where the INP concentration is strongly decreasing with altitude and thus confined to near the surface as for MOA results in negligible changes in freezing rate despite an overall increase in concentration at all levels in autumn.

Chapter 5

Impact of black carbon deposition on snow on the surface albedo

5.1 Introduction

Despite relatively lower mass concentrations in the atmosphere compared to other aerosol species, black carbon (BC) is of particular importance due to its ability to absorb shortwave radiation. In the atmosphere, this leads to a semi-direct effect of warming of the surrounding air which may alter the atmospheric relative humidity and therefore cloud cover (e.g. Johnson et al., 2006; Hansen et al., 1997). Once deposited on the surface, on the other hand, BC can also alter the albedo of highly reflective surfaces such as snow (e.g. Doherty et al., 2010). In this study, focus is placed on the forcing exerted by the latter process on the climate system. In particular, as BC is scavenged from the atmosphere along with falling snow or without concurrent precipitation, it is deposited onto the surface and mixes in with snow, creating a BC-snow mixture whose albedo then varies with the concentration of BC and the property of the snow.

Darkening of surface snow by BC has been examined previously in various studies, focusing on the impact on various scales. Of particular relevance for the current study is the publication by Flanner (2013), where the Arctic's sensitivity to BC is investigated. With a suite of idealized simulations, they found the strongest influence of BC in the Arctic to be when it is present in the lowest atmospheric layer and in the surface snow, with a positive forcing that leads to warming in the Arctic. On the global scale in the present climate, Flanner et al. (2007) quoted a global annual mean radiative forcing of BC in snow of approximately 0.05 W m^{-2}, which is strongest during the melt season. This induced a stronger surface snow melt during the month prior to the peak melting month in their model and led to 2-metre temperature increases on the order of 0.1 °C on the global annual mean and between 0.5 and 1.6 °C in the Arctic. In the study by Namazi et al. (2015) using the Canadian Global Climate Model, on the other hand, no significant difference was found between the forcing exerted by BC in snow from pre-industrial emissions compared to that from present day emissions. They postulated that the difference may stem from models' transient versus equilibrium response to BC in snow, as well as differences in the feedback processes such as the snow-albedo feedback.

5.2 Model implementation

Representation of the snow darkening effect of deposited BC is applied in ECHAM-HAM based on a previous implementation into the ECHAM model (without an explicit aerosol

module) which is documented in detail in Engels (2016). The original implementation considers only the effect of deposited BC on the snow albedo over land, and this is further extended to include the impact on snow over sea ice in the current study. Due to the differing radiative properties of sea ice when compared to snow, and the different mixing process of BC on sea ice (more likely to accumulate at the surface), however, the effects of BC deposited on bare sea ice is not considered.

A two-step process thus needs to be considered in the implementation. Firstly, the concentration of BC in the top snow layer needs to be traced, and secondly, the change in snow albedo is then calculated based on this concentration.

5.2.1 Tracing the concentration of BC in snow

For the purpose of examining the changes in surface snow albedo, only the BC concentration in the topmost snow layer (defined to be the top 2 cm of snow (Engels, 2016), converted into mass for calculations in the model based on a fixed snow density of 300 kg m^{-3} in ECHAM) is considered. This concentration is in turn controlled by the separately considered influx of BC and snow from the atmosphere and their respective removal from the surface due to melting and melt water scavenging.

BC is removed from the atmosphere through dry deposition, sedimentation, and wet deposition to the surface. Dry deposition is defined as the mechanical process of surface turbulence removal and biomass scavenging of aerosol particles from the atmosphere, and mostly concerns only aerosol in the near-surface layers (Ganzeveld et al., 1998). Sedimentation refers to the downward movement of aerosol particles due to gravity, and is considered only for larger particles in the current model (Zhang et al., 2012; Stier et al., 2005). Wet deposition, on the other hand, can occur both in-cloud and below-cloud (Croft et al., 2010; Stier et al., 2005). Both cases refer to the depletion of aerosol particles from the air by precipitating hydrometeors, which can occur through collection of ambient aerosol particles by the falling hydrometeors or through activation of the hydrometeors by the aerosol particles (by acting as cloud condensation nuclei, CCN, or ice nucleating particles, INPs). It should be noted, however, that as the aerosol particles are not removed upon activation and not traced separately during droplet activation, the exact number and mass of aerosol particles scavenged through droplet activation is a diagnosed property calculated based on the grid aerosol mass mixing ratio during precipitation formation and an aerosol mode-dependent scavenging parameter. Lastly, as is consistent with the original model set-up and similarly treated in other global climate models (e.g. Rasch and Kristjánsson, 1998), precipitation is assumed to fall to the surface within one time step, removing the aerosol particles by wet scavenging. Reduction in the scavenged aerosol reaching the surface is considered, however, due to below-cloud evaporation of the droplet which leads to release of the scavenged aerosol (Stier et al., 2005).

The surface snow mass, on the other hand, is computed for the sole purpose of determining the BC concentration in snow by accumulating the snowfall and snow melt mass over time. The latter variable (snow melt) is calculated in the land surface model (JSBACH) by considering the surface temperature, heat capacity of the uppermost soil layer, and latent heating due to the melting process. BC in the snow can also be removed during this melting process by subsequent run-off. As these particles are not as easily removed as the snow melt, the scavenging coefficient for BC internally mixed with other aerosol species is 0.2 and 0.03 for externally mixed BC (Flanner et al., 2007). This results in an increase in the concentration of BC in the remaining snow, as is consistent with observations (e.g. Doherty et al., 2010; Sterle et al., 2013).

To obtain the concentration of BC in the top snow layer, 5 different cases are considered. This is slightly modified from the implementation by Engels (2016), in which only

four cases are considered, in order to more consistently keep track of only the BC mass in the top layer (up to 2 cm) of snow:

1. If there is no snow on the surface:
   The deposited BC has no impact on the surface albedo

2. The updated snow mass on the surface is less than the 2 cm layer considered:
   The BC concentration in snow is calculated from the total mass of both BC and snow already present at the surface as well as considering sinks and sources from the current time step

3. New snowfall is greater than the 2 cm layer:
   BC concentration is calculated only from the new influx of BC and snow

4. New snowfall is less than the 2 cm layer but the total snow mass is more than 2 cm deep: All of the new flux of BC and snow as well as whatever amount of snow (with the mass of BC it contains) already on the surface that is needed to reach the 2 cm threshold are used to calculate the BC concentration in snow, after first updating the concentration at the surface with the runoff amount

5. No fresh snow but there is snow on the surface which remains:
   Newly deposited BC is added to the previous BC mass and spread through the snow layer to a maximum of 2 cm of snow, after first considering concentration changes in the old snow layer due to melt scavenging and run-off

In all cases, decrease of the BC concentration in snow only occurs through fresh snowfall coinciding with lower BC deposition rates, and the canvas is refreshed after complete snow melt.

5.2.2 Considering the impact of BC concentration in snow on the albedo

Once the BC concentration in the topmost 2 cm of surface snow is determined at each time step, its impact on the snow albedo is diagnosed by linearly interpolating between the pre-calculated albedo values for a set of conditions. A single-layer implementation of the Snow, Ice, and Aerosol Radiation (SNICAR) model (SNICAR-online; Flanner et al., 2007) is used to calculate the albedo values for three different BC-in-snow concentrations (0, 100, and 1500 ng of BC per g of snow). For each of the chosen BC concentrations, two different snow grain sizes are considered in order to account for differences in the age of snow. This determines the albedo of pure snow and thus directly limits the relative influence BC can have on the surface albedo (Flanner et al., 2007). With increasing BC concentration, the choices of snow grain sizes used for the calculations are 50 and 150 μm, 150 and 500 μm, and 500 and 1000 μm, respectively. While the snow grain size increases with age due to processes such as melting and refreezing, the BC concentration in snow is also expected to scale with snow age as the aerosol accumulates over time.

This part of the implementation is directly applied following Engels (2016) and extended to snow over sea ice without further changes. The lookup table of albedo values for these pre-determined conditions is produced by Engels and the background conditions chosen for these simulations are described in Appendix A of the aforementioned reference. Notably, while the SNICAR-online set-up also allows for consideration of other impurities such as deposited dust particles, they are not included in the current implementation.

5.3 Simulations

In the current study, analyses are based on four different simulations:

- "BCinSnow": a 20-year atmosphere-only simulation (plus an additional 3 months of spin-up) from 2003 to 2023, where the impact of deposited BC on the surface snow albedo is considered as described in the previous sections
- "noBCinSnow": identical in set-up as "BCinSnow" but where the impact of BC in snow is turned off
- "BCinSnow_1yr": a rerun of the "BCinSnow" simulation with additional diagnostics, but only for one year (2003)
- "futureESM": a 55-year coupled earth system model (ESM) simulation from 2000 to 2055, starting from a historical run, including the effects of BC in snow on the surface albedo. This is the same simulation analysed and described in more detail in chapter 4.

For the atmosphere-only simulations (all but "futureESM"), the monthly mean sea ice cover and sea surface temperature are prescribed based on the AMIP (Taylor et al., 2000) climatology averaged over the years 1979 to 2008, and do not vary throughout the 20-year simulations. The prescribed aerosol and precursor gases emissions, on the other hand, are time-dependent in order to take into account variabilities in their emission rate. Emission files for the Representative Concentration Pathway (RCP) 8.5 scenario (Riahi et al., 2007) from the Atmospheric Chemistry and Climate Model Intercomparison Project (ACCMIP; Lamarque et al., 2013) are used. For the ESM simulation, the aerosol and atmosphere part of the model (ECHAM6.3-HAM2.3; Tegen et al., 2018; Zhang et al., 2012; Stier et al., 2005) is coupled to a full ocean model (MPIOM; Marsland et al., 2003; Jungclaus et al., 2013), and thus the sea ice cover and sea surface temperature are prognosed online. Prescribed emissions not calculated online by the aerosol module (HAM) are obtained from the same ACCMIP dataset for the ESM run as for the atmosphere-only simulations.

5.4 Results

5.4.1 Comparison to BC concentration in snow simulated in other studies

To give a first order validation of the BC concentration in snow simulated by the current model set-up, comparisons are made to the present-day concentrations published in Namazi et al. (2015) and Flanner et al. (2007) and shown in Fig. 5.1. Overall, the model compares well with the concentration simulated by previous studies, with a slight underestimation over Europe, the Tibetan plateau, and over the Eurasian Arctic when compared to Flanner et al. (2007). Compared to Namazi et al. (2015), on the other hand, ECHAM-HAM shows an overestimation that is most pronounced over North America. Disagreement between the two previous publications and the current simulation is indicative of the uncertainty of the simulated values. However, the general order of magnitude agreement between the studies is notable considering possible model differences in the simulated meteorology. When compared to measurements reported in Doherty et al. (2010), a general agreement can also be found, although the comparison is largely qualitative without rigorous co-location of the sampling sites and times.

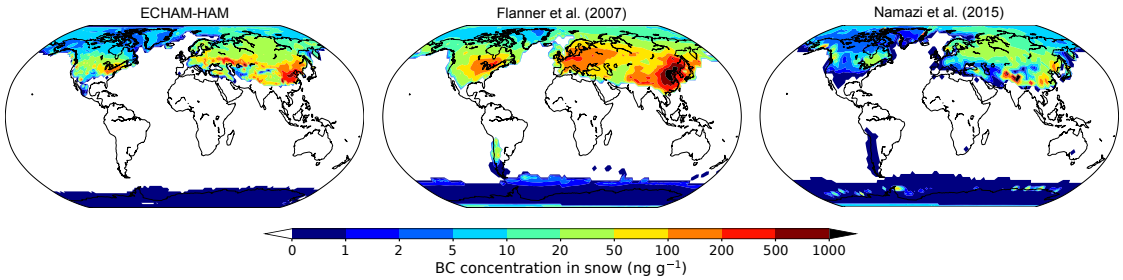

Figure 5.1: BC concentration in snow as simulated by the current model (left, from the "BCinSnow_1yr" simulation) and from Flanner et al. (2007) (middle, for the year 1998) and Namazi et al. (2015) (right, averaged over the years 2000 to 2009). Note that the BC concentration in snow plotted for ECHAM-HAM is only averaged over time steps where the snow depth is greater than 5 mm. The reasoning behind this analysis procedure is discussed in Sect. 5.4.3.

5.4.2 Global seasonal impacts

On the global scale, the seasonal mean instantaneous decrease in surface albedo lies in the 0.001 to 0.005 range, with local peak decreases of up to 0.02 and 0.03 found in north-eastern China during boreal winter and along coastal regions in Greenland during summer, respectively. As can be noted in Fig. 5.2, a poleward shift of the instantaneous radiative forcing due to deposited BC in snow can be observed as the latitudinal extent of available incoming solar radiation moves poleward. This coincides also with the melting of snow at the surface. While the trend is most pronounced in the Northern Hemisphere, a symmetric pattern can also be observed in the Southern Hemisphere, though with weaker decreases in surface albedo overall due to the lower BC burden and with no observable radiative forcing during austral autumn and winter due to the limited coverage of snow-covered landmass or sea ice reaching equatorward of the Antarctic Circle. Aside from some localized peaks, the instantaneous clear-sky shortwave (SW) radiative forcing due to BC deposited on snow-covered surfaces lies in the range of 0.01 to 0.5 W m^{-2}, with the strongest forcing during spring/summer and the weakest forcing in autumn.

When the atmosphere is allowed to respond freely to the initial forcing (by comparing the "BCinSnow" and "noBCinSnow" simulations), the resulting differences in the surface albedo and net surface radiative balance can be dominated by internal variability in the system (bottom two rows in Fig. 5.2). For the surface albedo, variations in snowfall occurring as part of the year-to-year variability can lead to a stronger signal in the difference in mean surface albedo than that induced by the darkening of snow by deposited BC. As none of the changes is statistically significant, one cannot deduce any possible linkage between the initial perturbation at the surface due to the deposited BC and the change in snowfall rate through any feedback processes. For changes in the clear-sky SW radiative balance at the surface, on the other hand, large differences can be noted to result from variations in the atmospheric aerosol burden. This is particularly notable for regions highly influenced by dust aerosol (e.g. downstream of the Sahara desert and of Australia), which has a strong variability associated with its sensitivity to wind speeds (Tegen et al., 2002).

Despite the overall lack to statistical significance due to the weak signal in the face of strong background variability, one region which shows a consistent pattern in the instantaneous forcing as well as in the effective radiative forcing (ERF) that accounts for feedbacks in the atmosphere, is the Arctic during late spring and early summer (Fig. 5.2). Possible explanations for this include the lack of strong forcing agents and the important

role of surface properties to the local climate system in the Arctic. While a strong signal can also be noted near major source regions in China and Russia during boreal winter, the focus of the current study is placed on the Arctic. Thus in the subsequent sections, a more detailed analysis is performed for the Arctic during the melting season (April to June).

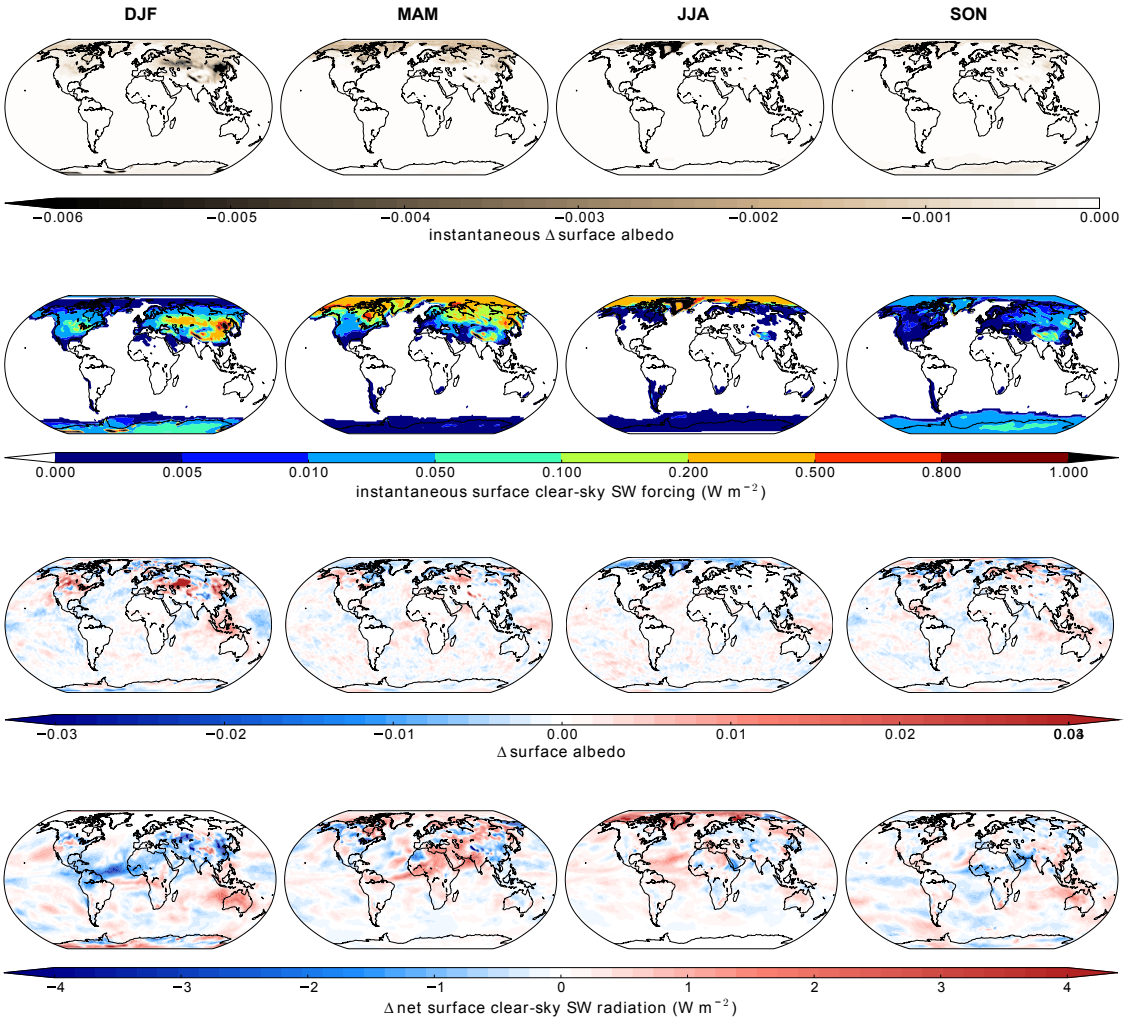

Figure 5.2: 20-year seasonal mean instantaneous change in surface albedo (top row), instantaneous surface clear-sky radiative forcing (second row), difference in surface albedo between the "BCinSnow" and "noBCinSnow" simulations (third row), and the respective difference in the clear-sky surface net SW radiation (bottom row). Statistical significance at the 90 % level but following the stricter Wilks (2016) method for controlling the false discovery rate for data with moderate to strong spatial correlations (which results in temporally variable but overall much stricter significance level) is plotted in hatches for all properties except that shown in the second row.

5.4.3 Accumulation of BC in the surface snow layer

The mass of BC transported and deposited into the Arctic region (on the order of 10^{-2} to 10^{-1} mg per month) is in general at least one order of magnitude lower than the amount deposited in lower latitudes. The property which is most relevant for consideration of its

impact on the snow albedo, however, is the concentration of BC in the top snow layer. As described in Sect. 5.2.1, this property in turn depends on the in- and out-fluxes of both BC and snow on the surface. Given a relatively steady (in terms of the order of magnitude) influx of BC from the lower latitudes, the concentration of BC on the surface is largely controlled by the snowfall and snow melt rates. Increased fresh snowfall dilutes the relative concentration of BC in the surface snow layer, while snow melt increases the concentration as the mass of snow removed is more than that of the BC. Thus the strongest impact of deposited BC on the surface snow albedo occurs in the Arctic during the late spring melting season (April to June). The monthly mean BC concentration in snow for these three months is therefore shown in Fig. 5.3 along with properties that control this concentration.

Firstly, it can be noted that during the month of April, the melting season is just beginning in the Arctic region, with snow mass decreasing in Alaska, Canada (south of the Canadian Arctic archipelago), and northern Europe, while over the Arctic Ocean, northern Siberia, and Greenland, the net flux of snow is still positive. This trend is reflected in the mass of BC in the top snow layer (at most the top 2 cm), where a greater amount can be noted in regions with higher snow melt (Fig. 5.3). This is resulting from the accumulation of BC at the surface due to inefficient scavenging by the melted snow and from the absence of fresh snowfall.

A similar correspondence between the net snow flux and the surface BC mass burden can be observed in the subsequent months, with the melting region moving poleward each month. While a general trend of a poleward shift and increase in BC-in-snow concentration can also be noted, the direct relationship cannot always be clearly identified. In particular, during the month of May, a sharp decrease in the BC-in-snow concentration can be observed when moving from land to sea ice regions, despite a higher BC mass in the top snow layer over sea ice. Due to the fast-changing surface conditions during this time of the year, a high BC-in-snow concentration can dominate over land where very little snow is left at the end of the month. This can occur despite a relatively moderate monthly mean snow depth in some regions. A relatively low BC mass in the top snow layer over these land regions also indicates that the surface snow layer may be completely melted away during the course of the month, thus removing completely the accumulated BC in the snow, and new snow layers may be formed within the month due to subsequent snow events. Another evidence to support this theory is the mean snow depth in the subsequent month (June), which is nearly zero everywhere over land, pointing to a depletion process occurring mostly in the previous month.

To examine the hypothesis that occurrence of a very thin snow cover at the surface is causing the observed high monthly-mean concentration of BC in snow over land as compared to that over sea ice (especially in May), an additional simulation ("BCinSnow_1yr") is performed for one year with additional diagnostic outputs. In particular, the monthly frequency of occurrence of surface snow depths greater than 5 mm and the respective mean BC-in-snow concentration diagnostic excluding the cases where the surface snow depth is thin (< 5 mm) is shown in Fig. 5.4. Here it can be seen that indeed, the regions over land with exceptionally high BC concentration in snow (greater than 200 ng g^{-1}) are where snow depths greater than 5 mm are rare. Examples include regions in northern Europe in April and over much of Canada and Siberia in May. When these time steps with BC accumulated in very thin snow over land are excluded from the analysis, the mean BC concentration in snow becomes more consistent across the entire Arctic region, with most areas having concentrations below 50 ng g^{-1}. Notably, increased occurrence of surface snow depths less than 5 mm can also be observed in the Pacific sector of the Arctic Ocean during June, but no spurious peak BC concentrations are found. Indeed, the

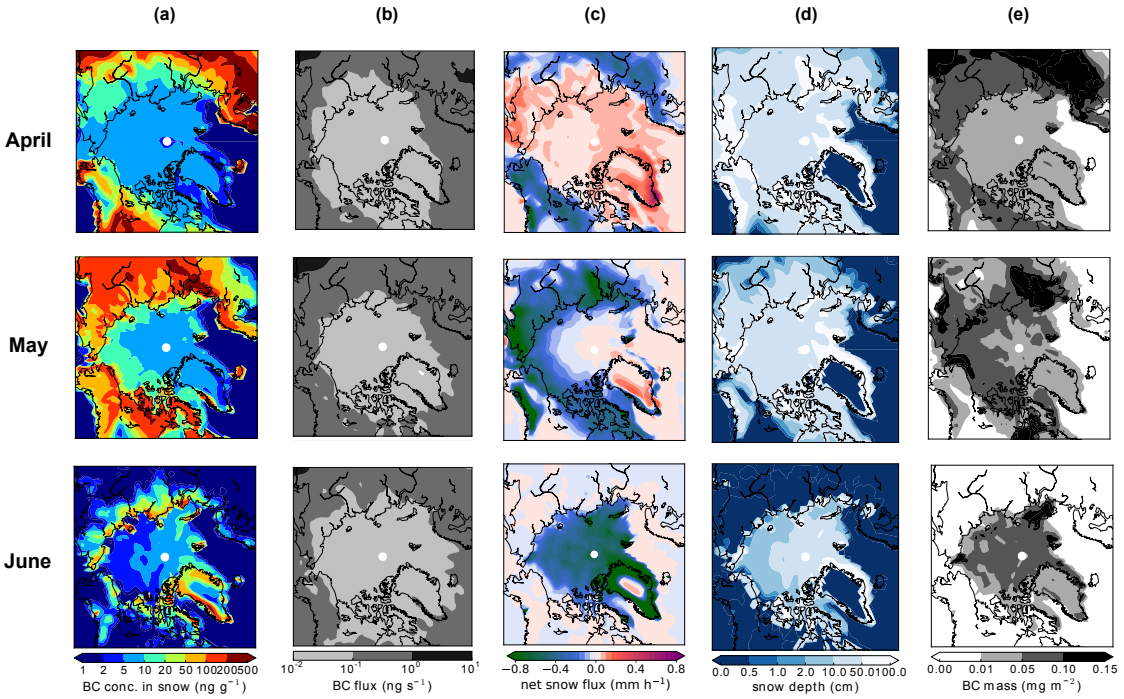

Figure 5.3: 20-year monthly mean (a) BC concentration in snow, (b) BC flux from the atmosphere to the surface, (c) net snow flux at the surface, defined as the snowfall rate minus the melting rate, (d) surface snow depth, and (e) BC mass burden in at most the top 2 cm of snow, for the month of April (top row), May (second row), and June (third row).

concentration of BC in the top snow layer remains the same regardless of the inclusion or exclusion of time steps when the snow depth is thin. This points to a possible difference in the processes controlling the net surface snow flux over land and over sea ice in our model. Indeed, further analysis (Fig. 5.5) shows that should there be any snow present on the sea ice, the snow depth is always greater than 5 mm, otherwise the sea ice remains bare. This does not appear to be driven by changes in the sea ice extent, which is prescribed in the simulation. It should be noted, however, that while this hypothesis serves to explain the results found in the current model study, its applicability in the real world would still need to be examined. Regardless, the spurious thin snow cases leading to exceptionally high BC-in-snow concentrations over land do not further translate into monthly mean changes in the surface albedo and instantaneous radiative forcing, as discussed in Sect. 5.4.4.

5.4.4 Instantaneous radiative forcing

The instantaneous change in surface albedo due to consideration of the deposited BC concentration is calculated by computing an additional diagnostic at each time step of the surface albedo without consideration of the deposited BC. While not used in the model to determine the radiative balance at the surface, this albedo value is output as a monthly average and contrasted with the actual albedo seen by the model (including consideration of the BC concentration at the surface). The resulting instantaneous change in the albedo is shown in Fig. 5.6. It reaches a maximum decrease of 0.005 over the Arctic Ocean and up to 0.03 along the western coast of Greenland. As opposed to the monthly mean BC concentration in snow, which can be dominated by spurious days with very low surface snow mass resulting in a high relative BC concentration, the change in albedo can be

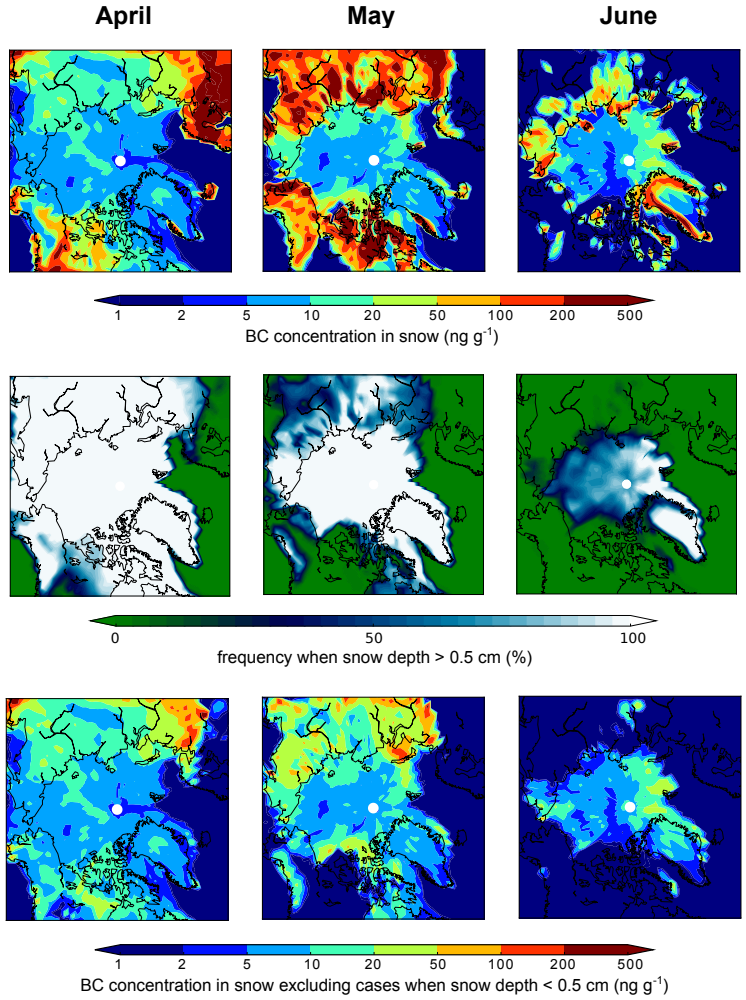

Figure 5.4: Monthly mean diagnostics from the additional "BCinSnow_1yr" simulation for the months of April (left), May (middle), and June (right). Shown in the top row is the direct monthly mean BC concentration in the top snow layer, the middle row shows the frequency when snow depth is greater than 5 mm, and in the bottom the BC concentration in snow averaged over only the time steps when the surface snow depth is greater than 5 mm.

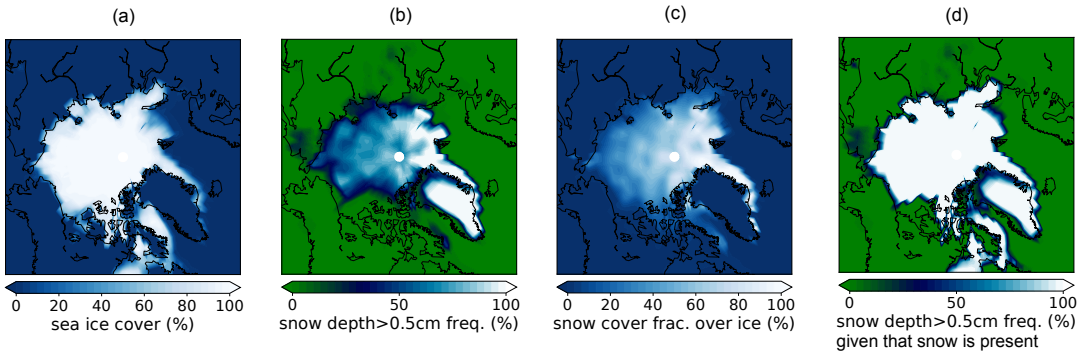

Figure 5.5: For the month of June and from the "BCinSnow_1yr" simulation, the monthly mean: (a) sea ice cover, (b) frequency of occurrence when the surface snow depth is greater than 5 mm (same plot as in Fig. 5.4), (c) snow cover fraction over sea ice, and (d) the frequency of time when snow depth is greater than 5 mm, given that there is snow present on the sea ice.

well described in general by the mean snow depths and BC mass concentration in the top snow layer in the individual months (shown in Fig. 5.3). The decrease in surface albedo can then be translated to an instantaneous surface clear-sky radiative forcing, defined as the difference in the stated radiation between one calculation with consideration of the deposited BC in the surface snow and one without, and is shown in Fig. 5.6. A forcing of up to 1.3 W m^{-2} is found over the central Arctic Ocean in June, and up to 2 W m^{-2} in isolated regions along the coastline in May. Here it can also be noted that despite the higher mean BC concentration in snow over land resulting from cases with very thin snow cover, the mean impact on the surface albedo and the instantaneous radiative forcing both peak over the sea ice regions in May, corresponding to the highest mean BC mass burden in the top snow layer in this month.

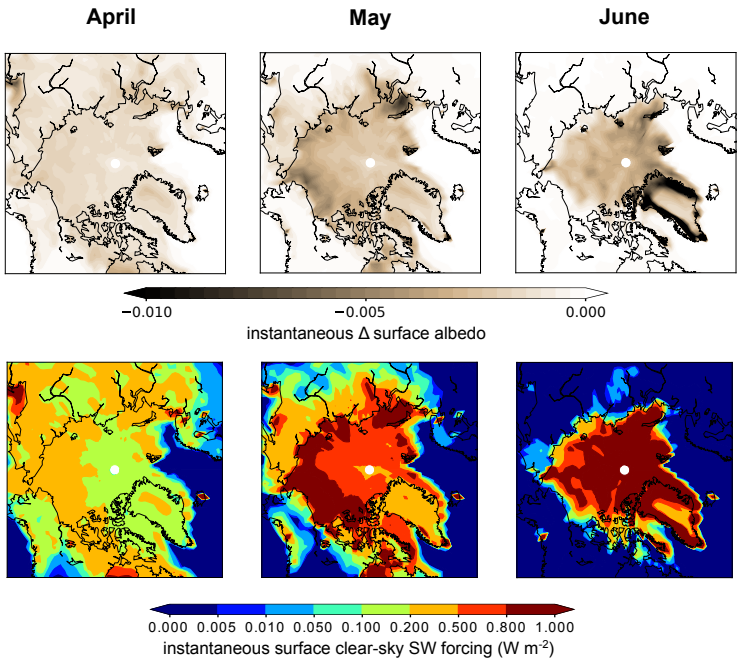

Figure 5.6: 20-year mean instantaneous change in surface albedo due to mixing of BC in the top snow layer (top row), and the respective instantaneous clear-sky surface SW forcing (bottom row), for the months of April, May and June (left, centre, and right column, respectively). Statistical significance is tested for the change in surface albedo using the Wilks (2016) method described in the caption of Fig. 5.2, but not found in any of the shown regions.

5.4.5 Changes including feedbacks and variability in the atmosphere

By comparing a simulation with consideration of the deposited BC on snow to one without (i.e. "BCinSnow"-"noBCinSnow"), the impact of the darkened snow albedo on the climate system is examined and shown in Fig. 5.7. In contrast to the instantaneous analyses discussed in Sect. 5.4.4, this includes fast feedback processes in the atmosphere (i.e. the ERF is computed) and considers other concurrent processes in the system which can mask or compound the impact of the deposited BC on snow.

Corresponding to the instantaneous clear-sky radiative forcing discussed in the previous section, the net clear-sky surface SW radiation is compared between the two separate model simulations with and without consideration of the BC concentration in snow. Here a consistent increase in the net SW radiation can be noted over the sea ice regions when

compared to the instantaneous forcing diagnostics. The difference in the radiative balance between the "BCinSnow" and "noBCinSnow" simulations is most pronounced over the Arctic Ocean in June and over the Canadian Arctic Archipelago in May, with more SW radiation retained at the surface by up to 9 W m^{-2}, except over isolated regions near the coastline in June where an increase by up to 16 W m^{-2} can be observed. This is also reflected in the decrease in surface albedo of up to 0.03 in the respective regions.

South of the Arctic Circle, however, less consistent signals in the changes in surface albedo and radiative balance can be found between the ERF and the instantaneous diagnostics discussed in the previous section (i.e. comparing Fig. 5.7 to Fig. 5.6). Rather, variability in other processes dominates in the signal. For instance, the "BCinSnow" simulation produces a lower net clear-sky SW radiation at the surface in much of Canada and Alaska in April, when compared to the "noBCinSnow" simulation. This is despite the solely positive forcing of deposited BC on snow. Rather, the lower net radiative balance is associated with an increase in surface albedo correlated to a deeper snow layer in this region in the "BCinSnow" simulation. A similarly strong cooling is found over the north-eastern tip of Siberia in May. As no statistical significance in the changes is found, however, the differences are likely simply resulting from internal variability of the system.

Additionally, when the all-sky radiative balance is considered (including the influence of clouds), the radiative impact of deposited BC in surface snow becomes largely masked by the intrinsic variability of the system (Fig. 5.9). The magnitude of the increase in the net surface SW radiation that can be attributed to the deposited BC on the surface snow based the clear-sky diagnostics is on the same order as the spatial variability resulting from differences in cloud properties between the "BCinSnow" and "noBCinSnow" simulations. For the month of April, the sign of the net radiative balance even reverses over the central Arctic Ocean between the clear-sky and all-sky diagnostics, indicating the more dominating impact of variability in clouds.

To further investigate possible feedback processes originating from the relatively weak initial forcing due to BC in snow, the difference in simulated 2-metre temperature and snow melt rate between the "BCinSnow" and "noBCinSnow" simulations are shown in Fig. 5.8. Notable increases in near-surface temperature can be noted over the Arctic Ocean in April, over the Canadian Archipelago and Greenland in May, and over much of northern Canada in June, but no statistical significance can be found. In the snow melt rate, however, a statistically significant increase on the order of 0.1 mm h^{-1} is observed over the Canadian Archipelago and north eastern Russia in May. While the signal over Canada is consistent with a decrease in surface albedo (Fig. 5.7), that over north eastern Russia rather coincides with an increase in surface albedo and snow depth, indicating a possible strong meteorological difference between the two simulations.

Overall, therefore, it can be noted that the radiative impact of the deposited BC on the snow-covered surfaces is on the same order of magnitude or even weaker than the often strong internal variability associated with clouds. Thus statistical significance is not found in any of the SW radiative balance or surface albedo comparisons (Fig. 5.7 and 5.9). Exceptions are in the changes in the net snow flux at the surface and the snow melt rate, where a significant increase (on the order of 0.1 mm h^{-1}) in snow melt (and thus decrease in net surface snow flux) can be observed in May, as well as the converse signal in June over the Canadian Arctic Archipelago (Fig. 5.7).

5.4.6 Future vs. present day

To investigate potential changes in the impact of BC deposition on snow, analyses of the instantaneous radiative forcing are performed for a 55-year simulation with an earth-system model following the RCP8.5 scenario, as described in Sect. 5.3. 10-year mean

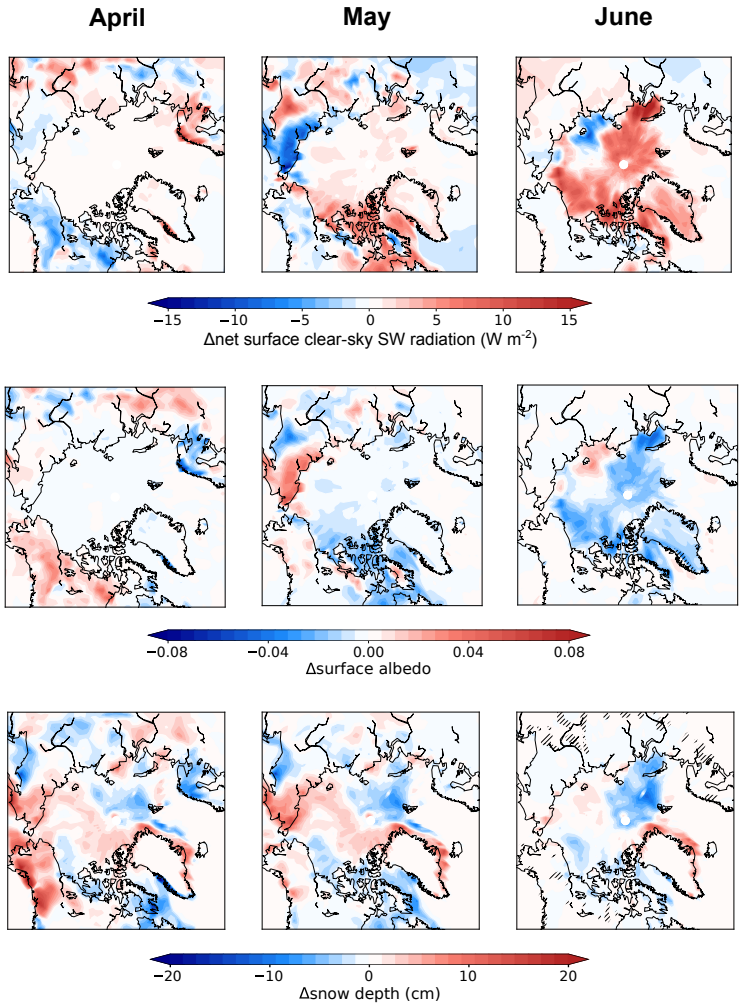

Figure 5.7: Impact of BC deposited on snow surfaces diagnosed as the 20-year mean value from the "BCinSnow" simulation minus that from the "noBCinSnow" simulation. Shown are the difference in clear-sky SW radiation balance (ERF) at the surface (top row), the difference in surface albedo (middle row), and the difference in snow depth (bottom row), for the months of April to June (left to right column). Hatching indicates statistical significance tested using the Wilks (2016) method described in the caption of Fig. 5.2.

analyses are performed for the period from 2005 to 2014, defined as the present day (PD), and for 2045 to 2054, defined as the future, and shown in Fig. 5.10 for the three late spring to early summer months when the strongest forcing in the Arctic is found. Here a decrease in both the magnitude and spatial coverage of the instantaneous radiative forcing can be noted. Aside from the expected decrease in spatial coverage of the forcing due to decreased sea ice cover in the future, contribution also comes from shrinking of the surface snow cover, as can be recognized in the area where non-zero radiative forcing extends over land in the individual monthly comparisons.

In areas covered by snow in both the PD and the future, however, a general decrease in the instantaneous forcing can also be found. This is associated with a statistically significant decrease in the BC burden in the top layer (up to 2 cm) of snow, as shown in Fig. 5.11. While the RCP scenario predicts a decrease in the global mean anthropogenic emissions of BC following economic and technological developments, the influx of BC from the atmosphere to the surface does not show statistically significant changes in the Arctic

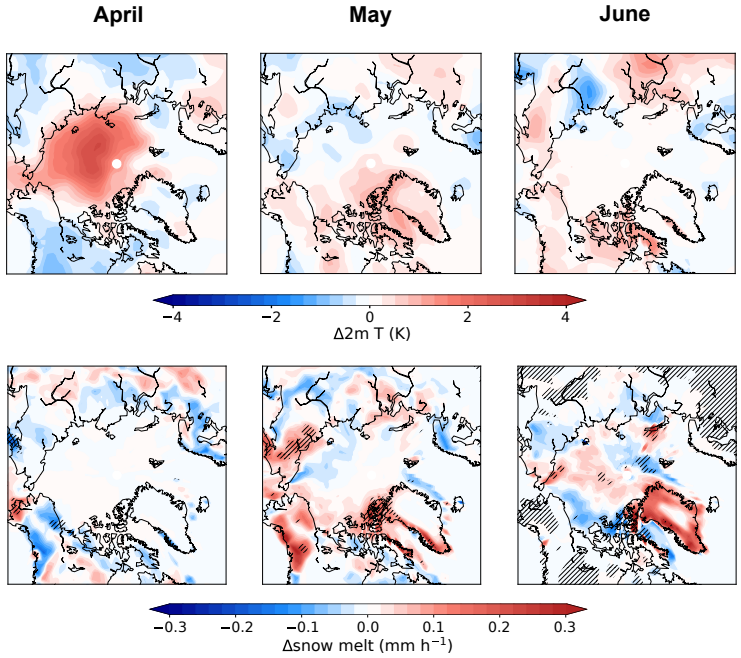

Figure 5.8: Difference in the 2-metre temperature (top row) and snow melt rate (bottom row; converted from a mass melt rate using a constant snow density of 300 kg m^{-3}) due to consideration of BC in snow (diagnosed as the 20-year mean value from the "BCinSnow" simulation minus that from the "noBCinSnow" simulation) for the three melting season months. Hatching indicates statistically significant differences following the Wilks (2016) method for significance testing of data with moderate to strong spatial correlation, as described in the caption of Fig. 5.2.

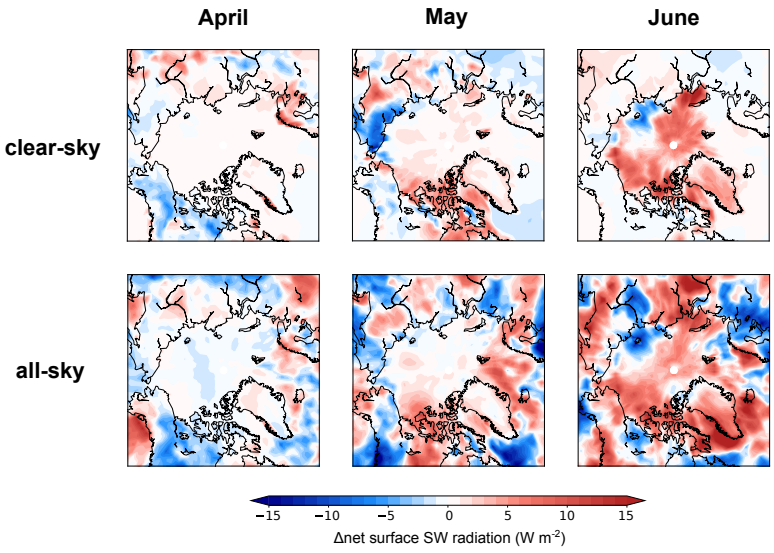

Figure 5.9: 20-year mean difference ("BCinSnow"-"noBCinSnow") in the net SW radiation at the surface under clear-sky (top row) and all-sky (bottom row) conditions for, from left to right, April, May, and June.

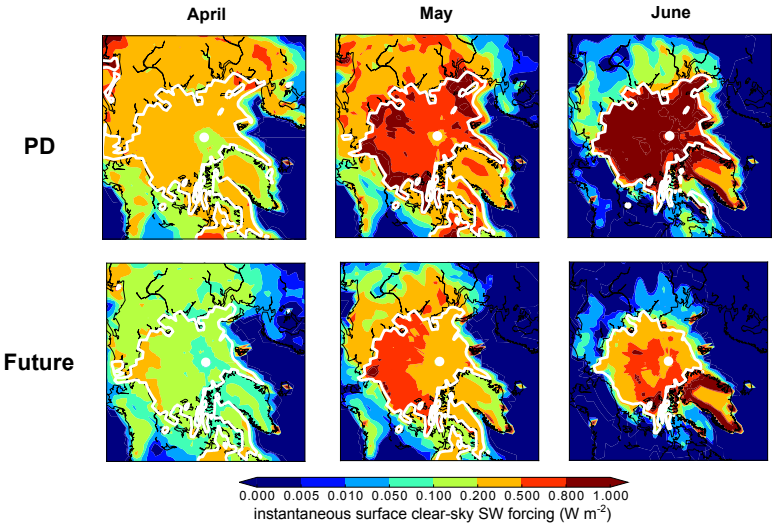

Figure 5.10: Instantaneous clear-sky surface SW radiative forcing from the ESM simulation for the months of April, May, and June, averaged over ten year periods centered around 2010 for the present day case (top row) and centered around 2050 for the future case (bottom row). The white contour indicates the spatial extent of sea ice defined as grid boxes with more than 50 % sea ice cover.

between PD and the future. Since aerosol is mostly transported from lower latitudes, the influx of BC into the Arctic can be dominated by variability in the transport patterns and biased by relatively extreme cases. For the months of May and June, the monthly mean influx even shows an increase (though not significant) in the future. Changes in the snow fluxes, on the other hand, are driven by an increase in the melting rate especially over the Arctic Ocean in May and June, while in lower latitudes, the net change is positive due to the decrease in snow melt resulting from the decrease in overall snow cover. Neither the changes in the BC influx nor that in the net surface snow flux, however, can clearly explain the observed decrease in BC concentration in the top surface snow layer.

5.5 Conclusions

In the current study, darkening effects of deposited BC on snow covered surfaces are implemented into the ECHAM-HAM model. The instantaneous as well as more long term impacts are investigated for the Arctic region during melting season (April to June). A general decrease of up to 0.005 in surface albedo over the Arctic sea ice is found during May and June, which corresponds to an instantaneous clear-sky SW forcing at the surface of up to 1.3 W m^{-2}. When feedback processes and internal variability of the system are considered, the change in the clear-sky SW radiative balance at the surface reaches up to 9 W m^{-2}, most pronounced over the Canadian Arctic Archipelago in May and over the Arctic Ocean in June. This in turn corresponds to albedo decreases of up to 0.03. Changes in neither of the properties is found to be statistically significant, however, and the signal blends into the background variability when clouds are also considered in the radiative balance diagnostics (all-sky case). When comparing the instantaneous forcing in the PD with that in the future (2050), a decrease in the forcing due to the presence of BC in surface snow can be observed. In addition to decreased spatial extent of the forcing resulting from decreased sea ice and snow cover in the future, a decrease in magnitude of the forcing can also be noted, due to a statistically significant decrease in BC concentration

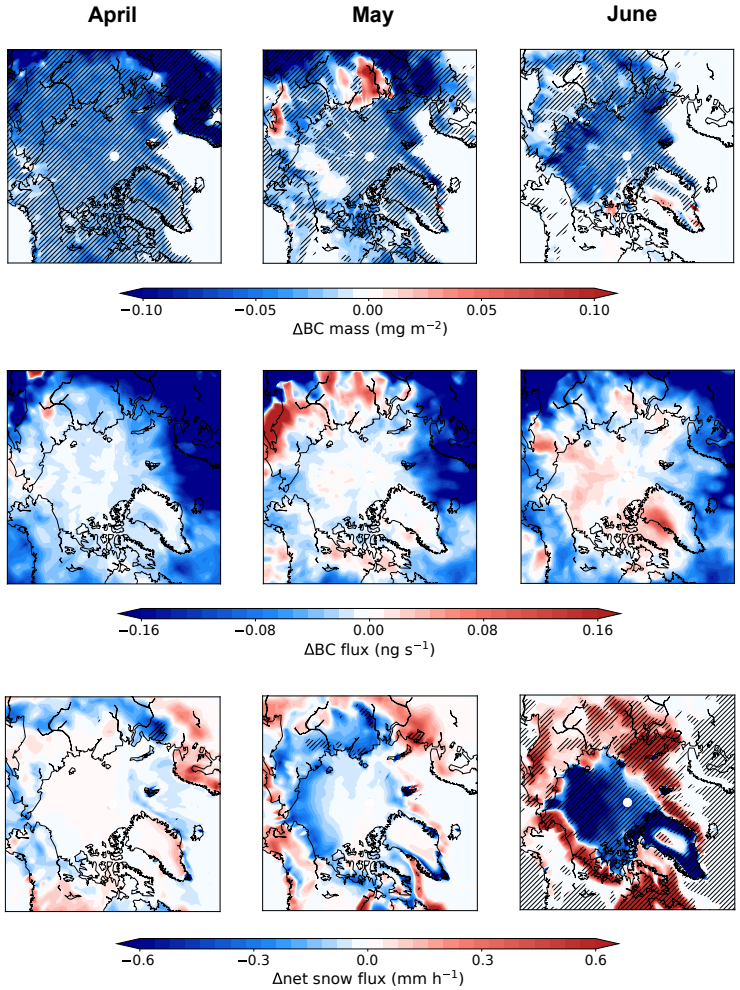

Figure 5.11: For the months of April to June (left to right), the changes (future-PD) in the mass of BC contained in the topmost snow layer (at most the top 2 cm; top row), the influx of BC from the atmosphere to the surface (second row), and the net surface snow flux defined as the snowfall rate minus the snow melt rate (bottom row). Hatches indicate statistically significant differences between the future and PD following the Wilks (2016) method as described in the caption of Fig. 5.2. It should be noted that much of the increase in net snow flux outside of the Arctic Ocean is associated with a decrease in snow melt as there is in general less snow available for melting in these regions during this time of year in the future.

in the surface snow layer. This change in BC concentration, however, cannot be clearly attributed to either the changes in influx of BC from the atmosphere, or the net flux of snow at the surface. Future increases in Arctic BC emissions due to increased shipping in the Arctic Ocean is not considered in the current study, but is discussed in a separate study by Gilgen et al. (2018) where the current implementation of the BC impact on surface albedo is used. There, an increase in BC deposition on snow in the Arctic is found, which results in a slight local warming in early autumn.

Despite statistical insignificance of the changes in surface albedo and SW radiative balance due to deposited BC on snow surfaces when investigated on a global scale, various previous studies have found BC in snow to be highly relevant in regulating the hydrological cycle in mountainous regions, where the source of water during spring and summer is often originating from melting of snow in high elevation regions (e.g. Qian et al., 2011; Wu et al., 2018). Indeed, signals over the Tibetan plateau can also be identified in our global analysis of the albedo and radiative balance changes (Fig. 5.2), though without statistical significance. Thus despite the current finding of a weak global significance of BC in snow due to dominating variability in other processes, darkening of snow surfaces due to deposited BC should not be disregarded as a potentially important process, especially at the regional and local scale.

Chapter 6

Summary and outlook

6.1 Summary

In this thesis, aerosol-induced cloud and climate processes are investigated with the global aerosol-climate model ECHAM6.3-HAM2.3 and the earth system model MPI-ESM1.2-HAM. Focus is placed on processes involving aerosols that may be important in the Arctic environment, in the present day or in the future. In particular, two main aspects are examined in detail: heterogeneous ice nucleation in mixed-phase clouds and the darkening effects of BC deposited on snow.

In terms of heterogeneous ice nucleation, interest for the Arctic is mainly placed on potential changes in the future due to increased local emission from the exposed ocean surface, following sea ice retreat. For this, a sensitivity analysis is first performed on the relevance of MOA as an ice nucleating particle under present day conditions on the global scale. Different factors contributing to differences in the emission rate of MOA are investigated, and when a chlorophyll-based parametrisation is used (as is the case for all parametrisations examined), the strongest dependence stems from using modelled chlorophyll concentrations as opposed to satellite observations. Regardless, when compared to dust as an INP on the global scale, the amount of immersed particles frozen is more strongly controlled by the ice activity of the relevant aerosol species rather than its abundance. Thus also when comparing the relative contribution of each INP species over a time span, a strong dependence is found on the choice of ice nucleation parametrisation for each species. In particular, this varies with the onset temperature of each parametrisation. When the case with the strongest relative contribution from MOA is investigated, an increase in the zonal mean ICNC and frequency of cloud ice occurrence is observed in the high latitude regions near the surface during their respective summer months, when the temperature is too warm for formation of ice crystals through other processes included in the model. On the annual average, this also leads to a slight but consistent (throughout the year) decrease in ice crystal radii near the surface in polar regions, due to nucleation of ice crystals near the surface. This decreases the average size of ice crystals as those formed higher up in the atmosphere would have grown to larger sizes during sedimentation. Overall, however, forcing induced by the addition of MOA as an INP is weak and does not lead to a strong impact on the radiative balance and the global climate.

Moving on to the future, changes in heterogeneous ice nucleation in the Arctic are examined relative to the present day. Impacts are found to result from changes in the aerosol concentration and shifting of the isotherms. In particular, a strong decrease in the global dust burden is found due to greening of the Sahel region and subsequent decreases in near-surface wind speeds. Local emissions of marine aerosols (SS and MOA), on the other hand, show a significant increase in the future, though the impact on the aerosol

mass concentration is largely confined to the lowest two kilometres above the surface. In terms of the number concentration, a general decrease is found in the accumulation and coarse soluble modes in the future Arctic. This can be attributed to decreases in transported aerosol aloft and possible increases in aerosol coalescence associated with warming temperatures. Together with the shifting of the isotherms, heterogeneous ice nucleation is found to decrease in the Arctic in the future, with the exception of near the surface in summer, where an increase in freezing rate is observed due to the increased availability of MOA. Ice nucleation occurrence at warmer temperatures is also found more frequently in autumn and winter due to shifting of the isotherms. When both aerosol and environmental changes are considered, a compensating effect is found in autumn near the surface, as diminishing INP ice activity due to warming temperatures occurs concurrently with an increase in INP concentration due to enhanced local emissions of MOA.

To consider the impact of BC deposition on the surface snow albedo, snow mass at the surface and accumulation of BC in the top 2 cm of the snow layer is tracked. The corresponding albedo of the snow is determined based on the concentration of BC in the snow and the snow age, which is then used for interpolating between offline calculated albedos from a single-layer implementation of the SNICAR model. When its effects are considered, BC in snow leads to most consistent effects in the Arctic during May and June, with instantaneous albedo decreases of up to 0.005 and an instantaneous clear-sky SW forcing of up to 1.3 W m^{-2} at the surface. When feedback processes are considered, this results in a clear-sky ERF of up to 9 W m^{-2}. The impacts are, however, not statistically significant due to the same order of magnitude or stronger contributions from internal variability associated with clouds. When comparing the impact of BC in snow in the present day to that in the future, a weaker instantaneous SW forcing is found overall, with a decrease in both the spatial extent and the magnitude. The former is expected due to decreased snow and sea ice cover associated with global warming, while the latter is associated with a lower concentration of BC in the top snow layer in the future. This does not, however, include consideration for a possible increase in local BC emissions from Arctic ship traffic in the future.

6.2 Outlook

A common theme in the results found in this thesis is the weak influence of the processes considered on the global climate. The reasons behind the weak sensitivity, however, varies. For heterogeneous ice nucleation, it has been found that the process contributes very little to the model ice water content (Ickes et al., in preparation). Rather, most of the ice crystals found in the model originate from homogeneously formed sedimenting ice. Considering the strong influence of this aspect on the model sensitivity to heterogeneous ice nucleation, it is important to examine its validity in the real world. More specifically, it would be of great interest and essential for further studies on global modelling of heterogeneous ice nucleation to quantify the global contribution of ice crystals from the different ice formation processes. Considering the great uncertainty in also other ice formation processes such as ice multiplication/secondary ice production (e.g. Hallett and Mossop, 1974), it may be a good first step, especially for validating the ECHAM-HAM model, to quantify the global frequency of occurrence of seeder-feeder processes. An initial attempt at investigating this has already started through the employment of a student for a short project on analysing satellite data for overlapping cirrus and mixed-phase clouds, but further effort is warranted to continue the investigation.

For BC deposited on snow, the weak influence on the overall climate is due to its weak forcing which is in turn largely masked by internal variability in other atmospheric

processes. This does not, however, rule out its importance on a regional scale, especially for the hydrological cycle in mountainous regions (e.g. Wu et al., 2018). Thus a more regional to local perspective would be recommended for further studies on this topic.

While some of the work contained in this thesis includes the first scientific studies utilizing the newly coupled MPI-ESM-HAM model, this mostly translates to performing a transient future simulation and examining differences between the present day and the future. The strength of the ESM, however, lies rather in its ability to include feedback processes that involve the ocean and sea ice. To continue in the investigation of the same processes, ensembles of ESM simulations can be performed with and without the process of interest (e.g. MOA as INP or BC in surface snow) to examine their potential influence on the sea ice cover. As the forcing from these processes is generally weak (especially in this model), however, a large ensemble of runs would likely be required to detect a signal amidst the noise from internal variability of the system.

Bibliography

Abdul-Razzak, H. and Ghan, S. J.: A parameterization of aerosol activation: 2. Multiple aerosol types, Journal of Geophysical Research: Atmospheres, 105, 6837–6844, doi: 10.1029/1999JD901161, 2000.

Acosta Navarro, J. C., Varma, V., Riipinen, I., Seland, Ø., Kirkevåg, A., Struthers, H., Iversen, T., Hansson, H.-C., and Ekman, A. M. L.: Amplification of Arctic warming by past air pollution reductions in Europe, Nature Geoscience, 9, 277–281, doi: 10.1038/ngeo2673, 2016.

Alterskjær, K., Kristjánsson, J. E., and Hoose, C.: Do anthropogenic aerosols enhance or suppress the surface cloud forcing in the Arctic?, Journal of Geophysical Research: Atmospheres, 115, doi:10.1029/2010JD014015, 2010.

Atkinson, J. D., Murray, B. J., Woodhouse, M. T., Whale, T. F., Baustian, K. J., Carslaw, K. S., Dobbie, S., O'Sullivan, D., and Malkin, T. L.: The importance of feldspar for ice nucleation by mineral dust in mixed-phase clouds, Nature, 498, 355–358, doi: 10.1038/nature12278, 2013.

Barrie, L. A.: Arctic Aerosols: Composition, Sources and Transport, in: Ice Core Studies of Global Biogeochemical Cycles, edited by Delmas, R. J., pp. 1–22, Springer Berlin Heidelberg, Berlin, Heidelberg, 1995.

Bathiany, S., Claussen, M., and Brovkin, V.: CO2-Induced Sahel Greening in Three CMIP5 Earth System Models, Journal of Climate, 27, 7163–7184, doi:10.1175/JCLI-D-13-00528.1, 2014.

Bekryaev, R. V., Polyakov, I. V., and Alexeev, V. A.: Role of Polar Amplification in Long-Term Surface Air Temperature Variations and Modern Arctic Warming, Journal of Climate, 23, 3888–3906, doi:10.1175/2010JCLI3297.1, 2010.

Bergman, T., Kerminen, V.-M., Korhonen, H., Lehtinen, K. J., Makkonen, R., Arola, A., Mielonen, T., Romakkaniemi, S., Kulmala, M., and Kokkola, H.: Evaluation of the sectional aerosol microphysics module SALSA implementation in ECHAM5-HAM aerosol-climate model, Geoscientific Model Development, 5, 845–868, doi:10.5194/gmd-5-845-2012, 2012.

Bigg, E. K.: Ice Nucleus Concentrations in Remote Areas, Journal of the Atmospheric Sciences, 30, 1153–1157, doi:10.1175/1520-0469(1973)030<1153:INCIRA>2.0.CO;2, 1973.

Bonsang, B., Polle, C., and Lambert, G.: Evidence for marine production of isoprene, Geophysical Research Letters, 19, 1129–1132, doi:10.1029/92GL00083, 1992.

Brinkop, S. and Roeckner, E.: Sensitivity of a general circulation model to parameterizations of cloud–turbulence interactions in the atmospheric boundary layer, Tellus A, 47, 197–220, doi:10.1034/j.1600-0870.1995.t01-1-00004.x, 1995.

Brock, C. A., Cozic, J., Bahreini, R., Froyd, K. D., Middlebrook, A. M., McComiskey, A., Brioude, J., Cooper, O. R., Stohl, A., Aikin, K. C., de Gouw, J. A., Fahey, D. W., Ferrare, R. A., Gao, R.-S., Gore, W., Holloway, J. S., Hübler, G., Jefferson, A., Lack, D. A., Lance, S., Moore, R. H., Murphy, D. M., Nenes, A., Novelli, P. C., Nowak, J. B., Ogren, J. A., Peischl, J., Pierce, R. B., Pilewskie, P., Quinn, P. K., Ryerson, T. B., Schmidt, K. S., Schwarz, J. P., Sodemann, H., Spackman, J. R., Stark, H., Thomson, D. S., Thornberry, T., Veres, P., Watts, L. A., Warneke, C., and Wollny, A. G.: Characteristics, sources, and transport of aerosols measured in spring 2008 during the aerosol, radiation, and cloud processes affecting Arctic Climate (ARCPAC) Project, Atmospheric Chemistry and Physics, 11, 2423–2453, doi:10.5194/acp-11-2423-2011, 2011.

Brovkin, V., Boysen, L., Raddatz, T., Gayler, V., Loew, A., and Claussen, M.: Evaluation of vegetation cover and land-surface albedo in MPI-ESM CMIP5 simulations, Journal of Advances in Modeling Earth Systems, 5, 48–57, doi:10.1029/2012MS000169, 2013.

Browse, J., Carslaw, K. S., Mann, G. W., Birch, C. E., Arnold, S. R., and Leck, C.: The complex response of Arctic aerosol to sea-ice retreat, Atmospheric Chemistry and Physics, 14, 7543–7557, doi:10.5194/acp-14-7543-2014, 2014.

Burkhart, J. F., Bales, R. C., McConnell, J. R., and Hutterli, M. A.: Influence of North Atlantic Oscillation on anthropogenic transport recorded in northwest Greenland ice cores, Journal of Geophysical Research: Atmospheres, 111, doi:10.1029/2005JD006771, 2006.

Burrows, S. M., Hoose, C., Pöschl, U., and Lawrence, M. G.: Ice nuclei in marine air: biogenic particles or dust?, Atmospheric Chemistry and Physics, 13, 245–267, doi:10.5194/acp-13-245-2013, 2013.

Burrows, S. M., Ogunro, O., Frossard, A. A., Russell, L. M., Rasch, P. J., and Elliott, S. M.: A physically based framework for modeling the organic fractionation of sea spray aerosol from bubble film Langmuir equilibria, Atmospheric Chemistry and Physics, 14, 13 601–13 629, doi:10.5194/acp-14-13601-2014, 2014.

Caroline, L. and Keith, B. E.: Source and evolution of the marine aerosol—A new perspective, Geophysical Research Letters, 32, doi:10.1029/2005GL023651, 2005.

Ceburnis, D., O'Dowd, C. D., Jennings, G. S., Facchini, M. C., Emblico, L., Decesari, S., Fuzzi, S., and Sakalys, J.: Marine aerosol chemistry gradients: Elucidating primary and secondary processes and fluxes, Geophysical Research Letters, 35, doi:10.1029/2008GL033462, 2008.

Cesana, G., Kay, J. E., Chepfer, H., English, J. M., and de Boer, G.: Ubiquitous low-level liquid-containing Arctic clouds: New observations and climate model constraints from CALIPSO-GOCCP, Geophysical Research Letters, 39, doi:10.1029/2012GL053385, 2012.

Chang, R. Y.-W., Leck, C., Graus, M., Müller, M., Paatero, J., Burkhart, J. F., Stohl, A., Orr, L. H., Hayden, K., Li, S.-M., Hansel, A., Tjernström, M., Leaitch, W. R., and Abbatt, J. P. D.: Aerosol composition and sources in the central Arctic Ocean during ASCOS, Atmospheric Chemistry and Physics, 11, 10 619–10 636, doi:10.5194/acp-11-10619-2011, 2011.

Coluzza, I., Creamean, J., Rossi, M. J., Wex, H., Alpert, P. A., Bianco, V., Boose, Y., Dellago, C., Felgitsch, L., Fröhlich-Nowoisky, J., Herrmann, H., Jungblut, S., Kanji, Z. A., Menzl, G., Moffett, B., Moritz, C., Mutzel, A., Pöschl, U., Schauperl, M., Scheel, J., Stopelli, E., Stratmann, F., Grothe, H., and Schmale, D. G.: Perspectives on the Future of Ice Nucleation Research: Research Needs and Unanswered Questions Identified from Two International Workshops, Atmosphere, 8, doi:10.3390/atmos8080138, 2017.

Connolly, P. J., Möhler, O., Field, P. R., Saathoff, H., Burgess, R., Choularton, T., and Gallagher, M.: Studies of heterogeneous freezing by three different desert dust samples, Atmospheric Chemistry and Physics, 9, 2805–2824, doi:10.5194/acp-9-2805-2009, 2009.

Croft, B., Lohmann, U., Martin, R. V., Stier, P., Wurzler, S., Feichter, J., Hoose, C., Heikkilä, U., van Donkelaar, A., and Ferrachat, S.: Influences of in-cloud aerosol scavenging parameterizations on aerosol concentrations and wet deposition in ECHAM5-HAM, Atmospheric Chemistry and Physics, 10, 1511–1543, doi:10.5194/acp-10-1511-2010, 2010.

Curry, J. A.: Interactions among aerosols, clouds, and climate of the Arctic Ocean, Science of The Total Environment, 160-161, 777 – 791, doi:10.1016/0048-9697(95)04411-S, 1995.

Curry, J. A., Schramm, J. L., Rossow, W. B., and Randall, D.: Overview of Arctic Cloud and Radiation Characteristics, Journal of Climate, 9, 1731–1764, doi:10.1175/1520-0442(1996)009<1731:OOACAR>2.0.CO;2, 1996.

de Boer, G., Eloranta, E. W., and Shupe, M. D.: Arctic Mixed-Phase Stratiform Cloud Properties from Multiple Years of Surface-Based Measurements at Two High-Latitude Locations, Journal of the Atmospheric Sciences, 66, 2874–2887, doi:10.1175/2009JAS3029.1, 2009.

DeMott, P. J., Hill, T. C. J., McCluskey, C. S., Prather, K. A., Collins, D. B., Sullivan, R. C., Ruppel, M. J., Mason, R. H., Irish, V. E., Lee, T., Hwang, C. Y., Rhee, T. S., Snider, J. R., McMeeking, G. R., Dhaniyala, S., Lewis, E. R., Wentzell, J. J. B., Abbatt, J., Lee, C., Sultana, C. M., Ault, A. P., Axson, J. L., Diaz Martinez, M., Venero, I., Santos-Figueroa, G., Stokes, M. D., Deane, G. B., Mayol-Bracero, O. L., Grassian, V. H., Bertram, T. H., Bertram, A. K., Moffett, B. F., and Franc, G. D.: Sea spray aerosol as a unique source of ice nucleating particles, Proceedings of the National Academy of Sciences, 113, 5797–5803, doi:10.1073/pnas.1514034112, 2016.

Doherty, S. J., Warren, S. G., Grenfell, T. C., Clarke, A. D., and Brandt, R. E.: Light-absorbing impurities in Arctic snow, Atmospheric Chemistry and Physics, 10, 11 647–11 680, doi:10.5194/acp-10-11647-2010, 2010.

Dou, T.-F. and Xiao, C.-D.: An overview of black carbon deposition and its radiative forcing over the Arctic, Advances in Climate Change Research, 7, 115 – 122, doi:10.1016/j.accre.2016.10.003, including special topic on atmospheric black carbon and its effects on cryosphere, 2016.

Dreischmeier, K., Budke, C., Wiehemeier, L., Kottke, T., and Koop, T.: Boreal pollen contain ice-nucleating as well as ice-binding 'antifreeze' polysaccharides, Scientific Reports, 7, doi:10.1038/srep41890, 2017.

Eckhardt, S., Stohl, A., Beirle, S., Spichtinger, N., James, P., Forster, C., Junker, C., Wagner, T., Platt, U., and Jennings, S. G.: The North Atlantic Oscillation controls air pollution transport to the Arctic, Atmospheric Chemistry and Physics, 3, 1769–1778, doi:10.5194/acp-3-1769-2003, 2003.

Engels, J.: The impact of black carbon aerosol induced snow darkening on the radiation balance in ECHAM6: Quantifying the contribution of wildfires for present and future conditions, Ph.D. thesis, Universität Hamburg, Hamburg, doi:10.17617/2.2308910, 2016.

Facchini, M. C., Rinaldi, M., Decesari, S., Carbone, C., Finessi, E., Mircea, M., Fuzzi, S., Ceburnis, D., Flanagan, R., Nilsson, E. D., de Leeuw, G., Martino, M., Woeltjen, J., and O'Dowd, C. D.: Primary submicron marine aerosol dominated by insoluble organic colloids and aggregates, Geophysical Research Letters, 35, doi:10.1029/2008GL034210, 2008.

Fan, J., Ovtchinnikov, M., Comstock, J. M., McFarlane, S. A., and Khain, A.: Ice formation in Arctic mixed-phase clouds: Insights from a 3-D cloud-resolving model with size-resolved aerosol and cloud microphysics, Journal of Geophysical Research: Atmospheres, 114, doi:10.1029/2008JD010782, 2009.

Fan, J., Wang, Y., Rosenfeld, D., and Liu, X.: Review of Aerosol–Cloud Interactions: Mechanisms, Significance, and Challenges, Journal of the Atmospheric Sciences, 73, 4221–4252, doi:10.1175/JAS-D-16-0037.1, 2016.

Flanner, M. G.: Arctic climate sensitivity to local black carbon, Journal of Geophysical Research: Atmospheres, 118, 1840–1851, doi:10.1002/jgrd.50176, 2013.

Flanner, M. G., Zender, C. S., Randerson, J. T., and Rasch, P. J.: Present-day climate forcing and response from black carbon in snow, Journal of Geophysical Research: Atmospheres, 112, doi:10.1029/2006JD008003, 2007.

Flanner, M. G., Zender, C. S., Hess, P. G., Mahowald, N. M., Painter, T. H., Ramanathan, V., and Rasch, P. J.: Springtime warming and reduced snow cover from carbonaceous particles, Atmospheric Chemistry and Physics, 9, 2481–2497, doi:10.5194/acp-9-2481-2009, 2009.

Freud, E., Krejci, R., Tunved, P., Leaitch, R., Nguyen, Q. T., Massling, A., Skov, H., and Barrie, L.: Pan-Arctic aerosol number size distributions: seasonality and transport patterns, Atmospheric Chemistry and Physics, 17, 8101–8128, doi:10.5194/acp-17-8101-2017, 2017.

Fröhlich-Nowoisky, J., Hill, T. C. J., Pummer, B. G., Yordanova, P., Franc, G. D., and Pöschl, U.: Ice nucleation activity in the widespread soil fungus Mortierella alpina, Biogeosciences, 12, 1057–1071, doi:10.5194/bg-12-1057-2015, 2015.

Fu, S. and Xue, H.: The Effect of Ice Nuclei Efficiency on Arctic Mixed-Phase Clouds from Large-Eddy Simulations, Journal of the Atmospheric Sciences, 74, 3901–3913, doi:10.1175/JAS-D-17-0112.1, 2017.

Gantt, B., Meskhidze, N., Facchini, M. C., Rinaldi, M., Ceburnis, D., and O'Dowd, C. D.: Wind speed dependent size-resolved parameterization for the organic mass fraction of sea spray aerosol, Atmospheric Chemistry and Physics, 11, 8777–8790, doi:10.5194/acp-11-8777-2011, 2011.

Gantt, B., Xu, J., Meskhidze, N., Zhang, Y., Nenes, A., Ghan, S. J., Liu, X., Easter, R., and Zaveri, R.: Global distribution and climate forcing of marine organic aerosol – Part 2: Effects on cloud properties and radiative forcing, Atmospheric Chemistry and Physics, 12, 6555–6563, doi:10.5194/acp-12-6555-2012, 2012.

Ganzeveld, L., Lelieveld, J., and Roelofs, G.-J.: A dry deposition parameterization for sulfur oxides in a chemistry and general circulation model, Journal of Geophysical Research, 103, 5679–5694, doi:10.1029/97JD03077, 1998.

Garrett, T. J. and Zhao, C.: Increased Arctic cloud longwave emissivity associated with pollution from mid-latitudes, Nature, 440, 787–789, doi:10.1038/nature04636, 2006.

Garrett, T. J., Radke, L. F., and Hobbs, P. V.: Aerosol Effects on Cloud Emissivity and Surface Longwave Heating in the Arctic, Journal of the Atmospheric Sciences, 59, 769–778, doi:10.1175/1520-0469(2002)059<0769:AEOCEA>2.0.CO;2, 2002.

Garrett, T. J., Zhao, C., Dong, X., Mace, G. G., and Hobbs, P. V.: Effects of varying aerosol regimes on low-level Arctic stratus, Geophysical Research Letters, 31, doi:10.1029/2004GL019928, 2004.

Gilgen, A., Huang, W. T. K., Ickes, L., Neubauer, D., and Lohmann, U.: How important are future marine and shipping aerosol emissions in a warming Arctic summer and autumn?, Atmospheric Chemistry and Physics, 18, 10 521–10 555, doi:10.5194/acp-18-10521-2018, 2018.

Giorgetta, M. A., Jungclaus, J., Reick, C. H., Legutke, S., Bader, J., Böttinger, M., Brovkin, V., Crueger, T., Esch, M., Fieg, K., Glushak, K., Gayler, V., Haak, H., Hollweg, H., Ilyina, T., Kinne, S., Kornblueh, L., Matei, D., Mauritsen, T., Mikolajewicz, U., Mueller, W., Notz, D., Pithan, F., Raddatz, T., Rast, S., Redler, R., Roeckner, E., Schmidt, H., Schnur, R., Segschneider, J., Six, K. D., Stockhause, M., Timmreck, C., Wegner, J., Widmann, H., Wieners, K., Claussen, M., Marotzke, J., and Stevens, B.: Climate and carbon cycle changes from 1850 to 2100 in MPI-ESM simulations for the Coupled Model Intercomparison Project phase 5, Journal of Advances in Modeling Earth Systems, 5, 572–597, doi:10.1002/jame.20038, 2013a.

Giorgetta, M. A., Roeckner, E., Mauritsen, T., Bader, J., Crueger, T., Esch, M., Rast, S., Kornblueh, L., Schmidt, H., Kinne, S., Hohenegger, C., Möbis, B., Krismer, T., Wieners, K.-H., and Stevens, B.: The atmospheric general circulation model ECHAM6 - Model description, doi:10.17617/2.1810480, 2013b.

Gorbunov, B., Baklanov, A., Kakutkina, N., Windsor, H., and Toumi, R.: Ice nucleation on soot particles, Journal of Aerosol Science, 32, 199 – 215, doi:10.1016/S0021-8502(00)00077-X, 2001.

Graham, R. M., Rinke, A., Cohen, L., Hudson, S. R., Walden, V. P., Granskog, M. A., Dorn, W., Kayser, M., and Maturilli, M.: A comparison of the two Arctic atmospheric winter states observed during N-ICE2015 and SHEBA, Journal of Geophysical Research: Atmospheres, 122, 5716–5737, doi:10.1002/2016JD025475, 2016.

Graversen, R. G. and Wang, M.: Polar amplification in a coupled climate model with locked albedo, Climate Dynamics, 33, 629–643, doi:10.1007/s00382-009-0535-6, 2009.

Guelle, W., Schulz, M., Balkanski, Y., and Dentener, F.: Influence of the source formulation on modeling the atmospheric global distribution of sea salt aerosol, Journal of Geophysical Research: Atmospheres, 106, 27 509–27 524, doi:10.1029/2001JD900249, 2001.

Hallett, J. and Mossop, S. C.: Production of secondary ice particles during the riming process, Nature, 249, 26–28, doi:10.1038/249026a0, 1974.

Hansen, J., Sato, M., and Ruedy, R.: Radiative forcing and climate response, Journal of Geophysical Research: Atmospheres, 102, 6831–6864, doi:10.1029/96JD03436, 1997.

Held, A., Brooks, I. M., Leck, C., and Tjernström, M.: On the potential contribution of open lead particle emissions to the central Arctic aerosol concentration, Atmospheric Chemistry and Physics, 11, 3093–3105, doi:10.5194/acp-11-3093-2011, 2011.

Holland, M. M. and Bitz, C. M.: Polar amplification of climate change in coupled models, Climate Dynamics, 21, 221–232, doi:10.1007/s00382-003-0332-6, 2003.

Hoose, C. and Möhler, O.: Heterogeneous ice nucleation on atmospheric aerosols: a review of results from laboratory experiments, Atmospheric Chemistry and Physics, 12, 9817–9854, doi:10.5194/acp-12-9817-2012, 2012.

Hoose, C., Lohmann, U., Erdin, R., and Tegen, I.: The global influence of dust mineralogical composition on heterogeneous ice nucleation in mixed-phase clouds, Environmental Research Letters, 3, 025 003, 2008.

Hoose, C., Kristjánsson, J. E., and Burrows, S. M.: How important is biological ice nucleation in clouds on a global scale?, Environmental Research Letters, 5, 024 009, doi:10.1088/1748-9326/5/2/024009, 2010.

Hu, C., Lee, Z., and Franz, B.: Chlorophyll a algorithms for oligotrophic oceans: A novel approach based on three-band reflectance difference, Journal of Geophysical Research: Oceans, 117, doi:10.1029/2011JC007395, 2012.

Huang, W. T. K., Ickes, L., Tegen, I., Rinaldi, M., Ceburnis, D., and Lohmann, U.: Global relevance of marine organic aerosol as ice nucleating particles, Atmospheric Chemistry and Physics, 18, 11 423–11 445, doi:10.5194/acp-18-11423-2018, 2018.

Huffman, J. A., Prenni, A. J., DeMott, P. J., Pöhlker, C., Mason, R. H., Robinson, N. H., Fröhlich-Nowoisky, J., Tobo, Y., Després, V. R., Garcia, E., Gochis, D. J., Harris, E., Müller-Germann, I., Ruzene, C., Schmer, B., Sinha, B., Day, D. A., Andreae, M. O., Jimenez, J. L., Gallagher, M., Kreidenweis, S. M., Bertram, A. K., and Pöschl, U.: High concentrations of biological aerosol particles and ice nuclei during and after rain, Atmospheric Chemistry and Physics, 13, 6151–6164, doi:10.5194/acp-13-6151-2013, 2013.

Hurtt, G. C., Frolking, S., Fearon, M. G., Moore, B., Shevliakova, E., Malyshev, S., Pacala, S. W., and Houghton, R. A.: The underpinnings of land-use history: three centuries of global gridded land-use transitions, wood-harvest activity, and resulting secondary lands, Global Change Biology, 12, 1208–1229, doi:10.1111/j.1365-2486.2006.01150.x, 2006.

Ickes, L., Welti, A., and Lohmann, U.: Classical nucleation theory of immersion freezing: sensitivity of contact angle schemes to thermodynamic and kinetic parameters, Atmospheric Chemistry and Physics, 17, 1713–1739, doi:10.5194/acp-17-1713-2017, 2017.

Ickes, L., Neubauer, D., and Lohmann, U.: What is triggering ice in mixed-phase clouds in ECHAM-HAM: the importance of ice nucleation, Journal of Geophysical Research, in preparation, 2018.

Ilyina, T., Six, K. D., Segschneider, J., Maier-Reimer, E., Li, H., and Núñez-Riboni, I.: Global ocean biogeochemistry model HAMOCC: Model architecture and performance as component of the MPI-Earth system model in different CMIP5 experimental realizations, Journal of Advances in Modeling Earth Systems, 5, 287–315, doi:10.1029/2012MS000178, 2013.

Inness, A., Baier, F., Benedetti, A., Bouarar, I., Chabrillat, S., Clark, H., Clerbaux, C., Coheur, P., Engelen, R. J., Errera, Q., Flemming, J., George, M., Granier, C., Hadji-Lazaro, J., Huijnen, V., Hurtmans, D., Jones, L., Kaiser, J. W., Kapsomenakis, J., Lefever, K., Leitão, J., Razinger, M., Richter, A., Schultz, M. G., Simmons, A. J., Suttie, M., Stein, O., Thépaut, J.-N., Thouret, V., Vrekoussis, M., Zerefos, C., and the MACC team: The MACC reanalysis: an 8 yr data set of atmospheric composition, Atmospheric Chemistry and Physics, 13, 4073–4109, doi:10.5194/acp-13-4073-2013, 2013.

Intrieri, J. M., Fairall, C. W., Shupe, M. D., Persson, P. O. G., Andreas, E. L., Guest, P. S., and Moritz, R. E.: An annual cycle of Arctic surface cloud forcing at SHEBA, Journal of Geophysical Research: Oceans, 107, SHE 13–1–SHE 13–14, doi:10.1029/2000JC000439, 2002a.

Intrieri, J. M., Shupe, M. D., Uttal, T., and McCarty, B. J.: An annual cycle of Arctic cloud characteristics observed by radar and lidar at SHEBA, Journal of Geophysical Research: Oceans, 107, SHE 5–1–SHE 5–15, doi:10.1029/2000JC000423, 2002b.

Iversen, T.: On the atmospheric transport of pollution to the Arctic, Geophysical Research Letters, 11, 457–460, doi:10.1029/GL011i005p00457, 1984.

Jiao, C., Flanner, M. G., Balkanski, Y., Bauer, S. E., Bellouin, N., Berntsen, T. K., Bian, H., Carslaw, K. S., Chin, M., De Luca, N., Diehl, T., Ghan, S. J., Iversen, T., Kirkevåg, A., Koch, D., Liu, X., Mann, G. W., Penner, J. E., Pitari, G., Schulz, M., Seland, Ø., Skeie, R. B., Steenrod, S. D., Stier, P., Takemura, T., Tsigaridis, K., van Noije, T., Yun, Y., and Zhang, K.: An AeroCom assessment of black carbon in Arctic snow and sea ice, Atmospheric Chemistry and Physics, 14, 2399–2417, doi:10.5194/acp-14-2399-2014, 2014.

Johnson, B. T., Shine, K. P., and Forster, P. M.: The semi-direct aerosol effect: Impact of absorbing aerosols on marine stratocumulus, Quarterly Journal of the Royal Meteorological Society, 130, 1407–1422, doi:10.1256/qj.03.61, 2006.

Jungclaus, J. H., Fischer, N., Haak, H., Lohmann, K., Marotzke, J., Matei, D., Mikolajewicz, U., Notz, D., and Storch, J. S.: Characteristics of the ocean simulations in the Max Planck Institute Ocean Model (MPIOM) the ocean component of the MPI-Earth system model, Journal of Advances in Modeling Earth Systems, 5, 422–446, doi:10.1002/jame.20023, 2013.

Kanji, Z. A., Ladino, L. A., Wex, H., Boose, Y., Burkert-Kohn, M., Cziczo, D. J., and Krämer, M.: Overview of Ice Nucleating Particles, Meteorological Monographs, 58, 1.1–1.33, doi:10.1175/AMSMONOGRAPHS-D-16-0006.1, 2017.

Kay, J. E. and Gettelman, A.: Cloud influence on and response to seasonal Arctic sea ice loss, Journal of Geophysical Research: Atmospheres, 114, doi:10.1029/2009JD011773, 2009.

Kinne, S.: Remote sensing data combinations: superior global maps for aerosol optical depth, pp. 361–381, Springer Berlin Heidelberg, Berlin, Heidelberg, doi:10.1007/978-3-540-69397-0_12, 2009.

Kinne, S., O'Donnel, D., Stier, P., Kloster, S., Zhang, K., Schmidt, H., Rast, S., Giorgetta, M., Eck, T. F., and Stevens, B.: MAC-v1: A new global aerosol climatology for climate studies, Journal of Advances in Modeling Earth Systems, 5, 704–740, doi:10.1002/jame.20035, 2013.

Knopf, D. A., Alpert, P. A., Wang, B., and Aller, J. Y.: Stimulation of ice nucleation by marine diatoms, Nature Geoscience, 4, 88–90, doi:10.1038/ngeo1037, 2011.

Korolev, A.: Limitations of the Wegener–Bergeron–Findeisen Mechanism in the Evolution of Mixed-Phase Clouds, Journal of the Atmospheric Sciences, 64, 3372–3375, doi:10.1175/JAS4035.1, 2007.

Lamarque, J.-F., Shindell, D. T., Josse, B., Young, P. J., Cionni, I., Eyring, V., Bergmann, D., Cameron-Smith, P., Collins, W. J., Doherty, R., Dalsoren, S., Faluvegi, G., Folberth, G., Ghan, S. J., Horowitz, L. W., Lee, Y. H., MacKenzie, I. A., Nagashima, T., Naik, V., Plummer, D., Righi, M., Rumbold, S. T., Schulz, M., Skeie, R. B., Stevenson, D. S., Strode, S., Sudo, K., Szopa, S., Voulgarakis, A., and Zeng, G.: The Atmospheric Chemistry and Climate Model Intercomparison Project (ACCMIP): overview and description of models, simulations and climate diagnostics, Geoscientific Model Development, 6, 179–206, doi:10.5194/gmd-6-179-2013, 2013.

Langmann, B., Scannell, C., and O'Dowd, C.: New Directions: Organic matter contribution to marine aerosols and cloud condensation nuclei, Atmospheric Environment, 42, 7821 – 7822, doi:10.1016/j.atmosenv.2008.09.002, 2008.

Lapina, K., Heald, C. L., Spracklen, D. V., Arnold, S. R., Allan, J. D., Coe, H., McFiggans, G., Zorn, S. R., Drewnick, F., Bates, T. S., Hawkins, L. N., Russell, L. M., Smirnov, A., O'Dowd, C. D., and Hind, A. J.: Investigating organic aerosol loading in the remote marine environment, Atmospheric Chemistry and Physics, 11, 8847–8860, doi:10.5194/acp-11-8847-2011, 2011.

Law, K. S. and Stohl, A.: Arctic Air Pollution: Origins and Impacts, Science, 315, 1537–1540, doi:10.1126/science.1137695, 2007.

Le Quéré, C., Buitenhuis, E. T., Moriarty, R., Alvain, S., Aumont, O., Bopp, L., Chollet, S., Enright, C., Franklin, D. J., Geider, R. J., Harrison, S. P., Hirst, A. G., Larsen, S., Legendre, L., Platt, T., Prentice, I. C., Rivkin, R. B., Sailley, S., Sathyendranath, S., Stephens, N., Vogt, M., and Vallina, S. M.: Role of zooplankton dynamics for Southern Ocean phytoplankton biomass and global biogeochemical cycles, Biogeosciences, 13, 4111–4133, doi:10.5194/bg-13-4111-2016, 2016.

Leck, C. and Bigg, E. K.: Aerosol production over remote marine areas–A new route, Geophysical Research Letters, 26, 3577–3580, doi:10.1029/1999GL010807, 1999.

Leck, C. and Bigg, E. K.: New Particle Formation of Marine Biological Origin, Aerosol Science and Technology, 44, 570–577, doi:10.1080/02786826.2010.481222, 2010.

Levkov, L., Rockel, B., Kapitza, H., and Raschke, E.: 3D mesoscale numerical studies of cirrus and stratus clouds by their time and space evolution, Beiträge zur Physik der Atmosphäre, 65, 35–58, 1992.

Liu, Y., Key, J. R., Liu, Z., Wang, X., and Vavrus, S. J.: A cloudier Arctic expected with diminishing sea ice, Geophysical Research Letters, 39, doi:10.1029/2012GL051251, 2012.

Lohmann, U.: A glaciation indirect aerosol effect caused by soot aerosols, Geophysical Research Letters, 29, 11–1–11–4, doi:10.1029/2001GL014357, 2002.

Lohmann, U. and Diehl, K.: Sensitivity Studies of the Importance of Dust Ice Nuclei for the Indirect Aerosol Effect on Stratiform Mixed-Phase Clouds, Journal of the Atmospheric Sciences, 63, 968–982, doi:10.1175/JAS3662.1, 2006.

Lohmann, U., Feichter, J., Chuang, C. C., and Penner, J. E.: Prediction of the number of cloud droplets in the ECHAM GCM, Journal of Geophysical Research: Atmospheres, 104, 9169–9198, doi:10.1029/1999JD900046, 1999.

Lohmann, U., Stier, P., Hoose, C., Ferrachat, S., Kloster, S., Roeckner, E., and Zhang, J.: Cloud microphysics and aerosol indirect effects in the global climate model ECHAM5-HAM, Atmospheric Chemistry and Physics, 7, 3425–3446, doi:10.5194/acp-7-3425-2007, 2007.

Long, M. S., Keene, W. C., Kieber, D. J., Erickson, D. J., and Maring, H.: A sea-state based source function for size- and composition-resolved marine aerosol production, Atmospheric Chemistry and Physics, 11, 1203–1216, doi:10.5194/acp-11-1203-2011, 2011.

Lubin, D. and Vogelmann, A. M.: Expected magnitude of the aerosol shortwave indirect effect in springtime Arctic liquid water clouds, Geophysical Research Letters, 34, doi:10.1029/2006GL028750, 2006a.

Lubin, D. and Vogelmann, A. M.: A climatologically significant aerosol longwave indirect effect in the Arctic, Nature, 439, 453–456, doi:10.1038/nature04449, 2006b.

MacCracken, M. C., Cess, R. D., and Potter, G. L.: Climatic effects of anthropogenic arctic aerosols: An illustration of climate feedback mechanisms with one- and two-dimensional climate models, Journal of Geophysical Research: Atmospheres, 91, 14 445–14 450, doi:10.1029/JD091iD13p14445, 1986.

Manabe, S. and Stouffer, R. J.: Sensitivity of a global climate model to an increase of CO2 concentration in the atmosphere, Journal of Geophysical Research: Oceans, 85, 5529–5554, doi:10.1029/JC085iC10p05529, 1980.

Mann, K. and Lazier, J.: Vertical Structure in Coastal Waters: Coastal Upwelling Regions, pp. 163–215, Blackwell Publishing Ltd., doi:10.1002/9781118687901.ch5, 2005.

Marsland, S., Haak, H., Jungclaus, J., Latif, M., and Röske, F.: The Max-Planck-Institute global ocean/sea ice model with orthogonal curvilinear coordinates, Ocean Modelling, 5, 91 – 127, doi:10.1016/S1463-5003(02)00015-X, 2003.

McCluskey, C. S., Hill, T. C. J., Malfatti, F., Sultana, C. M., Lee, C., Santander, M. V., Beall, C. M., Moore, K. A., Cornwell, G. C., Collins, D. B., Prather, K. A., Jayarathne, T., Stone, E. A., Azam, F., Kreidenweis, S. M., and DeMott, P. J.: A Dynamic Link between Ice Nucleating Particles Released in Nascent Sea Spray Aerosol and Oceanic Biological Activity during Two Mesocosm Experiments, Journal of the Atmospheric Sciences, 74, 151–166, doi:10.1175/JAS-D-16-0087.1, 2017.

Meskhidze, N., Xu, J., Gantt, B., Zhang, Y., Nenes, A., Ghan, S. J., Liu, X., Easter, R., and Zaveri, R.: Global distribution and climate forcing of marine organic aerosol: 1. Model improvements and evaluation, Atmospheric Chemistry and Physics, 11, 11 689–11 705, doi:10.5194/acp-11-11689-2011, 2011.

Morrison, H., Pinto, J. O., Curry, J. A., and McFarquhar, G. M.: Sensitivity of modeled arctic mixed-phase stratocumulus to cloud condensation and ice nuclei over regionally varying surface conditions, Journal of Geophysical Research: Atmospheres, 113, doi: 10.1029/2007JD008729, 2008.

Morrison, H., de Boer, G., Feingold, G., Harrington, J., Shupe, M. D., and Sulia, K.: Resilience of persistent Arctic mixed-phase clouds, Nature Geoscience, 5, 11–17, doi: 10.1038/ngeo1332, 2012.

Namazi, M., von Salzen, K., and Cole, J. N. S.: Simulation of black carbon in snow and its climate impact in the Canadian Global Climate Model, Atmospheric Chemistry and Physics, 15, 10 887–10 904, doi:10.5194/acp-15-10887-2015, 2015.

Niemand, M., Möhler, O., Vogel, B., Vogel, H., Hoose, C., Connolly, P., Klein, H., Bingemer, H., DeMott, P., Skrotzki, J., and Leisner, T.: A Particle-Surface-Area-Based Parameterization of Immersion Freezing on Desert Dust Particles, Journal of the Atmospheric Sciences, 69, 3077–3092, doi:10.1175/JAS-D-11-0249.1, 2012.

O'Dowd, C., Ceburnis, D., Ovadnevaite, J., Bialek, J., Stengel, D. B., Zacharias, M., Nitschke, U., Connan, S., Rinaldi, M., Fuzzi, S., and et al.: Connecting marine productivity to sea-spray via nanoscale biological processes: Phytoplankton Dance or Death Disco?, Scientific Reports, 5, 14 883, doi:10.1038/srep14883, 2015.

Orbe, C., Newman, P. A., Waugh, D. W., Holzer, M., Oman, L. D., Li, F., and Polvani, L. M.: Airmass Origin in the Arctic. Part I: Seasonality, Journal of Climate, 28, 4997–5014, doi:10.1175/JCLI-D-14-00720.1, 2015.

Pinto, J. O.: Autumnal Mixed-Phase Cloudy Boundary Layers in the Arctic, Journal of the Atmospheric Sciences, 55, 2016–2038, doi:10.1175/1520-0469(1998)055<2016:AMPCBL>2.0.CO;2, 1998.

Pithan, F. and Mauritsen, T.: Arctic amplification dominated by temperature feedbacks in contemporary climate models, Nature Geoscience, 7, 181–184, doi:10.1038/ngeo2071, 2014.

Pithan, F., Medeiros, B., and Mauritsen, T.: Mixed-phase clouds cause climate model biases in Arctic wintertime temperature inversions, Climate Dynamics, 43, 289–303, doi:10.1007/s00382-013-1964-9, 2014.

Popp, T., de Leeuw, G., Bingen, C., Brühl, C., Capelle, V., Chedin, A., Clarisse, L., Dubovik, O., Grainger, R., Griesfeller, J., Heckel, A., Kinne, S., Klüser, L., Kosmale, M., Kolmonen, P., Lelli, L., Litvinov, P., Mei, L., North, P., Pinnock, S., Povey, A., Robert, C., Schulz, M., Sogacheva, L., Stebel, K., Stein Zweers, D., Thomas, G., Tilstra, L. G., Vandenbussche, S., Veefkind, P., Vountas, M., and Xue, Y.: Development, Production and Evaluation of Aerosol Climate Data Records from European Satellite Observations (Aerosol_cci), Remote Sensing, 8, doi:10.3390/rs8050421, 2016.

Pruppacher, H. and Klett, J.: Microphysics of Clouds and Precipitation, Springer, 2 edn., 1997.

Pueschel, R. and Kinne, S.: Physical and radiative properties of Arctic atmospheric aerosols, Science of The Total Environment, 160-161, 811 – 824, doi:10.1016/0048-9697(95)04414-V, 1995.

Qian, Y., Flanner, M. G., Leung, L. R., and Wang, W.: Sensitivity studies on the impacts of Tibetan Plateau snowpack pollution on the Asian hydrological cycle and monsoon climate, Atmospheric Chemistry and Physics, 11, 1929–1948, doi:10.5194/acp-11-1929-2011, 2011.

Rasch, P. J. and Kristjánsson, J. E.: A Comparison of the CCM3 Model Climate Using Diagnosed and Predicted Condensate Parameterizations, Journal of Climate, 11, 1587–1614, doi:10.1175/1520-0442(1998)011<1587:ACOTCM>2.0.CO;2, 1998.

Reick, C. H., Raddatz, T., Brovkin, V., and Gayler, V.: Representation of natural and anthropogenic land cover change in MPI-ESM, Journal of Advances in Modeling Earth Systems, 5, 459–482, doi:10.1002/jame.20022, 2013.

Riahi, K., Grübler, A., and Nakicenovic, N.: Scenarios of long-term socio-economic and environmental development under climate stabilization, Technological Forecasting and Social Change, 74, 887 – 935, doi:10.1016/j.techfore.2006.05.026, greenhouse Gases - Integrated Assessment, 2007.

Riahi, K., Rao, S., Krey, V., Cho, C., Chirkov, V., Fischer, G., Kindermann, G., Nakicenovic, N., and Rafaj, P.: RCP 8.5—A scenario of comparatively high greenhouse gas emissions, Climatic Change, 109, 33, doi:10.1007/s10584-011-0149-y, 2011.

Rinaldi, M., Fuzzi, S., Decesari, S., Marullo, S., Santoleri, R., Provenzale, A., von Hardenberg, J., Ceburnis, D., Vaishya, A., O'Dowd, C. D., and Facchini, M. C.: Is chlorophyll-a the best surrogate for organic matter enrichment in submicron primary marine aerosol?, Journal of Geophysical Research: Atmospheres, 118, 4964–4973, doi:10.1002/jgrd.50417, 2013.

Ritter, C., Notholt, J., Fischer, J., and Rathke, C.: Direct thermal radiative forcing of tropospheric aerosol in the Arctic measured by ground based infrared spectrometry, Geophysical Research Letters, 32, doi:10.1029/2005GL024331, 2005.

Roeckner, E., Bäuml, G., Bonaventura, L., Brokopf, R., Esch, M., Giorgetta, M., Hagemann, S., Kirchner, I., Kornblueh, L., Manzini, E., Rhodin, A., Schlese, U., Schulzweida, U., and Tompkins, A.: The atmospheric general circulation model ECHAM 5. PART I: model description, Tech. rep., Max Planck Institute for Meteorology, 2003.

Roeckner, E., Brokopf, R., Esch, M., Giorgetta, M., Hagemann, S., Kornblueh, L., Manzini, E., Schlese, U., and Schulzweida, U.: Sensitivity of Simulated Climate to Horizontal and Vertical Resolution in the ECHAM5 Atmosphere Model, Journal of Climate, 19, 3771–3791, doi:10.1175/JCLI3824.1, 2006.

Roelofs, G. J.: A GCM study of organic matter in marine aerosol and its potential contribution to cloud drop activation, Atmospheric Chemistry and Physics, 8, 709–719, doi:10.5194/acp-8-709-2008, 2008.

Rogers, R. R. and Yau, M. K.: A short course in cloud physics, Butterworth-Heinemann, Oxford, UK, 3 edn., 1989.

Schnell, R. C. and Vali, G.: Biogenic Ice Nuclei: Part I. Terrestrial and Marine Sources, Journal of the Atmospheric Sciences, 33, 1554–1564, doi:10.1175/1520-0469(1976)033<1554:BINPIT>2.0.CO;2, 1976.

Sciare, J., Favez, O., Sarda-Estève, R., Oikonomou, K., Cachier, H., and Kazan, V.: Long-term observations of carbonaceous aerosols in the Austral Ocean atmosphere: Evidence of a biogenic marine organic source, Journal of Geophysical Research: Atmospheres, 114, doi:10.1029/2009JD011998, 2009.

Seinfeld, J. H., Bretherton, C., Carslaw, K. S., Coe, H., DeMott, P. J., Dunlea, E. J., Feingold, G., Ghan, S., Guenther, A. B., Kahn, R., Kraucunas, I., Kreidenweis, S. M., Molina, M. J., Nenes, A., Penner, J. E., Prather, K. A., Ramanathan, V., Ramaswamy, V., Rasch, P. J., Ravishankara, A. R., Rosenfeld, D., Stephens, G., and Wood, R.: Improving our fundamental understanding of the role of aerosol-cloud interactions in the climate system, Proceedings of the National Academy of Sciences, 113, 5781–5790, doi:10.1073/pnas.1514043113, 2016.

Serreze, M. C. and Francis, J. A.: The Arctic Amplification Debate, Climatic Change, 76, 241–264, doi:10.1007/s10584-005-9017-y, 2006.

Shupe, M. D.: Clouds at Arctic Atmospheric Observatories. Part II: Thermodynamic Phase Characteristics, Journal of Applied Meteorology and Climatology, 50, 645–661, doi:10.1175/2010JAMC2468.1, 2011.

Shupe, M. D. and Intrieri, J. M.: Cloud Radiative Forcing of the Arctic Surface: The Influence of Cloud Properties, Surface Albedo, and Solar Zenith Angle, Journal of Climate, 17, 616–628, doi:10.1175/1520-0442(2004)017<0616:CRFOTA>2.0.CO;2, 2004.

Shupe, M. D., Walden, V. P., Eloranta, E., Uttal, T., Campbell, J. R., Starkweather, S. M., and Shiobara, M.: Clouds at Arctic Atmospheric Observatories. Part I: Occurrence and Macrophysical Properties, Journal of Applied Meteorology and Climatology, 50, 626–644, doi:10.1175/2010JAMC2467.1, 2011.

Sofiev, M., Soares, J., Prank, M., de Leeuw, G., and Kukkonen, J.: A regional-to-global model of emission and transport of sea salt particles in the atmosphere, Journal of Geophysical Research: Atmospheres, 116, doi:10.1029/2010JD014713, 2011.

Sotiropoulou, G., Sedlar, J., Tjernström, M., Shupe, M. D., Brooks, I. M., and Persson, P. O. G.: The thermodynamic structure of summer Arctic stratocumulus and the dynamic coupling to the surface, Atmospheric Chemistry and Physics, 14, 12 573–12 592, doi:10.5194/acp-14-12573-2014, 2014.

Spracklen, D. V., Arnold, S. R., Sciare, J., Carslaw, K. S., and Pio, C.: Globally significant oceanic source of organic carbon aerosol, Geophysical Research Letters, 35, doi:10.1029/2008GL033359, l12811, 2008.

Sterle, K. M., McConnell, J. R., Dozier, J., Edwards, R., and Flanner, M. G.: Retention and radiative forcing of black carbon in eastern Sierra Nevada snow, The Cryosphere, 7, 365–374, doi:10.5194/tc-7-365-2013, 2013.

Stevens, B., Giorgetta, M., Esch, M., Mauritsen, T., Crueger, T., Rast, S., Salzmann, M., Schmidt, H., Bader, J., Block, K., Brokopf, R., Fast, I., Kinne, S., Kornblueh, L., Lohmann, U., Pincus, R., Reichler, T., and Roeckner, E.: Atmospheric component of the MPI-M Earth System Model: ECHAM6, Journal of Advances in Modeling Earth Systems, 5, 146–172, doi:10.1002/jame.20015, 2013.

Stevens, B., Fiedler, S., Kinne, S., Peters, K., Rast, S., Müsse, J., Smith, S. J., and Mauritsen, T.: MACv2-SP: a parameterization of anthropogenic aerosol optical properties and an associated Twomey effect for use in CMIP6, Geoscientific Model Development, 10, 433–452, doi:10.5194/gmd-10-433-2017, 2017.

Stier, P., Feichter, J., Kinne, S., Kloster, S., Vignati, E., Wilson, J., Ganzeveld, L., Tegen, I., Werner, M., Balkanski, Y., Schulz, M., Boucher, O., Minikin, A., and Petzold, A.: The aerosol-climate model ECHAM5-HAM, Atmospheric Chemistry and Physics, 5, 1125–1156, doi:10.5194/acp-5-1125-2005, 2005.

Stocks, B. J., Fosberg, M. A., Lynham, T. J., Mearns, L., Wotton, B. M., Yang, Q., Jin, J.-Z., Lawrence, K., Hartley, G. R., Mason, J. A., and McKENNEY, D. W.: Climate Change and Forest Fire Potential in Russian and Canadian Boreal Forests, Climatic Change, 38, 1–13, doi:10.1023/A:1005306001055, 1998.

Stohl, A.: Characteristics of atmospheric transport into the Arctic troposphere, Journal of Geophysical Research: Atmospheres, 111, doi:10.1029/2005JD006888, 2006.

Stramler, K., Genio, A. D. D., and Rossow, W. B.: Synoptically Driven Arctic Winter States, Journal of Climate, 24, 1747–1762, doi:10.1175/2010JCLI3817.1, 2011.

Struthers, H., Ekman, A. M. L., Glantz, P., Iversen, T., Kirkevåg, A., Mårtensson, E. M., Seland, Ø., and Nilsson, E. D.: The effect of sea ice loss on sea salt aerosol concentrations and the radiative balance in the Arctic, Atmospheric Chemistry and Physics, 11, 3459–3477, doi:10.5194/acp-11-3459-2011, 2011.

Sundqvist, H., Berge, E., and Kristjánsson, J. E.: Condensation and Cloud Parameterization Studies with a Mesoscale Numerical Weather Prediction Model, Monthly Weather Review, 117, 1641–1657, doi:10.1175/1520-0493(1989)117<1641:CACPSW>2.0.CO;2, 1989.

Takahashi, K. and Battisti, D. S.: Processes Controlling the Mean Tropical Pacific Precipitation Pattern. Part II: The SPCZ and the Southeast Pacific Dry Zone, Journal of Climate, 20, 5696–5706, doi:10.1175/2007JCLI1656.1, 2007.

Taylor, K. E., Williamson, D., and Zwiers, F.: The sea surface temperature and sea ice concentration boundary conditions for AMIP II simulations, Tech. Rep. PCMDI Report 60, Program for Climate Model Diagnosis and Intercomparison, Lawrence Livermore National Laboratory, 2000.

Taylor, K. E., Stouffer, R. J., and Meehl, G. A.: An Overview of CMIP5 and the Experiment Design, Bulletin of the American Meteorological Society, 93, 485–498, doi:10.1175/BAMS-D-11-00094.1, 2012.

Tegen, I., Harrison, S. P., Kohfeld, K., Prentice, I. C., Coe, M., and Heimann, M.: Impact of vegetation and preferential source areas on global dust aerosol: Results from a model study, Journal of Geophysical Research: Atmospheres, 107, AAC 14–1–AAC 14–27, doi:10.1029/2001JD000963, 2002.

Tegen, I., Lohmann, U., Neubauer, D., Siegenthaler-Le Drian, C., Ferrachat, S., Bey, I., Stanelle, T., Stier, P., Schutgens, N., Watson-Parris, D., Schmidt, H., Rast, S., Schultz, M. G., Schroeder, S., Kokkola, H., Barthel, S., and Heinold, B.: The aerosol-climate model ECHAM6.3-HAM2.3: Aerosol evaluation, Geoscientific Model Development Discussions, in preparation, 2018.

Turpin, B. and Lim, H.: Species contributions to PM2.5 mass concentrations: Revisiting common assumptions for estimating organic mass, Aerosol Science and Technology, 35, 602–610, doi:10.1080/02786820119445, 2001.

Twomey, S.: The Influence of Pollution on the Shortwave Albedo of Clouds, Journal of the Atmospheric Sciences, 34, 1149–1152, doi:10.1175/1520-0469(1977)034<1149:TIOPOT>2.0.CO;2, 1977.

Vali, G., Christensen, M., Fresh, R. W., Galyan, E. L., Maki, L. R., and Schnell, R. C.: Biogenic Ice Nuclei. Part II: Bacterial Sources, Journal of the Atmospheric Sciences, 33, 1565–1570, doi:10.1175/1520-0469(1976)033<1565:BINPIB>2.0.CO;2, 1976.

Vergara-Temprado, J., Murray, B. J., Wilson, T. W., O'Sullivan, D., Browse, J., Pringle, K. J., Ardon-Dryer, K., Bertram, A. K., Burrows, S. M., Ceburnis, D., DeMott, P. J., Mason, R. H., O'Dowd, C. D., Rinaldi, M., and Carslaw, K. S.: Contribution of feldspar and marine organic aerosols to global ice nucleating particle concentrations, Atmospheric Chemistry and Physics, 17, 3637–3658, doi:10.5194/acp-17-3637-2017, 2017.

Vignati, E., Wilson, J., and Stier, P.: M7: An efficient size-resolved aerosol microphysics module for large-scale aerosol transport models, Journal of Geophysical Research: Atmospheres, 109, doi:10.1029/2003JD004485, 2004.

Vignati, E., Facchini, M., Rinaldi, M., Scannell, C., Ceburnis, D., Sciare, J., Kanakidou, M., Myriokefalitakis, S., Dentener, F., and O'Dowd, C.: Global scale emission and distribution of sea-spray aerosol: Sea-salt and organic enrichment, Atmospheric Environment, 44, 670 – 677, doi:10.1016/j.atmosenv.2009.11.013, 2010.

Wang, X., Sultana, C. M., Trueblood, J., Hill, T. C. J., Malfatti, F., Lee, C., Laskina, O., Moore, K. A., Beall, C. M., McCluskey, C. S., Cornwell, G. C., Zhou, Y., Cox, J. L., Pendergraft, M. A., Santander, M. V., Bertram, T. H., Cappa, C. D., Azam, F., DeMott, P. J., Grassian, V. H., and Prather, K. A.: Microbial Control of Sea Spray Aerosol Composition: A Tale of Two Blooms, ACS Central Science, 1, 124–131, doi:10.1021/acscentsci.5b00148, 2015.

Warren, S. G. and Wiscombe, W. J.: A Model for the Spectral Albedo of Snow. II: Snow Containing Atmospheric Aerosols, Journal of the Atmospheric Sciences, 37, 2734–2745, doi:10.1175/1520-0469(1980)037<2734:AMFTSA>2.0.CO;2, 1980.

Wiggert, J., Jones, B., Dickey, T., Brink, K., Weller, R., Marra, J., and Codispoti, L.: The Northeast Monsoon's impact on mixing, phytoplankton biomass and nutrient cycling in the Arabian Sea, Deep Sea Research Part II: Topical Studies in Oceanography, 47, 1353 – 1385, doi:10.1016/S0967-0645(99)00147-2, 2000.

Wilks, D. S.: "The Stippling Shows Statistically Significant Grid Points": How Research Results are Routinely Overstated and Overinterpreted, and What to Do about It, Bulletin of the American Meteorological Society, 97, 2263–2273, doi:10.1175/BAMS-D-15-00267.1, 2016.

Wilson, T. W., Ladino, L. A., Alpert, P. A., Breckels, M. N., Brooks, I. M., Browse, J., Burrows, S. M., Carslaw, K. S., Huffman, J. A., Judd, C., Kilthau, W. P., Mason, R. H., McFiggans, G., Miller, L. A., Nájera, J. J., Polishchuk, E., Rae, S., Schiller, C. L., Si, M., Temprado, J. V., Whale, T. F., Wong, J. P. S., Wurl, O., Yakobi-Hancock, J. D., Abbatt, J. P. D., Aller, J. Y., Bertram, A. K., Knopf, D. A., and Murray, B. J.: A marine biogenic source of atmospheric ice-nucleating particles, Nature, 525, 234–238, doi:10.1038/nature14986, 2015.

Wu, C., Liu, X., Lin, Z., Rahimi-Esfarjani, S. R., and Lu, Z.: Impacts of absorbing aerosol deposition on snowpack and hydrologic cycle in the Rocky Mountain region based on variable-resolution CESM (VR-CESM) simulations, Atmospheric Chemistry and Physics, 18, 511–533, doi:10.5194/acp-18-511-2018, 2018.

Yin, B. and Min, Q.: Climatology of aerosol and cloud optical properties at the Atmospheric Radiation Measurements Climate Research Facility Barrow and Atqasuk sites, Journal of Geophysical Research: Atmospheres, 119, 1820–1834, doi:10.1002/2013JD020296, 2014.

Yun, Y. and Penner, J. E.: An evaluation of the potential radiative forcing and climatic impact of marine organic aerosols as heterogeneous ice nuclei, Geophysical Research Letters, 40, 4121–4126, doi:10.1002/grl.50794, 2013.

Zhang, K., O'Donnell, D., Kazil, J., Stier, P., Kinne, S., Lohmann, U., Ferrachat, S., Croft, B., Quaas, J., Wan, H., Rast, S., and Feichter, J.: The global aerosol-climate model ECHAM-HAM, version 2: sensitivity to improvements in process representations, Atmospheric Chemistry and Physics, 12, 8911–8949, doi:10.5194/acp-12-8911-2012, 2012.

List of acronyms and symbols

Acronym	Full name
AATSR	Advanced Along-Track Scanning Radiometer
ACCMIP	Atmospheric Chemistry and Climate Model Intercomparison Project
AMIP	Atmospheric Model Intercomparison Project
AOD	aerosol optical depth
BC	black carbon
BVOC	biogenic volatile organic compound
CAMS	Copernicus Atmosphere Monitoring Service
CCN	cloud condensation nuclei
CDNC	cloud droplet number concentration
CMIP5	Coupled Model Intercomparison Project Phase 5
CNT	classical nucleation theory
DU	dust
ERF	effective radiative forcing
ESM	earth system model
FF	frozen fraction
GEOSCCM	Goddard Earth Observing System Chemistry-Climate Model
HAM	Hamburg aerosol module
HAMOCC	Hamburg ocean carbon cycle model
ICNC	ice crystal number concentration
ISCCP	International Satelite Cloud Climatology Project
INP	ice nucleating particle
IWC	ice water content (mass concentration)
IWP	ice water path (vertically integrated mass)
LW	longwave/terrestrial radiation
LWC	liquid water content (mass concentration)
LWP	liquid water path (vertically integrated mass)
MACC	Monitoring Atmospheric Composition and Climate
MACv2	Max-Planck-Institute Aerosol Climatology version 2
MOA	marine organic aerosol
MODIS	Moderate Resolution Imaging Spectroradiometer
MPIOM	Max Planck Institute ocean model
NAO	North Atlantic Oscillation
NH	Northern Hemisphere
OC	organic carbon
OMF	organic mass fraction
PD	present day
RCP	Representative Concentration Pathway
RH	relative humidity
SALSA	sectional aerosol model for large-scale applications
SeaWiFS	Sea-viewing Wide Field-of-view Sensor
SNICAR	Snow, Ice, and Aerosol Radiation
SS	sea salt
SW	shortwave/solar radiation
TKE	turbulent kinetic energy
TOA	top-of-atmosphere
WBF	Wegener-Bergeron-Findeisen
WIOM	water insoluble organic matter
WSOM	water soluble organic matter

Symbol	Unit	Description
m_{MOA}	kg	mean MOA particle mass
N_{frozen}	m^{-3}	number of droplets frozen per time step
N_{imm}	m^{-3}	number concentration of immersed aerosol in cloud droplets
$N_{\mathrm{TOT,act}}$	m^{-3}	number of aerosol particles that can be activated into cloud droplets
n_{m}	kg^{-1}	ice-active site density per unit mass
n_{s}	m^{-2}	ice-active site density per unit surface area
$\bar{r}$	m	median radius of all particles in the mode
$r_{\mathrm{eff,i}}$	m	ice crystal effective radius
$r_{\mathrm{eff,l}}$	m	cloud droplet effective radius
s_{mean}	m^2	mean surface area per aerosol particle
σ		standard deviation of the lognormal size distribution
T	K or °C	temperature
$T_{2\mathrm{m}}$	K	2-metre temperature
V_{species}	m^3	total volume of an aerosol species in a particular size mode, where species can be MOA for marine organic aerosol, SS for sea salt, or TOT for total/all aerosol species

Acknowledgements

This thesis was made possible by funding received from the European Union's Seventh Framework Programme (FP7/2007-2013) project BACCHUS under grant agreement n° 603445. Model simulations were performed on the high performance computing cluster Euler, maintained by ETH Zurich's High-Performance Computing (HPC) group under the Scientific IT Services (SIS) section, or through a grant from the Swiss National Supercomputing Centre (CSCS) under project ID 652.

But more importantly, the completion of this thesis would not be possible without the help of many people along the way:

I would first like to thank Ulrike, for giving me the opportunity to work on this research project, and for all of your enthusiasm and encouragement along the way. For truly caring about the betterment of the students, and for always being very responsive in case of need.

Thanks Risto and Luisa, for serving as co-examiners for my defence and for your feedback on my thesis.

Thanks David, for always being helpful when I have questions about the model or otherwise, for all the scientific support and discussions that helped clarify ideas, and for going out of your way to find an answer for me when the solution wasn't immediately obvious.

Thanks Sylvaine, for providing the model technical support that paved the road for all of my work in this thesis.

Thanks Remo, for sharing the code for producing histogram outputs from the model, without which chapter 4 would not exist, and in general for always sharing different ideas about how to look at the model outputs.

Thanks Luisa, additionally, for the detailed discussions about MOA, for providing the cover photo for this thesis, and for inviting me to all sorts of activities on the get-go when I first arrived in Zurich, so that I never had the chance to feel excluded.

Thanks Jörg and Annika, for being so kind and translating my abstract to German. And Franzi for popping by at exactly the right moment and offering to proof-read it.

Thanks Anina, for helping me with anything Arctic shipping-related.

Thanks to my officemates, Fabiola and Annika, and previously Baban and Jan, for the great company at work.

Thanks to all my fellow Wolke groupmates, for creating a great atmosphere for scientific exchange, and in general a great environment to work in. Special thanks are extended to Luisa, Blaž, Rob, Moni, Olga, Fabian, Gesa, Fabiola, and Annika for making the "life" part of my work-life balance at ETH.

Thanks to my Swing dancing friends, for bringing me so much joy. And to all the people that have showed me kindness since I arrived in Europe, for being so kind.

And very importantly, thanks to my family, for the unconditional support through everything.